TECHNICAL REPORT
WVT-RI-5907
REVISION 1

THE AUTOFRETTAGE PRINCIPLE AS APPLIED TO HIGH STRENGTH LIGHT WEIGHT GUN TUBES

BY
T. E. DAVIDSON
C. S. BARTON
A. N. REINER
D. P. KENDALL

OCTOBER 1959

INDUSTRIAL PREPAREDNESS MEASURE 8030-4231-03-46100-01

WATERVLIET ARSENAL
WATERVLIET, N. Y.

TECHNICAL REPORT
WVT-RI-5907
REVISION 1

THE AUTOFRETTAGE PRINCIPLE AS APPLIED TO HIGH STRENGTH LIGHT WEIGHT GUN TUBES

BY

T. E. DAVIDSON

C. S. BARTON

A. N. REINER

D. P. KENDALL

OCTOBER 1959

INDUSTRIAL PREPAREDNESS MEASURE 8030-4231-03-46100-01

WATERVLIET ARSENAL
WATERVLIET, N. Y.

~~CONFIDENTIAL~~ UNCLASSIFIED

This document is subject to special export controls and each transmittal to foreign governments or foreign nationals may be made only with prior approval of Army Watervliet Arsenal Watervliet, New York 12189

Publication of the photographs in this report are not authorized unless approved for release by a Public Information Office at any Army Activity or Installation and so noted hereon. Its use in commercial advertisement must be approved by the Public Information Division, Office of the Chief of Information and Education, Department of the Army, the Pentagon, Washington 25, D. C. If published, please credit as "U. S. Army Photograph."

NOTE: This revision is made to correct an erroneous assumption in the original report. Changes in test or formulation occur on pages 20, 31, 43; Appendix I, page vii and Appendix I, page viii. This revision does not obsolete the original report.

TABLE OF CONTENTS

TABLE OF CONTENTS
(Cont.)

LIST OF FIGURES

LIST OF FIGURES
(Cont.)

LIST OF TABLES

LIST OF SYMBOLS

σ	Stress, pounds per square inch
σ_y	Yield strength, pounds per square inch
δ	Unit strain
u	Radial displacement
E	Modulus of elasticity
ν	Poisson's ratio
W	Diameter ratio, $\frac{b}{a}$
a	Inside radius of cylinder
b	Outside radius of cylinder
R	Radius of elastic - plastic interface
K	Constant of proportionality
r	Variable radius
P	Pressure, pounds per square inch
P_f	Firing or operating pressure
P_m	Maximum applied internal pressure
P_{if}	Interface pressure
P_R	Pressure to produce plastic flow to depth R
P.F.	Pressure factor, $\frac{P}{\sigma_y}$
S.F.	Strain factor, $\frac{\delta_{\theta b} E}{\sigma_y}$
P.E.R.	Permanent enlargement ratio $\frac{u_a}{u_b}$

LIST OF SYMBOLS
(Cont.)

% P.B.E.	Percent permanent bore enlargement
$( )_t$	Tangential
$( )_r$	Radial
$( )_z$	Longitudinal
$( )_o$	100 percent overstrain condition
$( )_e$	Elastic condition
$( )_p$	Plastic condition
$( )_r$	Residual
$( )_c$	Container

General Title: Industrial Preparedness Measure

Authorization: Program Directive Number

8090-4231-03-46100-01

Project Title: COLD WORKING

Sub-Project Title: DEVELOPMENT OF ENGINEERING DESIGN DATA FOR APPLICATION OF AUTOFRETTAGE TO 165,000 POUNDS PER SQUARE INCH YIELD STRENGTH MATERIALS

OBJECTIVE

The objective of this program is the study of the autofrettage principle as applied to high strength thick-wall steel cylinders of intermediate diameter ratio and the development of the design criteria and procedures for the application of autofrettage to light weight gun tube design and fabrication.

SUMMARY

Those associated with the cannon field have long been interested in techniques for increasing the elastic strength of thick-wall cylinders. This interest is demonstrated by the early use in the cannon field of such techniques as bore quenching, wire wrapping and shrinking. Overstraining beyond the initial elastic breakdown pressure which is termed autofrettage, is another such technique that was introduced to the cannon field early in the Twentieth Century as a means of increasing the elastic operating range of gun tubes.

Up to, and during, World War II, autofrettage was widely utilized in the cannon field throughout the world. It was primarily limited, however, to materials in the 65,000 to 80,000 pounds per square inch yield strength range.

As a result of the metallurgical advances made after World War II which resulted in significant increases in material strengths, the autofrettage principle for cannon applications was thought unnecessary and rather impractical. Consequently, the design data and criteria along with the high pressure technology fell far behind the rapid increase in gun tube material strengths. Current and future warfare concepts, however, are confronting those in the cannon field with the requirement of designing and manufacturing weapons featuring greater mobility and higher firepower than ever before thought possible. To assist in meeting these requirements it is necessary to consider the application of autofrettage to current and future high strength light weight gun tube design and manufacture.

Developed and described are empirical data and design criteria for the application of the autofrettage principle to gun tubes in the current yield strength range of 160,000 - 190,000 pounds per square inch. The developed data, which is based on a nominal yield strength of 165,000 pounds per square inch, is compared to various thick-wall cylinder theories.

Empirical data and relationships are presented for the pressure-strain curve, the one hundred percent overstrain or optimum

autofrettage condition, permanent enlargement ratio, longitudinal strain and other phenomenon associated with the overstraining of thick-wall cylinders of intermediate diameter ratio.

Strain "stabilization", the hysteresis loop effect, effects of machining, and reverse yielding are briefly analysed and discussed.

A typical experimentally determined residual stress distribution is presented and compared to that predicted from theory based on various yield criteria.

The thick-wall cylinder theory for the various stages of overstrain is given and discussed.

The results obtained from the testing of miniature specimens in the diameter ratio range of 1.4 to 2.4 are complimented by the autofrettage of a series of four high strength 90mm gun tubes of various design safety factors. The design technique for autofrettage of gun tubes along with an example based on one of the above 90mm tubes is presented.

I - HISTORICAL REVIEW

Ever since approximately 1850, those in the field of cannon design and manufacture have used residual stresses, in one form or another, to counteract the operating stresses, thus increasing the effective elastic strength. The first attempt was made during the era of thick wall cast steel cannon which were bore quenched. This quenching procedure induced a thermal stress gradient of sufficient magnitude to cause favorable compressive residual stresses at the bore.

Other later attempts to induce compressive residual stresses at the bore involved the wrapping of steel wire under tension or the shrinking of one or more jackets onto a liner.

As early as 1872 Saint-Venant (20) and others reported the development of the mathematical relationships for the stresses induced by strains beyond the initial elastic breakdown condition in thick-walled cylinders. Following this, several investigators reported mathematical analyses of stresses resulting from overstrain, based upon several different criteria of flow.

Early in the 20th Century, Turner (25) proposed that overstrain produced by the application of a sufficient internal hydrostatic pressure could be used as a substitute for bore quenching, wire wrapping and shrinking as a means of producing compressive residual bore stresses. This concept was adapted by several European countries and the United States for application to cannon tubes in the material strength range 40 - 50,000 pounds per square inch.

Later during World War II the autofrettage process was applied to a large number of cannon tubes of all sizes by several countries. It was still generally limited however to material strengths of 65,000 - 80,000 pounds per square inch.

Following World War II, however, new steels and metallurgical advances made possible the increase of material strengths to the point where guns were able to meet warfare requirements without the use of autofrettage. Consequently the design criteria, data and technology associated with the use of autofrettage in cannon design and manufacture fell far behind the rapid increase in material strengths.

Several techniques for inducing residual stresses in gun tubes by overstraining have been developed. These basic autofrettage techniques are described briefly as follows:

A - Closed End

In this method, a schematic of which is shown in Figure 1, the ends of the tube are capped and hydraulic pressure introduced into the bore. The tube, before autofrettage, has a near constant cross section thus requiring a large amount of machining afterwards. No restraining containers are utilized, thus the process is limited to relatively low yield strength materials and small amounts of deformation.

B - Moveable Packing

This process was primarily utilized by the U.S. Navy. It consists of a moveable packing configuration which is moved along the bore and the pressure varied to accommodate a variable cross

section. This method does not utilize restraining containers but allows a near final configuration prior to autofrettage. A schematic of this process is also shown in Figure 1.

C - Open End

This process was originally used by the U.S. Army Ordnance Corps during World War II on materials of 65,000 - 80,000 pounds per square inch yield strength. The tube acts as an open end cylinder in that the pressure seals, or packings, are constrained by a press and not the tube as shown in Figure 2. Containers are utilized both to permit radial cross section changes along the tube length, and to permit the use of large permanent bore enlargements and high yield strength materials without the danger of "ballooning" or inhomogeneous radial deformation. This process which has previously been limited both from an equipment and design standpoint to low strength materials is currently being adapted to the material yield strength range of 160,000 - 190,000 pounds per square inch.

D - Swaging

A new method of autofrettage in which the sliding wedge principle is combined with direct or indirect hydrostatic pressure or mechanically applied force has recently been developed and is described in a previous report (1). In this process, which is still experimental, the deformation gradient is produced by forcing a mandrel, which is larger than the bore by a predetermined amount, through the tube. It has proven able to produce the same autofrettage effect at 75 percent less pressure than that required by the open end technique. One other added advantage is that since the

amount of radial deformation is controlled by the major diameter of the mandrel no external restraining containers are required. This process is shown in Figure 3.

II - INTRODUCTION

Current and future warfare concepts are confronting those in the cannon field with the problem of designing and manufacturing weapons featuring greater mobility and higher firepower than ever before thought possible. In terms of the gun proper, this means that it must withstand equal or higher chamber pressures than those of current monobloc or shrunk construction, but with radically reduced weight. The apparent solutions to this problem are the development and utilization of much higher strength to weight ratio materials and/or the use of design concepts and principles to increase the effectiveness of the load carrying capacity of the configuration. Autofrettage is one such principle.

The purpose of this program is to develop the design data and criteria, and to study the phenomenon associated with the application of the autofrettage principle to current materials utilized in gun construction which feature a yield strength range of 160,000 to 190,000 pounds per square inch. Since this yield strength is almost triple that on which the autofrettage principle was applied during the World War II era, previously developed design criteria and techniques are inadequate and not applicable for today's

application.

A - The Autofrettage Principle

The elastic breakdown pressure is defined as that pressure which just produces inelastic action or yielding at the bore of a cylinder. Assuming a perfectly plastic material, in a thin-wall cylinder, the elastic breakdown pressure is very nearly the ultimate or bursting pressure. For a diameter ratio larger than that defined as a "thin-wall cylinder", the inelastic region, which starts at the bore, proceeds towards the outside diameter as the internal pressure is increased. After this first application of sufficient pressure to cause initial yielding and the movement of the elastic-plastic interface either towards or to the outside diameter, a higher elastic breakdown pressure will result. This pressure, termed the autofrettage pressure, can theoretically be as much as 83 - 100 percent greater, depending on the yield criteria utilized, than that for initial elastic breakdown. This concept of increasing the elastic breakdown pressure by overstraining is known as autofrettage.

The mechanism by which the autofrettage effect is induced depends on the deformation gradient resulting from overstraining. Since the material near the bore has been deformed to a much greater extent than the material near the outside surface, the resultant effect upon release of the overstrain pressure, will be that the outside layers will squeeze the inner layers, thus

inducing a tangential residual stress that is compressive at the bore. "Self-hooping", the literal French translation for the term autofrettage, refers to this residual stress.

In order for re-yielding to occur in an autofrettaged cylinder, the residual stress, shown in Figure 4, must be overcome by the stresses induced by the next application of pressure. A schematic representation of the algebraic summation of the operating and residual stresses is shown in Figure 5. The limit of this summation where yielding will again start at the bore, utilizing the Von Mises yield criteria, is as follows:

$$2\sigma_y^2 = \left[(\sigma_t + \sigma_{tr}) - (\sigma_r + \sigma_{rr})\right]^2 + \left[(\sigma_r + \sigma_{rr}) - (\sigma_z + \sigma_{zr})\right]^2 + \left[(\sigma_z + \sigma_{zr}) - (\sigma_t + \sigma_{tr})\right]^2 \quad \ldots\ldots\ldots\ldots\ldots\ldots \quad (1)$$

were at the bore $\sigma_{rr} = 0$ and for the open end case considered herein, $\sigma_z = 0$.

The magnitude and distribution of the residual stresses, induced by subjecting a cylinder to pressures beyond initial elastic breakdown is a function of the internal pressure, yield strength of the material, diameter ratio, and location of the elastic-plastic interface.

Before discussing the mathematical development of residual stresses in thick-wall cylinders, it may be of assistance to understand the meaning of two terms, that are often, but incorrectly, used synonymously. The percent overstrain in a thick-walled

cylinder subjected to internal hydrostatic pressure is defined as the ratio of the distance to the elastic-plastic interface from the bore to the wall thickness of the cylinder; i.e.,

$$\text{percent overstrain} = \frac{R-a}{b-a} \times 100 \quad \ldots\ldots\ldots\ldots\ldots\ldots \quad (2)$$

One hundred percent overstrain results when the elastic-plastic interface diameter is equal to the outside diameter of the cylinder i.e. R = b. Overstrain pressure then is that pressure required to produce a given amount of overstrain.

The percent autofrettage, however, is the ratio of the attained residual stresses due to a given amount of overstrain to the maximum theoretically possible for a particular diameter ratio. This means that, depending on the diameter ratio, 100 percent autofrettage may be attained at less than 100 percent overstrain. This is the case, based on the Von Mises and Tresca yield criteria for open end cylinders, in diameter ratios of greater than approximately 2.0 and 2.2 respectively.

The magnitude and distribution of the induced residual stresses is found by taking the difference between the overstrain stresses, and the elastic stresses at the overstrain pressure as graphically shown in Figure 6. The derivation for the residual stresses in open end thick-wall cylinders is given in Appendix I.

A critical percent overstrain can be reached above which the induced residual stresses will cause yielding in the reverse

direction upon the release of pressure. This situation will occur assuming $\sigma_{rr} = 0$, where $\sigma_{tr} = \sigma_y$ which will result at values of 100 percent overstrain in diameter ratios greater than approximately 2.0 - 2.2. When this condition exists, the above method of defining and developing the relationships for the residual stresses is no longer valid.

B - Program of Study

The purpose of this program is:

a. to develop the design criteria and data necessary to apply the autofrettage principle to current and future high strength materials utilized in cannon and to study the elastic and plastic phenomena associated with such an application.

b. to develop the required techniques and facilities for the autofrettage of high strength gun tubes.

In the development of the design criteria and study of the elastic and plastic phenomena, the diameter ratios and yield strengths common to current cannon design and manufacture are considered. In view of these current high strength materials and the necessity for optimum weight conservation, the diameter ratio range considered is well below that associated with World War II cannon manufacture and that of prime concern to other current investigators.

Of prime importance along with the pressure and stress phenomenon, are the strains necessary to accomplish optimum benefits. If the same strain criterion was used today that was considered a

minimum during the World War II era, the tube would undergo serious damage and possibly rupture during autofrettage.

Developed under this program are the data necessary to design a high strength gun tube for optimum benefit from autofrettage. This includes the study of such variables as, autofrettage and overstrain pressures, permanent enlargement ratios, longitudinal strain and shrinkage, and the magnitude and distribution of the resultant residual stress. Other variables such as the effect of thermal treatment on non-linearity, reverse yielding on the release of overstrain pressure, and the effects of post machining on the strength of autofrettaged configurations are also investigated.

The primary data developed along with that for associated phenomenon, is compared to current theoretical elastic-plastic concepts and summarized into appropriate tables, charts and graphs that can be utilized for design purposes.

The practice or technique for autofrettage has, out of necessity, undergone radical modification and re-development from that utilized for World War II gun tubes. The pressure capacity has, of necessity been increased by 100 percent which has resulted in new equipment and procedure concepts.

III - DESCRIPTION OF TESTS AND APPARATUS

The description and discussion of the testing procedure and equipment will be divided into two categories consisting of that associated with 1" internal diameter miniature specimens and full scale 90mm gun tubes.

A - 1 Inch Bore Diameter Specimens

1 - Test Specimens

The specimen geometry consisted of a common initial 1 inch bore diameter with a length of 11 inches. This length was determined to be great enough to overcome end effects in the largest diameter ratio investigated.

The specimens were of a 4340 steel of the following chemical analysis:

Carbon	0.37	Nickel	2.39
Manganese	0.72	Chromium	0.98
Silicon	0.28	Molybdenum	0.38
Sulphur	0.035	Phosphorous	0.016

They were obtained from billets 80 inches long and 4.25 inches in diameter which were gun drilled and cut into two 40 inch lengths. These lengths were heat treated by austenizing at 1525° F, oil quenching in the longitudinal direction and tempering at 1075° F ∓ 25° with a resultant nominal yield strength of 165,000 pounds per

square inch. The 40 inch heat treated bars were then finish reamed to 1 inch I.D. and three 11 inch specimens cut from each bar. The seven inches of remaining material was utilized to obtain tensile and charpy specimens. The specimen physical property data is tabulated in Table I.

2 - Restraining Containers

Preliminary experimentation was conducted using several specimens, ranging in diameter ratio from 1.4 to 2.4, to determine the uniformity of strain along the specimen length. Due to the natural inhomogeneity of material, particularly at this high strength level, large variations in plastic dilation were noted, both along the length and circumferentially. To insure uniform deformation throughout, external restraining containers were utilized. These containers were split at the half-length point and recessed to allow the application of strain gages to the specimen surface as shown in Figure 11. They were fabricated from 1045 steel, heat treated to approximately 130,000 pounds per square inch yield strength. The diameter ratio was 1.5 for all containers, one set being provided for each nominal specimen diameter ratio.

3 - Pressure Seals

The seal configuration used as shown in Figure 7 was of the unsupported area type consisting of an "O" ring and an annealed 1020 steel ring which is forced up an inclined plane. This configuration was chosen as being the simplest and most troublefree

over the large range of pressures, permanent bore enlargements, and diameter ratios encountered in this investigation.

4 - Test Apparatus

The pressure source as shown in Figure 8 was a 200,000 pounds per square inch 10 cubic inch per minute intensifier type pumping system manufactured by the Harwood Engineering Company. This system has an intensification ratio of 100:1 with a low pressure source of 2000 pounds per square inch and a charging pressure of 10,000 pounds per square inch.

Pressures were measured with a Manganin cell and a Wheatstone bridge. This Manganin pressure measurement system was calibrated on a controlled clearance piston gage as shown in Figure 9 which utilizes a known weight supported on a free piston of known area. The unknown pressure, which the Manganin cell measures, is introduced into the bottom of the cylinder and the piston floated. From the known weight supported by the piston of a specified area the pressure can be determined to an accuracy of 0.1 percent.

The specimen strain during the application of pressure was measured by SR-4 type strain gages attached to the outside surface of the specimen midpoint. An SR-4 strain indicator was used on most tests for measuring the strain. A photograph of the physical strain measurement setup is shown in Figure 10. Supplemental data was obtained using a Moseley Model 2S X-Y recorder. This recorder

simultaneously measured and plotted outside surface strain and pressure. It was calibrated by the use of an accurate shunt resistance in one arm of a four arm bridge.

The overall experimental accuracy depended upon the manganin cell and Wheatstone bridge in the pressure measurement system, and strain gages, SR-4 indicator, X-Y recorder and associated strain recording equipment in the strain measurement circuit. The estimated error, including the human element was approximately 1 percent in the pressure measuring system and 4 percent in the strain measurement circuit.

5 - Test Procedure

As has been previously stated, all the data in this study was obtained from cylinders laterally supported by restraining containers during autofrettage. The predicted percent bore enlargement was controlled by varying the outside diameter of the specimen thus controlling the subsequent expansion of each specimen. In order to determine when the desired percent overstrain was obtained, the container was strain gaged using SR-4 type, A-7 gages tangentially directed and diametrically opposed at intervals along the length of the container. When a small but substantial reading (generally between 100 and 200 micro-inches per inch) was obtained on all container gages, it was assumed that the specimen had uniformly contacted the container and uniform plastic flow achieved.

Strain readings from the two tangential gages on the mid-section of the specimen were recorded at appropriate intervals of induced internal pressure. From these data, plots of internal pressure versus external surface strain from both tangential strain gages were made for increasing and decreasing pressure. On a few tests, longitudinal strain was measured by using longitudinally oriented strain gages.

Physical dimensions of the bore, external diameter, and length were measured before and after autofrettage utilizing screw micrometers and dial bore gages to an accuracy of ± .0002 inches.

The applied pressure, when using the SR-4 strain indicator, consisted of increments of 5000 pounds per square inch to the elastic breakdown pressure, 2000 pounds per square inch to within 2,000 pounds per square inch of the overstrain pressure as predicted from preliminary testing, 500 pounds per square inch to the overstrain pressure, and 5000 pounds per square inch on pressure release. When the X-Y pressure-strain recorder was utilized the pressure was continuously applied at a slow rate. Good agreement was obtained between the two procedures.

In order to duplicate, to the greatest extent possible, the conditions to be encountered in the full-scale autofrettage of gun tubes, the delay, or "stabilization" period for the measurement of the increment of strain produced by a pressure change was maintained at approximately 30 seconds per reading. Some specimens

were tested, however, allowing complete strain "stabilization" at each pressure increment. As will be discussed, the use of a short "stabilization" period did not significantly change the results as derived from the pressure-strain data and it allowed the testing of a large number of cylinders in a limited period of time.

B - Full Scale 90mm Gun Tubes

In order to fully evaluate the data obtained, a series of 90mm gun tubes were autofrettaged and service tested. These tubes were autofrettaged with a 200,000 pounds per square inch, 70 cubic inch per minute pumping system similar in principle to the smaller unit previously described. In this system as shown in Figure 12, two double-acting intensifiers operate in parallel. This arrangement yields a greater volumetric capacity and increased reliability under extreme pressure conditions.

For safety purposes the high pressure portion of the system as well as the holding press for the gun tube are installed below floor level. The controls for the system shown in Figure 13 are isolated from the high pressure portion of the facilities.

The four tubes were autofrettaged by the open-end process shown in Figure 2. They were placed in a ten million pound press, and constrained along the length by containers. In this process, the 10 million pound press serves to restrain the pressure seals, and also to force the gun tube out of the containers after autofrettage. This is necessitated by the tube being of near-final

configuration prior to autofrettage. Therefore the muzzle, which has a much lower diameter ratio than the breech-end, tends to fit rather tightly into the container after autofrettage. As previously mentioned the restraining containers insure uniformity of plastic deformation and control the amount of deformation in light of the diameter ratio variation over the length of the tube.

The pressure seals were of the same design as those utilized in the miniature scale testing. The technique for designing a tube for autofrettage is shown in Appendix II.

All tubes were service tested with the life criteria being .200 inch wear at, or just in front of the origin of rifling, or the development of serious inaccuracy.

III - TEST RESULTS AND DISCUSSION

A - End Condition Analysis

In the pressure seal configuration utilized in the 1 inch and full scale testing, the seal was not mechanically fixed to the tube or cylinder. However, since the steel ring moves up the inclined plane of the seal head, there is a tensile longitudinal stress induced in the cylinder from the frictional forces between the ring and the inner cylinder wall. As will be shown, however, this stress is of low enough magnitude so that the results obtained more closely approximated the open end than closed end condition.

Hookes Law defining the tangential strain in a thick wall cylinder is:

$$\delta_t = \frac{1}{E}\left[\sigma_t - \nu \quad (\sigma_r + \sigma_z)\right] \ldots\ldots\ldots\ldots\ldots\ldots (3)$$

The defining equations for the elastic tangential (σ_t) and radial (σ_r) stresses in a thick-wall cylinder exposed to internal pressure are:

$$\sigma_t = \frac{P}{W^2-1}\left(1 + \frac{b^2}{r^2}\right) \ldots\ldots\ldots\ldots\ldots\ldots (4)$$

$$\sigma_r = \frac{P}{W^2-1}\left(1 - \frac{b^2}{r^2}\right) \ldots\ldots\ldots\ldots\ldots\ldots (5)$$

From equations (3), (4), and (5), the slope of the elastic portion of the internal pressure-outside surface-strain curve for various ~~ex~~ conditions is as follows:

1 - Closed End

At r = b

$\sigma_r = 0$

$\sigma_z = \frac{P}{W^2-1}$

and

$$\frac{P}{E\delta_t} = \frac{W^2-1}{2-\nu} \ldots\ldots\ldots\ldots\ldots\ldots\ldots\ldots (6)$$

2 - Open End

At $r = b$

$$\sigma_r = 0$$

$$\sigma_z = 0$$

and

$$\frac{P}{E\delta_t} = \frac{K^2-1}{2} \quad \ldots\ldots\ldots\ldots\ldots\ldots\ldots\ldots\ldots\ldots (7)$$

3 - Restrained End

At $r = b$

$$\sigma_r = 0$$

$$\sigma_z = \frac{2\nu P}{K^2-1}$$

and

$$\frac{P}{E\delta_t} = \frac{K^2-1}{2(1-\nu^2)} \quad \ldots\ldots\ldots\ldots\ldots\ldots\ldots\ldots\ldots\ldots (8)$$

The slopes of the internal pressure outside surface strain curve as a function of the diameter ratios considered in this program for the closed, open and restrained end conditions and that experimentally determined are shown in Figure 14. From the figure it is seen that the physical condition encountered in this experimental program correlates closely with the open end condition.

B - Elastic Breakdown

The plot of internal pressure versus outside surface strain is linear up to the initial yield or elastic breakdown at the bore. The experimental values for the elastic breakdown pressure were averaged for each diameter ratio and plotted in Figure 15 as a function of pressure factor versus diameter ratio. For comparison the theoretical elastic breakdown pressure factor based on the Von Mises and Tresca yield criteria for the open end condition are also shown. Based on the Von Mises yield criterion elastic breakdown occurs when:

$$P.F. = \frac{R^2-1}{\sqrt{3R^4+1}} \quad \ldots\ldots\ldots\ldots\ldots\ldots\ldots\ldots \quad (9)$$

From the Tresca yield criterion elastic breakdown is:

$$P.F. = \frac{R^2-1}{2R^2} \quad \ldots\ldots\ldots\ldots\ldots\ldots\ldots\ldots \quad (10)$$

As can be seen from the figure, there is close correlation between the experimentally determined and the theoretical Von Mises elastic breakdown condition. This again justifies considering the test condition as open-end.

C - Overstrain

When the internal pressure exceeds the elastic breakdown pressure, the elastic-plastic interface moves from the bore towards the outside diameter. This movement is a function of the internal pressure, yield strength, diameter ratio and the strain hardening

coefficient or capabilities of the material. However, the strain hardening effect in the yield strength level considered is relatively small.

The theoretical relationship between the internal pressure and location of the elastic-plastic interface according to the Tresca criteria of yield is from equation (23) of Appendix I:

$$P_R = \frac{\sigma_y}{2}\left(1 - \frac{R^2}{b^2}\right) + \sigma_y \log \frac{R}{a} \quad \ldots\ldots\ldots\ldots \quad (11)$$

Since current and future cannon design will be based on diameter ratios rarely exceeding 2.2, this experimental program is primarily based on the 100 percent overstrain condition. At 100 percent overstrain, i.e. where R = b, equation 11 becomes

$$P_0 = \sigma_y \log \frac{b}{a} \quad \ldots\ldots\ldots\ldots\ldots\ldots\ldots\ldots \quad (12)$$

From the experimental data, the empirical relationship for the pressure required to produce 100 percent overstrain is:

$$P_0 = 1.08\ \sigma_y \log \frac{b}{a} \quad \ldots\ldots\ldots\ldots\ldots\ldots \quad (13)$$

This empirical relationship is compared to that for the Tresca yield criteria from equation 12 in Figure 15. It can be seen that as the diameter ratio increases, the ratio of 100 percent overstrain pressure to elastic breakdown pressure also increases for the range of diameter ratios considered. It should be noted, however, that due to the reverse yielding phenomenon, at diameter ratios of greater than approximately 2.0 - 2.2 the autofrettage pressure may be lower than the 100 percent overstrain pressure. This reverse yielding phenomenon will be discussed further.

As previously discussed, 100 percent overstrain is defined as the condition where the outside surface just becomes plastic. From a first approximation, this condition occurs when the tangential strain (δ_t) on the outside surface equals the strain associated with yielding of the material under uni-axial loading as follows:

$$\delta_t = \frac{\sigma_Y}{E} \quad \text{where } \sigma_t = \sigma_y$$

This condition, i.e. where $\delta_t = \frac{\sigma_Y}{E}$ is shown in Figure 16 which is a dimensionless plot of the pressure factor $\frac{P}{\sigma_y}$ versus outside surface

strain factor $\frac{E\delta t}{\sigma_y}$ for e diameter ratios investigated. These curves were derived by a raging at least three specimens for each nominal increment of permanent bore enlargement. From the significant leveling off of the curves, it can be seen that 100 percent overstrain was attained at the predicted value of outside surface strain.

Also shown in Figure 16 are theoretical pressure factor-strain factor curves for the diameter ratios investigated. This theoretical relationship will be developed based on the Tresca Yield Criterion. Assuming the Tresca Criterion will of course introduce a small inaccuracy at the elastic breakdown condition, i.e., when R = a, but it does not appreciably effect the overall curve shape.

Referring to the figure and equations (13), (17) and (18) of Appendix I, the stresses in the elastic region of a partially overstrained cylinder are:

$$\sigma_{te} = K\left(1 + \frac{b^2}{r^2}\right) \quad \ldots\ldots\ldots\ldots\ldots\ldots \quad (14)$$

$$\sigma_{re} = K\left(1 - \frac{b^2}{r^2}\right) \quad \ldots\ldots\ldots\ldots\ldots\ldots \quad (15)$$

$$\sigma_z = 0 \quad \ldots\ldots\ldots\ldots\ldots\ldots \quad (16)$$

Where it is shown that:

$$K = \frac{\sigma_y R^2}{2 b^2} \quad \ldots\ldots\ldots\ldots\ldots\ldots\ldots\ldots \quad (17)$$

At R = b, assuming $\sigma_z = 0$ and incorporating the experimentally determined proportionality factor of 1.08 for the 100 percent overstrain condition

$$1.08\ \sigma_{te} = \sigma_y$$

or

$$2.16\ K = \sigma_y \quad \ldots\ldots\ldots\ldots\ldots\ldots\ldots \quad (18)$$

By definition the 100 percent overstrain condition is:

$$\delta_{tbe}\ E = \sigma_y \quad \ldots\ldots\ldots\ldots\ldots\ldots\ldots \quad (19)$$

Substituting equations (18) and (19) into (18) and solving for R yields

$$R^2 = \frac{\delta_{tbe}\ E\ b^2}{1.08\ \sigma_y} \quad \ldots\ldots\ldots\ldots\ldots\ldots\ldots \quad (20)$$

From equation (23) of Appendix I and again incorporating experimental results for the constant, the pressure to produce plastic flow to a depth R is

$$P_R = 1.08\ \sigma_y \log \frac{R}{a} + 1.08\ \sigma_y\ \frac{b^2 - R^2}{2 b^2} \quad \ldots\ldots\ldots \quad (21)$$

Substituting equation (20) into (21) yields

$$P = \frac{1.08\ \sigma_y}{2} \left[\log \frac{\delta_{tbe}\ E\ W\ 2}{1.08\ \sigma_y} + 1 - \frac{\delta_{tbe}\ E}{1.08\ \sigma_y} \right] \quad (22)$$

converting equation (22) into terms of pressure factor and strain factor yields the following theoretical relationship for the pressure factor-strain factor curve.

$$P.F = .54\left[1 - \frac{S.F.}{1.08} + \log \frac{S.F.W^2}{1.08}\right] \quad \ldots\ldots\ldots\ldots \quad (23)$$

As can be seen in Figure 16, good agreement is obtained between this theoretical relationship and the experimental data.

From the inherent inhomogeneity of material, as exemplified by deformation bands, Luaders' lines, and minor variations in basic yield strength throughout the specimen, there will be some deviations in the measurement of the overstrain condition, i.e., one point of the specimen may be overstrained before another. The spread in overstrain data with respect to pressure, however, is not great and the average can be considered valid for design purposes.

D - Permanent Enlargement Ratio

Since it is much more economical and advantageous to autofrettage gun tubes in or near the final configuration, that is, with diameter ratios varying from 1.3 - 1.5 at the muzzle to 1.9 - 2.2 at the breech end, it is necessary to use some form of restraining containers. The internal diameter of these containers is designed to yield a given amount of deformation in the contained tube section. In the design of the tube and containers to obtain optimum autofrettage effect with minimal permanent bore enlargement, it is necessary to know the relationship between the permanent bore

and outside diameter enlargement.

Permanent enlargement ratio (P.E.R.) is defined as the ratio of the permanent enlargement of the bore to that of the outside diameter. From the data it appears that this ratio is independent of the amount of permanent enlargement for diameter ratios not exceeding 2.2. Therefore all data for a specific diameter ratio was averaged and plotted as a function of diameter ratio as shown in Figure 17.

Also shown in Figure 17 is a plot of a theoretical relationship for permanent enlargement ratio which is developed as follows assuming that:

1. The only volume changes in the plastic region are elastic.
2. The longitudinal strain is uniform throughout the cross section.
3. $\sigma_z = 0$

From Hookes law

$$\delta_t + \delta_r + \delta_z = \frac{(1-2\nu)}{E} (\sigma_t + \sigma_r + \sigma_z) \quad \ldots\ldots\ldots \quad (24)$$

Substituting equations (20), (21) and (22) of Appendix I into (24) and defining δ_t and δ_r in terms of u yields:

$$\frac{du}{dr} + \frac{u}{r} = \frac{\sigma_y}{E} \left[(1-2\nu) \left(2 \log \frac{r}{R} + \frac{R^2}{b^2}\right) + \frac{\nu R^2}{b^2} \right] \quad \ldots\ldots\ldots \quad (25)$$

Solving equation (25) for u using the continuity of displacement across R as shown in equation (19) of Appendix I results in the following relationship for radial displacement under internal pressure:

$$u = \frac{\sigma}{E}\left[r(1-2\nu)\left(\log\frac{r}{R} - \frac{1}{2}\right) + \frac{R^2 r}{2b^2}(1-\nu) + \frac{R^2}{2r}(2-\nu)\right] \quad . . \quad (26)$$

For the 100 percent overstrain condition, i.e., R = b, the enlargement ratio under internal pressure is from equation (26):

$$\left(\frac{u_a}{u_b}\right)_{P_o} = \left(1 - \frac{\nu}{2}\right)W - (1-2\nu)\left(\frac{\log W}{W} + \frac{\nu}{2W}\right) \quad . . . . . \quad (27)$$

The permanent enlargement ratio is determined by subtracting the elastic recovery at the bore and outside surfaces as determined from equation (11) of Appendix I from the displacement at pressure. Assuming $\nu = 0.3$ and the 100 percent overstrain condition where $P_o = \sigma_y \log W$, yields for the permanent enlargement ratio:

$$PER = \frac{.85W^2 - .4\log W + .15 - (.7 + 1.3W^2)\left(\frac{\log W}{W^2 - 1}\right)}{W - 2W\left(\frac{\log W}{W^2 - 1}\right)} \quad . . \quad (28)$$

This reduces to:

$$PER = .85W + \frac{.15}{W} \quad . . . . . \quad (29)$$

It can be shown that the above relationship for permanent enlargement ratio is valid for cases of less than 100 percent overstrain by simply determining the radial displacement as a function of the elastic-plastic interface radius, and subtracting the elastic recovery in much the same manner as in equation (28).

It is interesting to note that the same permanent enlargement ratio relationship can be developed from the basic assumption of no net volume change as a result of overstrain.

As can be seen in Figure 17, the experimental values for permanent enlargement ratio tend to coincide closely with the theoretical. It is interesting to note, that in those cases where 100 percent overstrain did not occur, the values for permanent enlargement ratio did not differ from those for 100 percent overstrain. This tends to substantiate the use of the theoretical relationship for overstrains of less than 100 percent.

Although the experimental data for Figure 17 were averaged for each diameter ratio, a very slight decrease in permanent enlargement ratio was noticed at permanent enlargements greater than 1.8 percent in the 2.4 diameter ratio. This phenomenon, although small, is assumed due to reverse yielding that is expected at 100 percent overstrain in diameter ratios greater than approximately 2.0.

E - Permanent Bore Enlargement

As shown in Figure 18 which is an engineering stress-strain curve for the material used in this program the margin between the defined yield and the ultimate tensile strength is extremely small. In the case of a thick-walled cylinder of this material then, the difference between the 100 percent overstrain pressure, and the ultimate or rupture pressure is also extremely small as can be noted from Figure 16 for various diameter ratios. In light of this small pressure increment between the 100 percent overstrain and rupture condition in the diameter ratios considered, it is necessary to know accurately how much permanent enlargement is required to attain the optimum amount of overstrain. It is also extremely important to utilize the smallest amount of plastic deformation necessary to attain 100 percent autofrettage in order to minimize possible impairment of the low temperature toughness properties of gun tubes.

In the diameter ratios considered in this program, it was verified, from both the pressure-strain and residual stress analysis data, that optimum or 100 percent autofrettage was essentially attained by 100 percent overstrain, which agrees with theory. As previously discussed, it may not be completely necessary to reach 100 percent overstrain in the 2.4 diameter ratio. However, since a small amount of reverse yielding is not considered harmful, 100 percent overstrain was considered optimum. This was considered so since the difference in permanent bore enlargement between the minimum amount of overstrain to get 100 percent autofrettage and 100 percent overstrain was small, and actually

within the allowable error on a full scale tube.

Figure 19 shows a plot of percent permanent bore enlargement to produce 100 percent overstrain. The experimental points were determined in the manner shown in Figure 20 by plotting the value of outside diameter strain (δ_b) versus the percent bore enlargement obtained. The percent bore enlargement that was required to produce 100 percent overstrain is determined for each diameter ratio by the intersection of the horizontal line for $\delta_{bo} = \frac{\sigma_Y}{E}$.

Also shown in Figure 19 is a curve showing theoretical values of percent bore enlargement to produce 100 percent overstrain. The theoretical relationship plotted is derived by substituting R = b and r = a into equation (26). The radial displacement of the bore at 100 overstrain is:

$$u_{a_o} = \frac{a\sigma_Y}{E}\left[\left(1 - \frac{\nu}{2}\right)W^2 - (1 - 2\nu)\log W + \frac{\nu}{2}\right] \quad \ldots\ldots (30)$$

The elastic recovery at the bore from equation (11) of Appendix I assuming $P_o = \sigma_Y \log W$ is:

$$u_{a_e} = \frac{a\sigma_Y}{E}\frac{\log W}{(W^2 - 1)}\left[(1+\nu)W^2 + (1-\nu)\right] \quad \ldots\ldots\ldots (31)$$

Subtracting equation (31) from (30) yields:

$$u_{a_p} = \frac{a\sigma_y}{E}\left[\left(1 - \frac{\nu}{2}\right)W^2 - (1 - 2\nu)\log W + \frac{1}{2} - \frac{\log W}{W^2 - 1}\left((1+\nu)\ W^2 + (1-\nu)\right)\right] \quad \ldots\ldots\ldots \quad (32)$$

For $\nu = 0.3$

$$\%\ \text{PSE} = \frac{\sigma_y}{E}\left[(.85\ W^2 + .15)\right]\left[1 - \frac{2\log W}{W^2 - 1}\right] \times 100 \quad \ldots \quad (33)$$

As can be seen in Figure 19, the experimental values correlate very well with, and substantiate the theoretical values.

F - Residual Stresses

Utilizing the stress analysis technique proposed by Sachs, the residual stress patterns induced were analyzed and compared with theory. The physical setup for this technique is shown in Figure 21.

Figure 4 shows a typical analysis for a 100 percent over-strained 2.0 diameter ratio cylinder. Also shown are the theoretical residual stress distributions based on the Tresca yield criterion. The theoretical relationship for these residual stresses based on the Tresca yield criterion are, as shown in Appendix I,

$$\sigma_{tr} = \sigma_y \left[1 - \log \frac{b}{r} - \frac{\log W}{W^2 - 1} \left(1 + \frac{b^2}{r^2} \right) \right] \quad \ldots\ldots\ldots \quad (34)$$

$$\sigma_{rr} = \sigma_y \left[- \log \frac{b}{r} - \frac{\log W}{W^2 - 1} \left(1 - \frac{b^2}{r^2} \right) \right] \quad \ldots\ldots\ldots \quad (35)$$

$$\sigma_{zr} = 0 \quad \ldots\ldots\ldots\ldots\ldots\ldots\ldots\ldots \quad (36)$$

As can be seen in Figure 4, good correlation is obtained between the theoretical and experimental results.

In the residual stress analysis, and as shown in Figure 4, a substantial longitudinal residual stress has been found. This longitudinal residual stress has been assumed by most investigators to be small and is usually neglected. It is of interest to note, however, that it does exist, and that it may be of sufficient magnitude to be considered. Although a more complete analysis of the longitudinal as well as the entire residual stress picture will be summarized in a future paper, data gathered to date indicates that it does vary with the amount of overstrain.

Closely associated with the "boring out" technique for the analysis of residual stresses is the effect of machining on the

autofrettage pressure and the residual stress distribution and magnitude. This is an important consideration since gun tubes are finished reamed and rifled after autofrettage.

Preliminary experimentation associated with the evaluation of the effects of machining after autofrettage have shown an unexplained deviation from theory. One such case consisted of a 2.2 diameter ratio specimen which was 100 percent overstrained and then bored out to a 1.8 ratio and repressurized. It would be expected that the resultant autofrettage pressure of the machined specimen would be equal to that for a fully overstrained non-machined specimen of equal diameter ratio. As shown in Figure 22, however, which is the pressure factor - outside surface strain factor curve for the reapplication of pressure, the autofrettage pressure for the machined 1.8 diameter ratio cylinder lies significantly above that for the non-machined. Also it should be noted that even though the autofrettage pressure was exceeded in the machined specimen, there is a decided decrease in non-linearity or hysteresis loop effect occurring without thermal treatment. This would be expected however since the more highly plastically deformed material was removed during boring. Although more work is planned

in this area in order to more fully understand this deviation from theory, it can be considered that the effect of machining is at least no greater and possibly less than anticipated from the diameter ratio decrease.

G - Reverse Yielding

As was previously stated, when the magnitude of the tangential residual stress exceeds the yield strength of the material, i.e. where $\sigma_{tr} = \sigma_y$ assuming $\sigma_{zr} = 0$, the cylinder will reverse yield, causing a redistribution of the residual stresses. By equating equation 34 to σ_y it can be shown based on the Tresca yield criterion that this condition will occur at 100 percent overstrain in cylinders of diameter ratios greater than approximately 2.22.

The maximum theoretical ratio of the autofrettage to initial elastic breakdown pressure can be determined by considering the condition for reyielding, at the bore, of an autofrettaged cylinder. Based on the Tresca yield criteria reyielding will occur when:

$$\sigma_y = (\sigma_t + \sigma_{tr}) - \sigma_r \quad \ldots\ldots\ldots\ldots\ldots\ldots \quad (37)$$

From this the 100 percent autofrettage pressure, assuming that

$\sigma_z = \sigma_{zr} = \sigma_{rr} = 0$ and $\sigma_{tr} = -\sigma_y$ is

$$P = \sigma_y \frac{W^2 - 1}{W^2} \quad \ldots\ldots\ldots\ldots\ldots\ldots \quad (38)$$

Comparing this to equation (10), it can be seen that the maximum autofrettage pressure is twice the initial elastic breakdown pressure and that this ratio is independent of diameter ratio.

Based on the Von Mises Yield Criterion the reyielding condition is defined by:

$$2\sigma_y^2 = \left[(\sigma_t + \sigma_{tr}) - \sigma_r\right]^2 + \sigma_r^2 + (\sigma_t + \sigma_{tr})^2 \quad \ldots \quad (39)$$

and making the same assumptions as in the case of equation (38) the 100 percent autofrettage pressure is:

$$P = \sigma_y \frac{3W^4 - 2W^2 - 1}{3W^4 \quad 1} \quad \ldots\ldots\ldots\ldots\ldots\ldots \quad (40)$$

Comparing equation (40) with equation (9), shows that the maximum attainable autofrettage pressure is 1.85 times the initial elastic breakdown pressure. It should be noted however, that this ratio is a maximum at a diameter ratio of 2.03 and decreases slightly as the diameter ratio increases as shown in Figure 23.

In order to evaluate the occurrence of reverse yielding in the upper end of the diameter ratio range investigated, s veral 100

cent overstrained specimens were thermal treated at 500° F for five hours and re-pressurized. Shown in Figure 24 are the internal pressure factor - outside surface strain factor curves for 2.2 and 2.4 diameter ratio specimens re-cycled to the initial 100 percent overstrain pressure. The larger amount of non-linearity in the upper portion of the 2.4 diameter ratio curve as compared to that for the 2.2 shown in the same figure and the 2.0 diameter ratio shown in Figure 26, indicates that some reverse yielding probably has occurred in the 2.4 specimens. The comparitively small amount of non-linearity in the 2.0 and 2.2 diameter ratios is considered due primarily to remaining hysteresis. Although it is extremely difficult to differentiate between non-linearity due to hysteresis and that associated with reverse yielding, it is indicated that the critical diameter ratio for reverse yielding may be closer to that predicted by the Tresca than the Von Mises yield criteria. A more thorough analysis of reverse yielding in intermediate diameter ratios will be included in a future report.

H - Hysteresis Loop Effect

Even in cylinders with a diameter ratio of equal to, or less than, the critical value above which reverse yielding occurs, a form of non-linearity is exhibited upon the re-application of the 100 percent overstrain pressure as shown in Figure 25 which is for a typical 2.0 diameter ratio specimen. From the figure, it can be seen that the effective limit of linearity on the continued

re-application of internal pressure equal to the initial overstrain pressure, that the hysteresis loop effect gradually diminishes with a resultant increase in the range of linearity and decreased permanent strain. In the case shown, this effect is significantly diminished by 7 reapplications of the 100 percent overstrain pressure.

Considering the great attrition of equipment when subjected to the overstrain pressures involved and potential progressive stress damage aspects of recycling, a more suitable technique for the elimination of the hysteresis loop effect should be considered. Based on prior investigations, it has long been the practice to thermal treat autofrettaged thick-wall cylinders at 500 - 600° F in order to eliminate this phenomenon. Throughout this investigation then, all cylinders were subjected to a low temperature stabilization treatment consisting of 500° F for five hours. In comparing Figure 25 to Figure 26 however, it is noted that the beneficial effects of this treatment in removing nonlinearity and the associated hysteresis loop are marginal if at all existant. Whether more beneficial affects may be obtained at other temperatures, along with the potential gains to be realized by strain aging phenomenon is the subject of another current experimental program.

I - Longitudinal Shrinkage

The external profile of a gun tube prior to autofrettage along with the internal profile of the restraining containers closely approaches that of the finished tube. It is necessary, therefore, to consider the longitudinal shrinkage occurring during autofrettage in order to obtain the desired amount of permanent bore enlargement in a configuration having one or several tapers.

The longitudinal shrinkage was measured as the total specimen shrinkage. There is, however, a short distance, usually less than .75 inches behind the specimen seal that is not strained the same as the midsection. Based on the data obtained by measuring the unit longitudinal strain with SR-4 gages, utilizing the total longitudinal shrinkage divided by the specimen length between the seals did not introduce a serious error.

Figure 27 shows the permanent longitudinal strain divided by the percent permanent bore enlargement as a function of diameter ratio. There was no systematic variation in longitudinal strain as a function of percent permanent bore enlargement in the diameter ratio range investigated so all data were averaged for a given diameter ratio.

Also shown in Figure 27 is a theoretical longitudinal unit strain curve as a function of diameter ratio which is developed as follows assuming that:

A. During expansion, at $r = b$

$$\sigma_z = \sigma_r = 0$$

B. All perpendicular planes remain perpendicular during deformation.

From the assumptions, at $r = b$

$$\delta_z = \nu \delta_{bp} \quad \ldots\ldots\ldots\ldots\ldots\ldots\ldots\ldots \quad (41)$$

and from equation (29) for permanent enlargement ratio

$$\delta_z = \frac{\nu \delta_{ap}}{.85 W^2 + .15} \quad \ldots\ldots\ldots\ldots\ldots\ldots \quad (42)$$

where

$$\delta_{ap} = \frac{\%\ \text{P.B.E.}}{100} \quad \ldots\ldots\ldots\ldots\ldots\ldots\ldots \quad (43)$$

Assuming $\nu = 0.3$ then

$$\frac{\delta_z}{\%\ \text{P.B.E.}} = \frac{1}{283 W^2 + 50} \quad \ldots\ldots\ldots\ldots\ldots \quad (44)$$

As can be noted, there is poor correlation between the theoretical and experimental results. The experimental data are satisfied by the following empirical relationship:

$$\frac{\delta_z}{\%\ \text{P.B.E.}} = \frac{1}{700 W^2 - 825} \quad \ldots\ldots\ldots\ldots\ldots \quad (45)$$

J - Strain Stabilization

The "stabilization" time allowed for the reading of the strain associated with a given pressure during testing was held to approximately 30 seconds in order to more closely duplicate the conditions encountered in the full-scale autofrettage process. In order to determine, however, how much the results of this testing procedure deviated from that for a true strain stabilized condition a series of tests were performed with the pressure being held at a given level until the strain attained an equilibrium value. Figure 28 shows a comparison of the internal pressure factor - outside surface strain factor curve for the strain "stabilized" condition as compared to the type encountered during normal testing practice. The change in strain with time at several internal pressure levels in a 2.0 diameter ratio specimen is shown in Figure 29. Although there is a significant change in strain with time, particularly as the pressure level approaches the 100 percent overstrain condition, it has little effect on the internal pressure outside surface strain results. The testing procedure then not only duplicates the full-scale autofrettage practice, but introduces only negligible experimental error as compared to the "stabilized" condition.

Also as a matter of interest, the specimens utilized for the study of the strain-time effect were re-cycled to the initial

overstrain pressure several times, with the pressure again being held at each point until the strain no longer changed. The type of internal pressure versus outside surface strain results obtained compared closely with that for a specimen re-cycled under normal testing practice. Although to be a subject taken up in a later report, it is indicated that the longer holding time at pressure has little effect on the magnitude of the hysteresis loop phenomenon in the steel and strength level investigated.

K - Full Size Gun Tubes

The data and design criteria developed in the miniature specimen program was complimented by its application to full size gun tubes. In the autofrettage of a series of four 90mm and subsequently a number of larger caliber gun tubes utilizing the experimental data for the design of the tube and containers, excellent correlation was obtained between the predicted and actual results. In all cases the empirical overstrain pressure to attain 100 percent overstrain correlated very well with the experimental data. The 100 percent overstrain condition in the full size tube was determined by using linear differential transformers inserted through the containers and bearing on the tube during deformation. The longitudinal shrinkage experimental data was also substantiated by these full scale applications.

There was a slightly lower permanent bore enlargement noted on the full size tube than as predicted by the data. This was

attributed to the yield strength variation normally found throughout a section as large and as long as a gun tube. In order to accommodate this yield strength variation 25 percent greater permanent bore enlargement than the predicted amount required to produce 100 percent overstrain is utilized in practice for tube and container design. This value, is not great enough to seriously effect the low temperature toughness properties, but large enough to insure 100 percent overstrain throughout the tube regardless of strength variations.

The four experimental 90mm tubes as schematically compared to the 90mm M41 in Figure 30 had a yield strength range of 171 - 180,000 pounds per square inch. Two tubes were designed with a design factor based on the data of 2.0 and the remaining two on 1.55. These factors yielded tube weights of 850 and 640 pounds respectively as compared to the 1580 pounds for the current 90mm M41 non-autofrettaged tube. This safety factor however may be somewhat misleading since it includes the conversion from copper to true pressure (approximately 1.2) and an allowance for the 115 percent overpressure rounds encountered during service and proof testing. The true factor of safety then, based on the developed design criteria was 1.45 and 1.12 respectively.

In the service testing of the four tubes, no permanent bore enlargement was noted, even as a result of the 115 percent over pressure rounds, and with the outside diameter of the tube being

at 500° F over a substantial portion of the test.

The accuracy of the tubes, which could be effected by the greater bore dilation and "whip" due to the thinner walls, was comparable to that for the current 90mm M41 gun. The erosion, or wear rate, which could also be effected by the greater bore dilation was not greater than, and in fact, was somewhat less than that expected in a comparable, thick-wall non-chromium plated tube.

V - CONCLUSIONS

Based on the miniature specimen study, and the successful autofrettage and service testing of a series of 90mm gun tubes, the autofrettage principle and process as described, represents a feasible means of increasing the elastic breakdown pressure of intermediate diameter ratio cylinders at the yield strength level of 165,000 pounds per square inch while maintaining design safety factor as small as 1.12. Utilizing the design data and criteria presented, and the open-end autofrettage process described, it is possible to design and manufacture high strength gun tubes featuring weight reductions of up to 60 percent or increased allowable chamber pressures of as great as 100 percent as compared to non-autofrettaged mono-block construction of the same basic strength level.

More work is currently under way in such fields as the progressive stress damage aspects of highly stressed autofrettaged cylinders at ambient and elevated temperatures, the effects of temperature from the standpoint of eliminating the hysteresis loop effect and stress relaxation, machining effects, reverse yielding phenomenon, the residual stress distributions characteristic of various autofrettage techniques, and the application of autofrettage to materials of over 200,000 pounds per square inch yield strength. However, from this study the following points concerning the application of autofrettage to materials of nominal 165,000 pounds per square inch yield strength have been established.

1. The experimentally determined initial elastic breakdown pressure over the range of diameter ratios investigated correlates more closely with that predicted by the Von Mises than the Tresca yield criteria.

2. The constant K in the relationship for the 100 percent overstrain pressure as a function of diameter ratio and yield strength, i.e., $P = K\sigma_y \log W$, was determined to be 1.08 as compared to 1.0 as predicted from the Tresca yield criterion.

3. The internal pressure - outside surface strain data for the diameter ratio range investigated can be predicted by an empirical relationship.

4. The experimentally determined permanent enlargement ratio for the 100 percent overstrained condition as a function of diameter ratio correlates well with that theoretically developed which is based on the assumption of uniform longitudinal strain throughout the cross section.

5. The permanent enlargement ratio is independent of the magnitude of overstrain in diameter ratios less than 2.2.

6. The experimentally determined permanent bore enlargement to obtain 100 percent overstrain substantiates that theoretically predicted if a Poisson's ratio of 0.3 is assumed.

7. The determined residual stress distribution correlates closely with that predicted by the Tresca yield criterion.

8. A substantial longitudinal residual stress exists and has shown to vary with the magnitude of overstrain.

9. Preliminary experimentation has shown that the damaging effects of machining after autofrettage are no greater, and possibly less, than would be predicted from the change in diameter ratio.

10. Reverse yielding was noted in the 100 percent overstrained 2.4 diameter ratio but was found to be insignificant in the 2.2 ratio which tends to substantiate that predicted from the Tresca yield criterion.

11. The maximum theoretical ratio of autofrettage to initial elastic breakdown pressure based on the Tresca yield criterion is a constant that is independent of diameter ratio above a diameter ratio of 2.2. Based on the Von Mises yield criterion, the ratio decreases above a critical diameter ratio of approximately 2.0.

12. The non-linearity associated with the hysteresis loop effect can be significantly decreased by a small number of re-applications of pressure up to the original overstrain pressure. The thermal treatment consisting of 500° F for five hours does not significantly reduce the hysteresis loop effect in the strength level investigated.

13. A large discrepancy between the experimental results and that theoretically predicted was noted in the case of the magnitude of the longitudinal strain as a function of percent permanent bore enlargement and diameter ratio. The empirical relationship based on the experimental results should be used for design purposes.

14. The magnitude of the permanent longitudinal strain does not vary with the magnitude of the overstrain in the ranges investigated.

15. The empirical data developed on miniature specimens is valid for full size gun tube applications.

16. No permanent bore enlargement was noted during service testing of autofrettaged full size gun tubes designed with a safety

factor of 1.12 even when the outside surface temperatures during firing approached 500° F. The accuracy and wear rates were comparable to non-autofrettaged thick-wall tubes of the same caliber and initial bore condition.

ACKNOWLEDGMENTS

Appreciation is expressed to R. A. Petell, High Pressure Laboratory Supervisor, and to G. E. Sogoian, S. J. Ball, P. J. Biocitelli, R. Young, C. W. Nelson, E. Nazarian and G. T. Langlois, Technicians, whose extreme care and accuracy in the test phase made this investigation possible, and to D. H. Newhall for his encouragement, suggestions and advice. Appreciation is also expressed to Col. E. S. Mathews, U. S. Army (Ret.) whose foresight and encouragement were instrumental in the initiation of this program.

BIBLIOGRAPHY

1. Davidson, T. E., Barton, C. S., Reiner, A. N. and Kendall, D. P. "A New Approach to the Autofrettage of High Strength Gun Tubes." Watervliet Arsenal, April 1959

2. Drucker, D. C. "The Significance of the Criterion for Additional Plastic Deformation of Metals." J. of Colloid Science. 4. p. 299-311. 1949.

3. Drucker, D. C. Greenberg, H. J. and Prager, W. "The Safety Factor of an Elastic-Plastic Body in Plane Strain." J. of Applied Mechanics. December, 1951. p. 371-378.

4. Drucker, D. C. and Stockton, F. D. "Instrumentation and Fundamental Experiments in Plasticity." November, 1951. Proceedings of the Society for Experimental Stress Analysis. X, no. 2, p. 127-142.

5. Faupel, J. H. "Residual Stresses in Heavy Wall Cylinders." J. of the Franklin Institute. May 1955. p. 409-419.

6. Faupel, J. H. "Some Considerations of the Mechanics and Design Limitations of Autofrettage." (Unpublished)

7. Faupel, J. H. and Furbeck, A. R. "Influence of Residual Stress on Behavior of Thick-Wall Closed-End Cylinders." Transactions of the ASME. 75, no. 3. April 1953. p. 345-354.

8. Gentil, L. "On the Principles of Cold Working." Memorial de L'Artillerie Francaise, Vol. XV, No. 2, 1936, p. 313-345 (Translation by F. M. O'Halloran, Watertown Arsenal Report No. 662/10)

9. Hill, R., Lee, E. H. and Tupper, S. J. "The Theory of Combined Plastic and Elastic Deformation with Particular Reference to a Thick Tube under Internal Pressure." 1947 Proceedings of the Royal Soc. of London. A. 191. p. 278-303.

10. Koiter, W. T. "On Partially Plastic Thick-Walled Tubes." "C. B. Biezeno Anniversary Volume on Applied Mechanics." N. V. de Technische Uitgeverij, H., Stam. Haarlem, 1953.

BIBLIOGRAPHY
(Cont.)

11. Langenberg, F. C. "Effect of Cold Working on the Strength of Hollow Cylinders." Trans. of the American Society for Steel Treating, Vol. 8, No. 4, October 1925.

12. Leto, J. and Newhall, D. H. "Cold Working of Guns." Watertown Arsenal Memorandum Report No. 662/21, October 1941.

13. Mac Gregor, C. W., Coffin, L. F., Jr., and Fisher, J. C. "Partially Plastic Thick-Walled Tubes." J. of the Franklin Institute. February 1948. p. 135-158.

14. Mickevics, E. J. "Experimental Stress Analysis in Super-pressure Design." Industrial and Engineering Chemistry. 48, No. 5. p.854-860.

15. Nadai, I. A. L. "Theory of Flow and Fracture of Solids." Vol. I, 2nd Ed. 1950 McGraw - Hill Inc.

16. Nadai, I. A. L. "The Flow of Metals under Various Stress Conditions." Proceedings of Institute of Mechanical Engineers. 157. p. 121-160. 1947

17. Newhall, D. H. "Selected Design Data Pertaining to Gun Tubes and High-Pressure Vessels." Watertown Arsenal Report No. WGD-4 December 1943

18. Newhall, D. H. "Plastic Strains in Thick Hollow Cylinders Overstrained by Internal Pressure." Watertown Arsenal Report No. WGD-7, January 1944

19. Prager, W. "Stress-Strain Laws of the Mathematical Theory of Plasticity Discussion." J. of Applied Mechanics. 70. p. 226-233. September 1948

20. de Saint-Venant. Sur l'intensite' des Forces Capables de De'former, avec Continuite, de Blocs Ductiles, Cylindriques, Pleins ou Evides, et Place's dans Diverses Circonstances. Comptes Rendus. April 1872. p. 1009-1016

BIBLIOGRAPHY
(Cont.)

21. Sopwith, D. G. and de G. Allen, D. N. "The Stresses and Strains in a Partially Plastic Thick Tube under Internal Pressure and End Load." Proceedings of the Royal Society London. Serial A. 205, 1951, p. 69-83

22. Steele, M. C. and Eichberger, L. C. "Nonhomogeneous Yielding of Steel Cylinders. 1-Mild Steel." Transactions of the ASME. October 1957. p. 1608-1618.

23. Steel, M. C. and Young, John. "An Experimental Investigation of Over-Straining in Mild-Steel Thick-Walled Cylinders by Internal Fluid Pressure." Transactions of the ASME. April 1952. p. 355-363

24. Timoshenko, S. "Strength of Materials, Part II." D. van Nostrand, Inc. 1942

25. Turner, L. B. "The Stresses in a Thick Hollow-Cylinder Subjected to Internal Pressure." Transactions of the Cambridge Philosophical Society XXI, No. XIV. p. 377-396

26. Voorhees, H. R., Sliepcevich, C. M., and Freeman, J. W. "Thick-Walled Pressure Vessels." Industrial and Engineering Chemistry. 48, No. 5. p. 872-881

27. Warren, A. G. "Autofrettage." Symposium on Internal Stresses in Metals and Alloys. 1947. Institute of Metals. p. 209-218.

28. Weiss, V. "Residual Stresses in Cylinders." Syracuse University Research Inst. Report No. MET 345-563T2 Watertown Arsenal Contract No. DAI-30-115-505-ORD-P-613

APPENDIX I

SUMMARY OF THEORY FOR THICK-WALL CYLINDERS SUBJECTED TO INTERNAL PRESSURE

The following summary of the elastic-plastic theory for open end thick-wall cylinders subjected to internal pressure will be divided into the different stages of deformation occurring upon the application of pressure. Also considered will be the variations occurring from the use of the Tresca and Von Mises yield criteria.

I - Elastic Case

By applying the condition of equilibrium to the forces in the radial direction on the element illustrated, the following general differential equation is obtained:

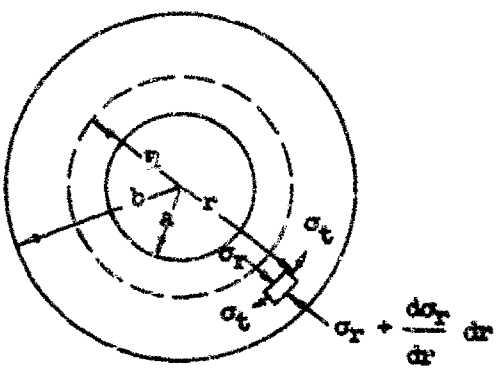

$$\sigma_t - \sigma_r - r\frac{d\sigma_r}{dr} = 0 \quad \ldots\ldots\ldots\ldots\ldots\ldots\ldots\ldots (1)$$

Utilizing the strain - displacement relations and Hookes law, assuming $\sigma_z = 0$, σ_t and σ_r are:

$$\sigma_t = \frac{E}{1-\nu^2}\left[\frac{u}{r} + \nu\frac{du}{dr}\right] \quad \ldots\ldots\ldots\ldots\ldots\ldots\ldots\ldots (2)$$

APPENDIX I

SUMMARY OF THEORY FOR THICK-WALL CYLINDERS SUBJECTED TO INTERNAL PRESSURE

The following summary of the elastic-plastic theory for open end thick-wall cylinders subjected to internal pressure will be divided into the different stages of deformation occurring upon the application of pressure. Also considered will be the variations occurring from the use of the Tresca and Von Mises yield criteria.

I - Elastic Case

By applying the condition of equilibrium to the forces in the radial direction on the element illustrated, the following general differential equation is obtained:

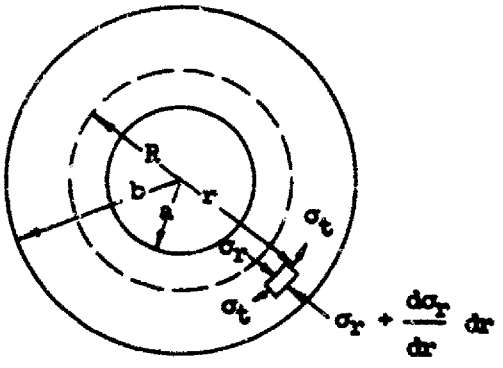

$$\sigma_t - \sigma_r - r\frac{d\sigma_r}{dr} = 0 \quad \ldots\ldots\ldots\ldots\ldots\ldots\ldots\ldots (1)$$

Utilizing the strain - displacement relations and Hookes law, assuming $\sigma_z = 0$, σ_t and σ_r are:

$$\sigma_t = \frac{E}{1-\nu^2}\left[\frac{u}{r} + \nu\frac{du}{dr}\right] \quad \ldots\ldots\ldots\ldots\ldots\ldots\ldots (2)$$

and

$$\sigma_r = \frac{E}{1-\nu^2}\left[\frac{du}{dr} + \nu\frac{u}{r}\right] \quad \ldots\ldots\ldots\ldots\ldots\ldots\ldots (3)$$

where

$$\delta_\theta = \frac{u}{r} \text{ and } \delta_r = \frac{du}{dr}$$

Substituting equations 2 and 3 into equation 1 yields a 2nd order differential equation which has the general solution:

$$u = C_1 r + \frac{C_2}{r} \quad \ldots\ldots\ldots\ldots\ldots\ldots (4)$$

placing equation 4 into equations 2 and 3 and using the boundary conditions

$$\sigma_{re} = -P$$

and

$$\sigma_{rb} = 0$$

yields the following well known equations for tangential and radial stresses for the internal pressure case:

$$\sigma_t = \frac{P}{R^2-1}\left(1+\frac{b^2}{r^2}\right) \quad \ldots\ldots\ldots\ldots\ldots (5)$$

$$\sigma_r = \frac{P}{R^2-1}\left(1-\frac{b^2}{r^2}\right) \quad \ldots\ldots\ldots\ldots\ldots (6)$$

$$\sigma_z = 0 \quad \ldots\ldots\ldots\ldots\ldots\ldots (7)$$

The maximum value of σ_t which is at r = a is

$$\sigma_{ta} = P\frac{W^2+1}{W^2-1} \quad \ldots\ldots\ldots\ldots\ldots\ldots\ldots\ldots \quad (8)$$

The minimum value of σ_t is at the outer surface where

$$\sigma_{tb} = \frac{2P}{W^2-1} \quad \ldots\ldots\ldots\ldots\ldots\ldots\ldots\ldots \quad (9)$$

The ratio $\frac{\sigma_{ta}}{\sigma_{tb}}$ approaches 1 as W approaches 1 which is the case for thin-wall cylinders.

The sum of the tangential and radial stresses is constant through the wall thickness. Hence they produce a uniform contraction in the direction of the axis of the cylinder, and planes perpendicular to the axis remain perpendicular. It is therefore justifiable to consider the cylinder as being in a state of plane stress, i.e., $\sigma_z = 0$.

Since

$$\sigma_t + \sigma_r = \frac{2P}{W^2-1}$$

then from Hookes' law, the longitudinal strain is

$$\epsilon_{ze} = -\frac{2\nu P}{E(W^2-1)} \quad \ldots\ldots\ldots\ldots\ldots\ldots\ldots \quad (10)$$

From equation (4), the radial displacement of any point in the wall becomes

$$u_a = \frac{P}{xE(k^2-1)} \left[(1-\nu)b^2 + (1-\nu)r^2\right] \quad \ldots\ldots\ldots\ldots \quad (11)$$

II - Elastic Breakdown

As the internal pressure is increased the elastic limit of the material is exceeded and the metal begins to yield at the bore. Utilising the Tresca criterion of yielding, i.e.

$$\sigma_t - \sigma_r = \sigma_y \quad \ldots\ldots\ldots\ldots\ldots\ldots\ldots\ldots \quad (12)$$

and substituting equations (5) and (6) into (12) for r = a where $\sigma_t - \sigma_r$ is the largest, then elastic breakdown begins on the internal surface at a pressure of

$$P_y = \sigma_y \frac{(k^2-1)}{2k^2} \quad \ldots\ldots\ldots\ldots\ldots\ldots\ldots \quad (13)$$

This pressure is the same for all end conditions.

If the Von Mises criterion of yielding is utilised as follows,

$$(\sigma_t-\sigma_r)^2 + (\sigma_r-\sigma_z)^2 + (\sigma_z-\sigma_t)^2 = 2\sigma_y^2 \quad \ldots\ldots\ldots \quad (14)$$

then substituting equations (5), (6) and (7) into (14) yields for the open end case,

$$P_y = \sigma_y \frac{k^2-1}{\sqrt{3k^4+1}} \quad \ldots\ldots\ldots\ldots\ldots\ldots \quad (15)$$

III - Partially Plastic Conditions

When the internal pressure exceeds the elastic breakdown pressure, the plastic region progresses towards the outside diameter. When the tube is partly plastic, the stresses in the elastic region are still of the form:

$$\sigma_{te} = K\left(\frac{b^2}{r^2} + 1\right)$$

and

$$\sigma_{re} = -K\left(\frac{b^2}{r^2} - 1\right)$$

Utilizing the Tresca criterion at r = R and solving for K yields

$$K = \frac{\sigma_y R^2}{2b^2}$$

The stresses in the elastic region from equations (5) and (6) for $R \leq r \leq b$ are:

$$\sigma_{te} = \frac{\sigma_y R^2}{2b^2}\left(\frac{b^2}{r^2} + 1\right) \quad \ldots\ldots\ldots\ldots\ldots\ldots\ldots (16)$$

$$\sigma_{re} = -\frac{\sigma_y R^2}{2b^2}\left(\frac{b^2}{r^2} - 1\right) \quad \ldots\ldots\ldots\ldots\ldots\ldots\ldots (17)$$

$$\sigma_{ze} = 0 \quad \ldots\ldots\ldots\ldots\ldots\ldots\ldots\ldots\ldots (18)$$

▼

Using Hookes' law and equations (16) and (17), the radial displacement in the elastic region is:

$$u_e = \frac{\sigma_y R^2}{2rEb^2}\left[(1+\nu)\,b^2 + (1-\nu)\,r^2\right] \quad \ldots\ldots\ldots \quad (19)$$

The longitudinal strain from equation (19) is

$$\delta_{ze} = -\frac{\nu\sigma_y R^2}{Eb^2} \quad \ldots\ldots\ldots\ldots\ldots\ldots\ldots \quad (20)$$

In the plastic region, the equation of equilibrium (1) combined with the Tresca yield criterion leads to

$$\sigma_{rp} = -\sigma_y \log\frac{R}{r} - \sigma_y\left(\frac{b^2-R^2}{2b^2}\right) \quad \ldots\ldots\ldots\ldots \quad (21)$$

$$\sigma_{tp} = -\sigma_y \log\frac{R}{r} + \sigma_y\left(\frac{b^2+R^2}{2b^2}\right) \quad \ldots\ldots\ldots\ldots \quad (22)$$

The internal pressure required to produce plastic flow up to the depth of r = R is from equation (21)

$$P_R = \sigma_y \log\frac{R}{a} + \sigma_y\left(\frac{b^2-R^2}{2b^2}\right) \quad \ldots\ldots\ldots\ldots\ldots \quad (23)$$

Equation (23) satisfies elastic breakdown at the bore and 100 percent overstrain which can be checked by letting R = a and R = b respectively.

Assuming that the only volume changes within the plastic region are elastic and that the longitudinal strain is uniform throughout

Using Hookes' law and equations (16) and (17), the radial displacement in the elastic region is:

$$u_e = \frac{\sigma_y R^2}{2rEb^2}\left[(1+\nu)\,b^2 + (1-\nu)\,r^2\right] \quad \ldots\ldots\ldots \quad (19)$$

The longitudinal strain from equation (19) is

$$\delta_{ze} = -\frac{\nu\sigma_y R^2}{Eb^2} \quad \ldots\ldots\ldots\ldots\ldots\ldots\ldots \quad (20)$$

In the plastic region, the equation of equilibrium (1) combined with the Tresca yield criterion leads to

$$\sigma_{rp} = -\sigma_y \log\frac{R}{r} - \sigma_y\left(\frac{b^2-R^2}{2b^2}\right) \quad \ldots\ldots\ldots\ldots \quad (21)$$

$$\sigma_{tp} = -\sigma_y \log\frac{R}{r} + \sigma_y\left(\frac{b^2+R^2}{2b^2}\right) \quad \ldots\ldots\ldots\ldots \quad (22)$$

The internal pressure required to produce plastic flow up to the depth of r = R is from equation (21)

$$P_R = \sigma_y \log\frac{R}{a} + \sigma_y\left(\frac{b^2-R^2}{2b^2}\right) \quad \ldots\ldots\ldots\ldots\ldots \quad (23)$$

Equation (23) satisfies elastic breakdown at the bore and 100 percent overstrain which can be checked by letting R = a and R = b respectively.

Assuming that the only volume changes within the plastic region are elastic and that the longitudinal strain is uniform throughout

the cross section, it has been shown that the radial displacement under internal overstrain pressure utilising the Tresca yield criterion is:

$$u_p = \frac{\sigma_Y}{E}\left[r\,(1-2\nu)\left(\log\frac{r}{R} - \frac{1}{2}\right) + \frac{R^2}{2b^2}\,(1-\nu) + \frac{R^2}{2r}\,(2-\nu)\right] \quad \ldots\ (24)$$

IV - Residual Stresses

The stresses which remain in the wall of the cylinder after bringing the material to a condition of yielding at least partly through the wall and then removing the internal pressure can be calculated based on the Tresca yield criterion and assuming that during unloading the material follows Hookes' law as follows:

$$\sigma(t,r)r = \sigma(t,r)\,\text{Pres.} - \sigma(t,r)\theta \quad \ldots\ (25)$$

For the elastic-plastic condition, from equations 16 and 17 the residual stresses in the elastic portion of the wall are:

$$\sigma_{tre} = \frac{\sigma_Y}{2}\left(1 + \frac{b^2}{r^2}\right)\left[\frac{R^2}{b^2} - \frac{a^2}{b^2-a^2}\left(\frac{b^2-R^2}{b^2} + 2\log\frac{R}{a}\right)\right] \quad \ldots\ (26)$$

$$\sigma_{rre} = \frac{\sigma_Y}{2}\left(1 - \frac{b^2}{r^2}\right)\left[\frac{R^2}{b^2} - \frac{a^2}{b^2-a^2}\left(\frac{b^2-R^2}{b^2} + 2\log\frac{R}{a}\right)\right] \quad \ldots\ (27)$$

and in the plastic portion,

$$\sigma_{\theta rp} = \frac{\sigma_y}{2}\left[\frac{b^2 + R^2}{b^2} + 2\log\frac{r}{R} - \frac{a^2}{b^2-a^2}\left(\frac{b^2-R^2}{b^2} + 2\log\frac{R}{a}\right)\left(1 + \frac{b^2}{r^2}\right)\right] \quad \ldots\ldots\ldots\ldots\ldots\ldots\ldots \quad (28)$$

$$\sigma_{rrp} = \frac{\sigma_y}{2}\left[\frac{R^2 - b^2}{b^2} + 2\log\frac{r}{R} - \frac{a^2}{b^2-a^2}\left(\frac{b^2-R^2}{b^2} + 2\log\frac{R}{a}\right)\left(1 - \frac{b^2}{r^2}\right)\right] \quad \ldots\ldots\ldots\ldots\ldots\ldots\ldots \quad (29)$$

APPENDIX II

AUTOFRETTAGE DESIGN PROCEDURE

The design of a gun tube or thick-wall cylinder utilising the autofrettage principle basically involves equating the desired operating pressure to the overstrain pressure in diameter ratios not exceeding approximately 2.2, and solving for the required diameter ratio in the following relationship.

(K) $P_f = (1.06)\ \sigma_y \log W$

K in this case is a factor of safety which, in light of the slight non-linearity exhibited in the diameter ratios and yield strength level investigated, has been preliminarily set at 1.2.

The design of a gun tube along with the associated restraining containers for the autofrettage process in order to obtain optimum results with the minimum amount of permanent bore enlargement is a more difficult problem and will be summarised in this appendix.

A - PROCESS CONSIDERATIONS

From experience and the physical arrangement utilised in the autofrettage of gun tubes, the following factors should be considered and incorporated into the basic design for autofrettage:

1 - Approximately .3 inches of material should be left on all diameters to facilitate the final machining operations. This

should be based on the tube configuration after autofrettage.

2 - The minimum taper to facilitate removal of the tube from the containers after autofrettage should be .005 inches/inch on the diameter, with a maximum of .020 inches/inch. Exceeding this maximum taper in anything but a very short section may introduce an excessive longitudinal component of the radial stresses between the outside tube surface and the container.

3 - A minimum length equal to the outside diameter and measured from the point of sealing should be discarded from each end of the tube. This is to eliminate the end effects caused by the sealing arrangement.

B - DESIGN PROCEDURE

The design for autofrettage by the open-end process utilizing containers can be divided into 3 basic parts consisting of that for the tube, containers and longitudinal shrinkage.

1 - Tube

The tube dimensions after autofrettage consist of that for the finished tube plus machining allowances. The design of the tube configuration for autofrettage then will be that required, including necessary tapers, to attain the predetermined dimensions after being overstrained. The determination of this initial configuration is accomplished by a trial and error technique as tabulated in Table II for one of the 90mm gun tubes shown in Figure 30. Each section of the tube must be considered separately.

In the initial trial, the final required dimensions are utilized to determine the amount of permanent bore enlargement resulting from the 100 percent overstrain condition. As an example, in tube Section 5, the required bore and outside diameters after autofrettage are 3.24 and 6.015 inches respectively. For this diameter ratio of 1.86, from Figure 19, it is seen that a permanent bore enlargement of 1.0 percent or .032 inches is required to attain 100 percent overstrain. Utilizing the permanent enlargement ratio for W = 1.86 from Figure 17, the change in outside diameter will be .019. These permanent diameter changes are subtracted from the original assumed or in this case final dimensions and the new diameters, adjusted slightly to simplify machining, utilized for the second trial. In the example shown, the second trial yielded satisfactory results. It should be noted that the required permanent bore enlargement to attain 100 percent overstrain is 1.25 times the experimental data in order to overcome material strength differences throughout the tube.

2 - Longitudinal Shrinkage

Since the outside diameter of the tube consists of one or several tapers, the longitudinal shrinkage must be considered in order to attain the desired amount of permanent bore enlargement in each tube section. Taking the mean diameter ratio for each section and the required amount of permanent bore enlargement, the longitudinal shrinkage can then be determined from Figure 27.

This amount then is added to the length of each section.

3 - Container Design

As previously stated, containers are utilized primarily to control the amount of permanent enlargement thus making possible the autofrettage of a tube of variable cross section. To determine the internal configuration of the containers which resemble very closely that of the tube, it is assumed that the tube-container interface pressure is equal to the difference between the maximum internal pressure for the tube and the overstrain pressure for the section in question. The maximum internal pressure is generally equal to or slightly greater than the maximum overstrain pressure for the tube. In this case 135,000 pounds per square inch is used. Again in the case of Section 5, the interface pressure is 135,000 - 115,000 or 20,000 pounds per square inch. Knowing the internal and interface pressure at a given section, the elastic recovery of the outside surface of the tube is:

$$w_{be} = \frac{b}{E(b^2-1)} \left[2 P_m - P_{if} (.7b^2 + 1.3)\right] \ldots\ldots\ldots (1)$$

where P_m = maximum internal pressure

P_{if} = interface pressure

Assuming that the internal diameter of the container equals the outside diameter of the tube when under pressure, the elastic

strain of the container can be similarly determined from:

$$\epsilon_{ec} = \frac{b\, P_{if}}{E(w^2-1)} \left(.7 + 1.3w_c^2\right) \quad \ldots\ldots\ldots\ldots\ldots\ldots \quad (2)$$

The internal diameter of the container to attain the desired permanent bore enlargement can now be determined by adding to the outside diameter of the tube after autofrettage the difference between the elastic recovery of the outside surface of the tube (equation 1) and the elastic expansion of the container (equation 2) as follows:

$$a_c = b + (u_{be} - u_{aec}) \ldots\ldots\ldots\ldots\ldots\ldots\ldots \quad (3)$$

strain of the container can be similarly determined from:

$$u_{ac} = \frac{b\,P_{if}}{E(N^2-1)}\left(.7 + 1.3N_c^2\right) \quad \ldots\ldots\ldots\ldots\ldots\ldots \quad (2)$$

The internal diameter of the container to attain the desired permanent bore enlargement can now be determined by adding to the outside diameter of the tube after autofrettage the difference between the elastic recovery of the outside surface of the tube (equation 1) and the elastic expansion of the container (equation 2) as follows:

$$a_o = b + (u_{be} - u_{aoc}) \ldots\ldots\ldots\ldots\ldots\ldots\ldots \quad (3)$$

▼

APPENDIX III

Figures and Tables

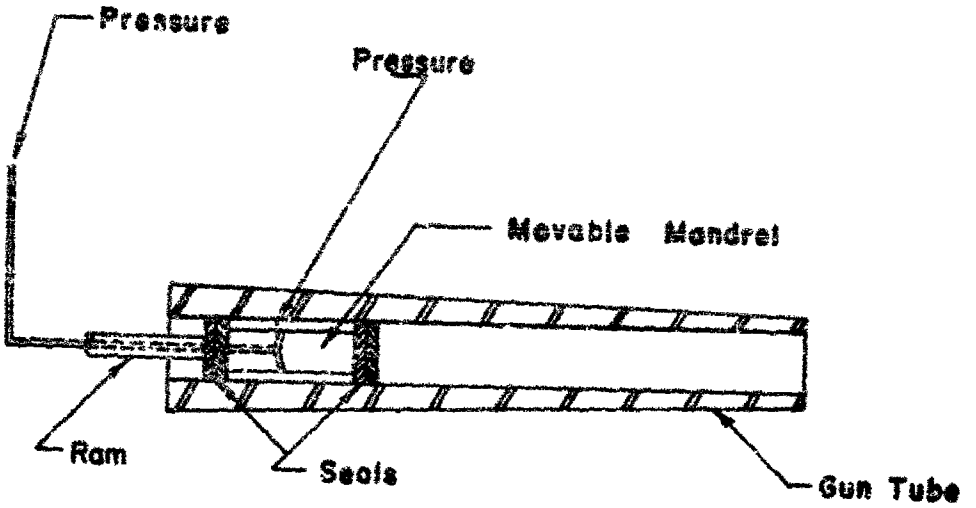

MOVABLE PACKING

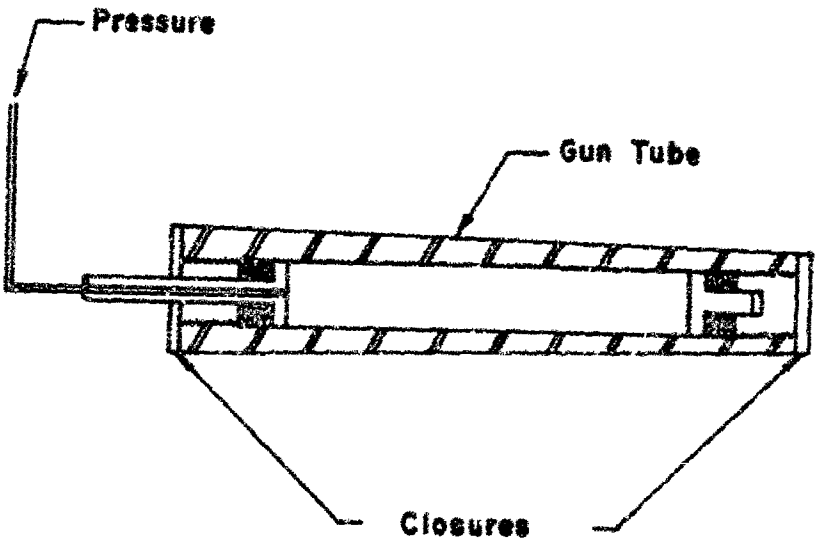

CLOSED END

CLOSED END AND MOVABLE PACKING
AUTOFRETTAGE PROCESSES

Figure 1.

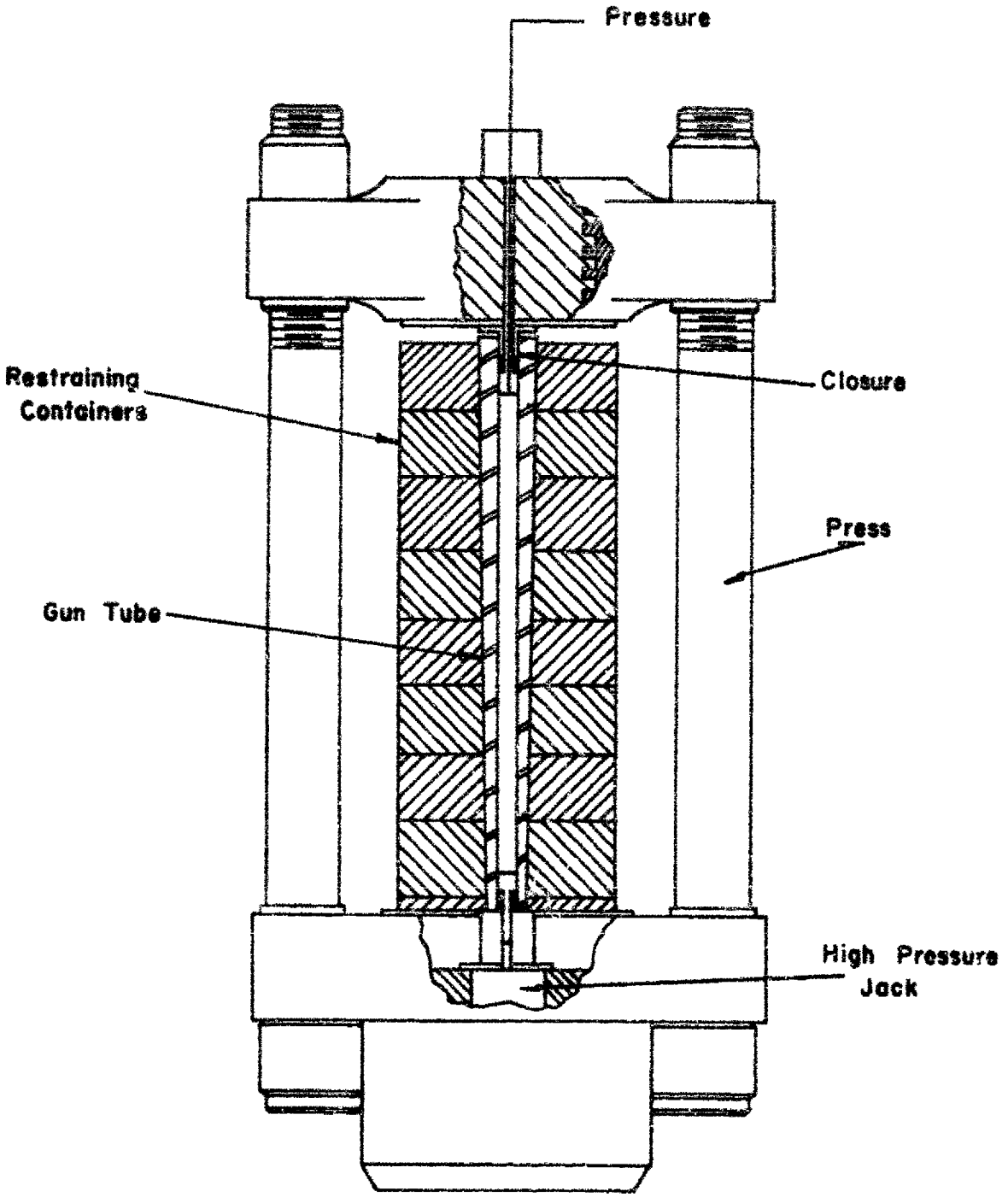

OPEN END AUTOFRETTAGE PROCESS

Figure 2.

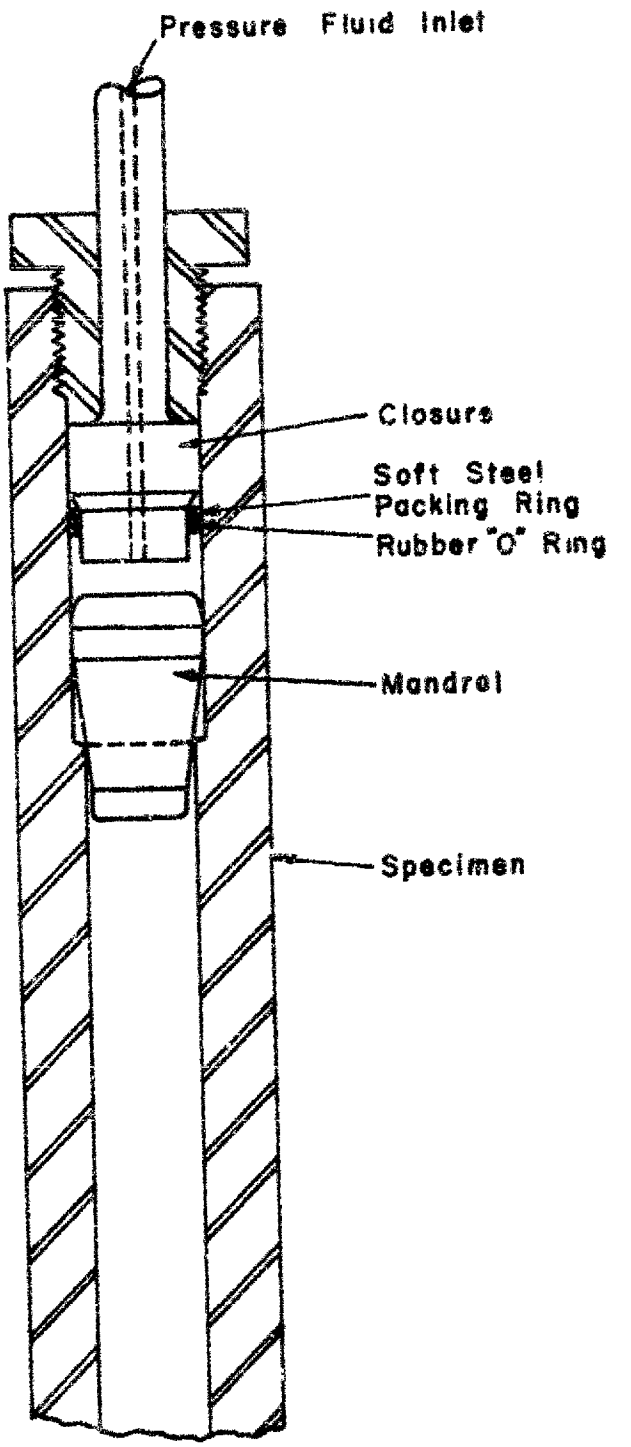

Figure 3. — SWAGING AUTOFRETTAGE PROCESS

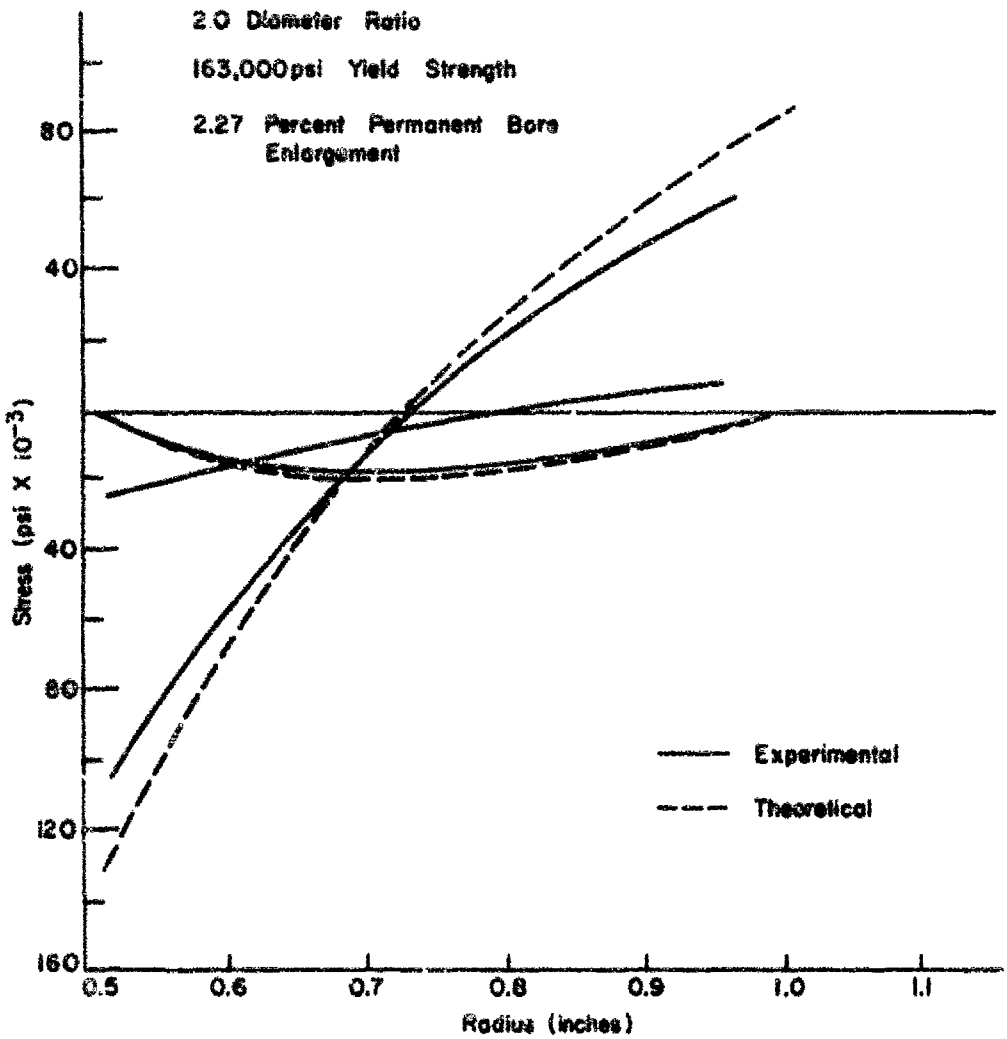

Figure 4. RESIDUAL STRESS DISTRIBUTION IN A 100 PERCENT OVERSTRAINED CYLINDER

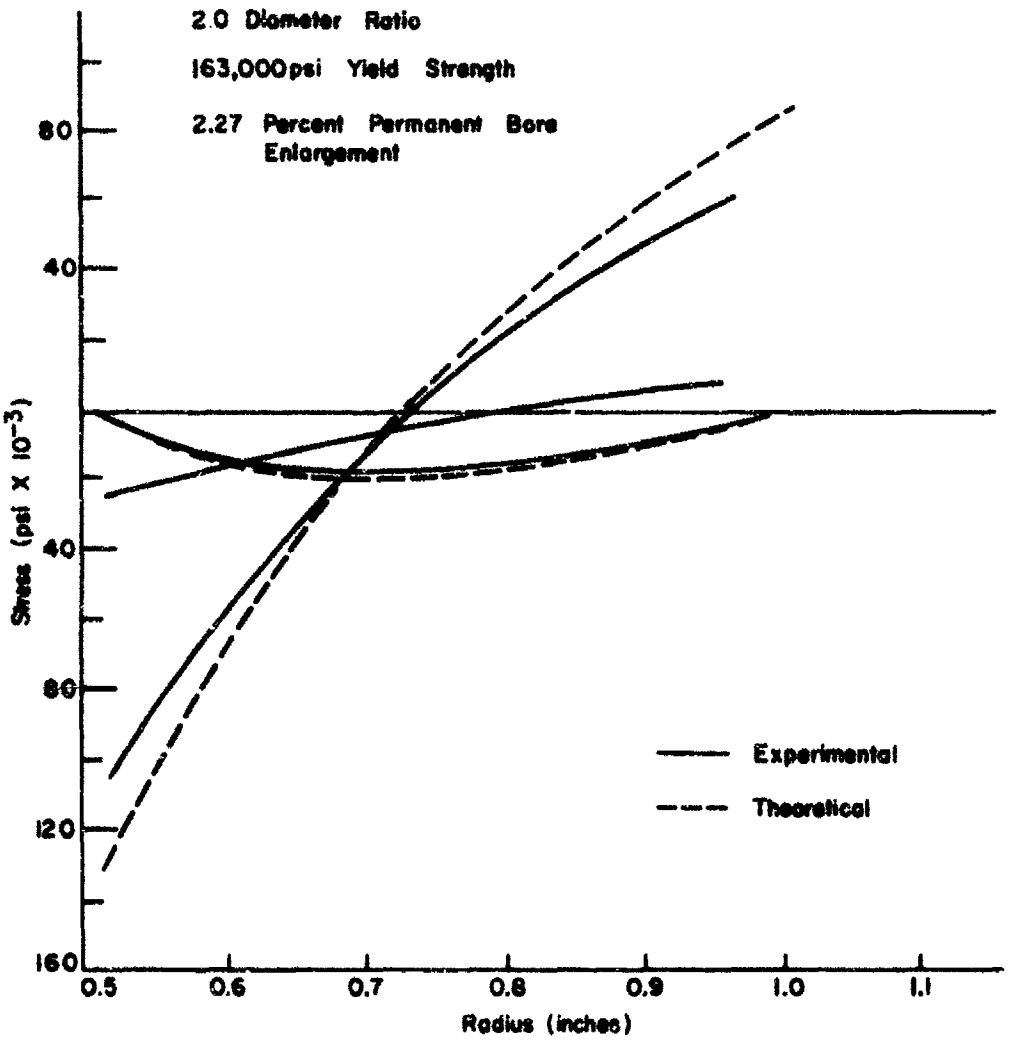

Figure 4. RESIDUAL STRESS DISTRIBUTION IN A 100 PERCENT OVERSTRAINED CYLINDER

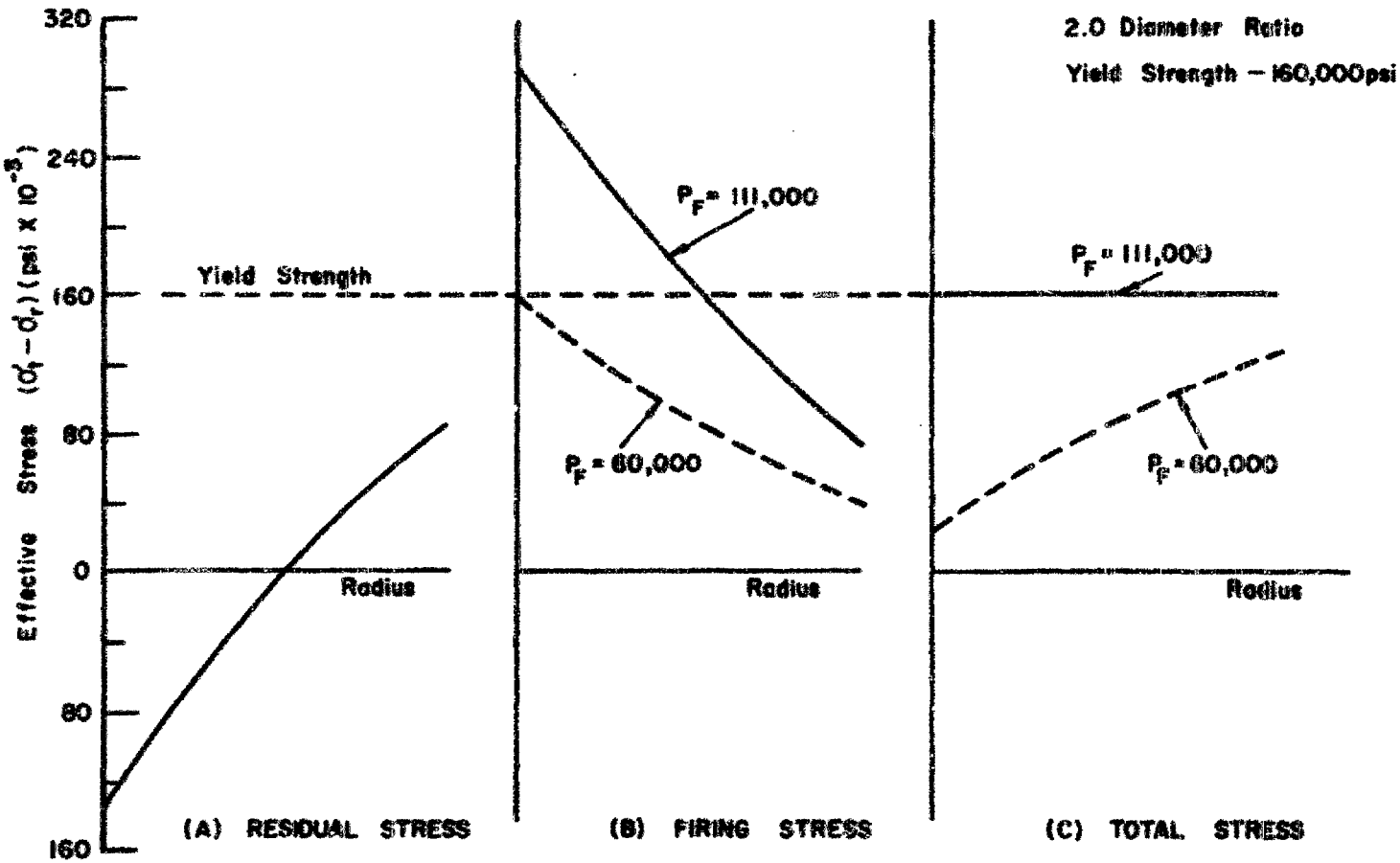

Figure 5. SUMMATION OF STRESSES IN A 100PERCENT OVERSTRAINED CYLINDER

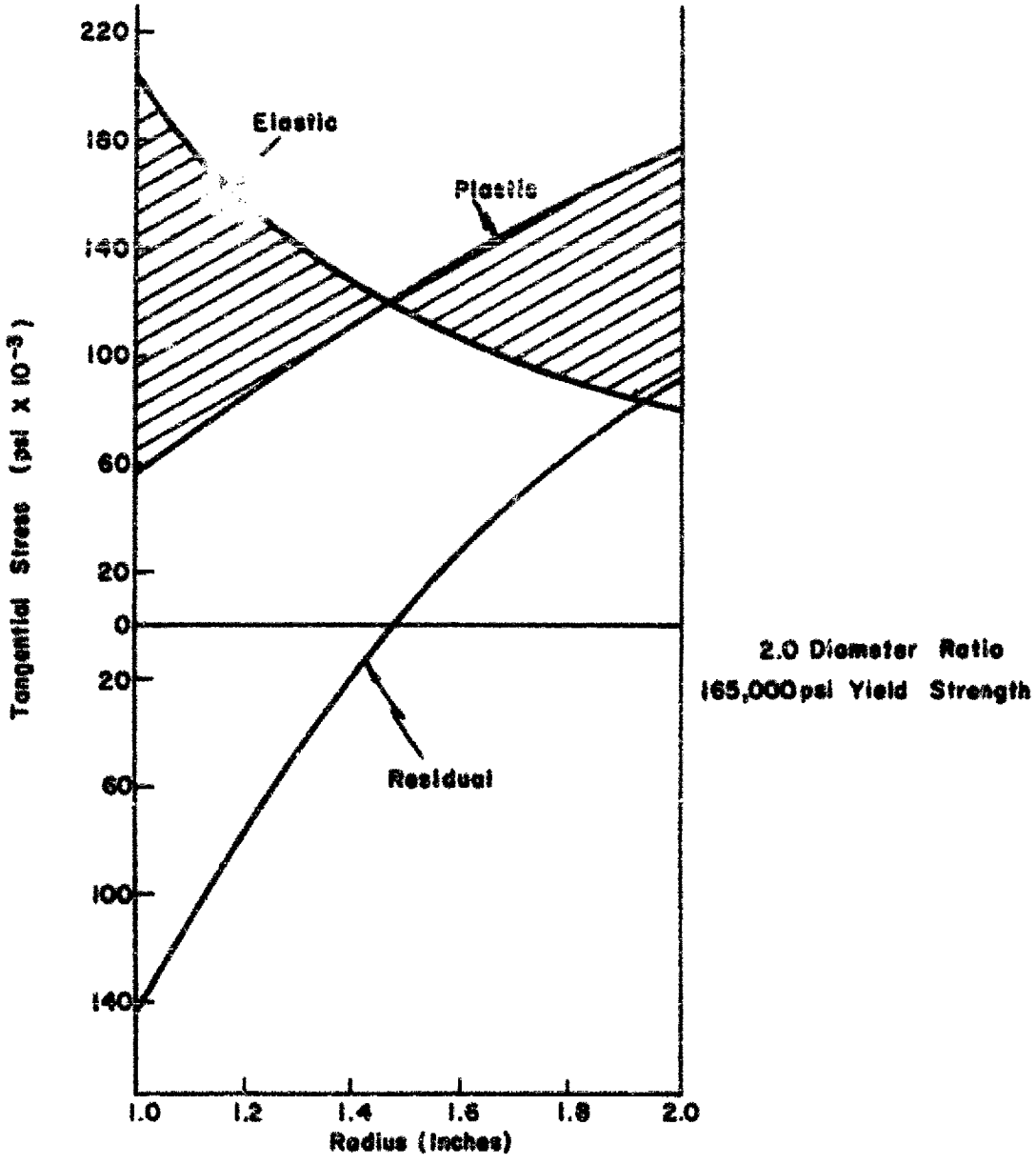

Figure 6. SUMMATION OF ELASTIC AND PLASTIC STRESSES

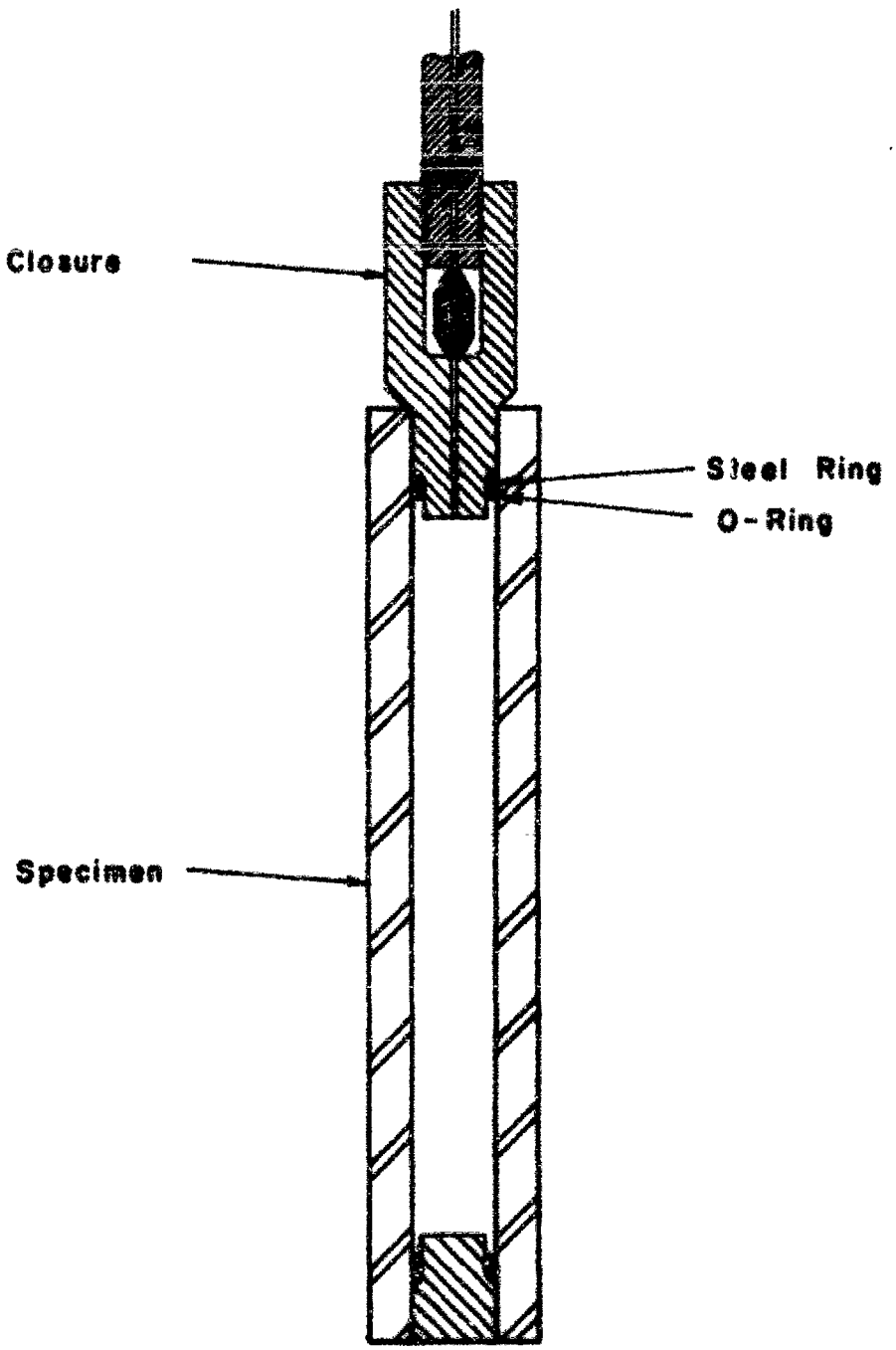

Figure 7. PRESSURE SEAL CONFIGURATION

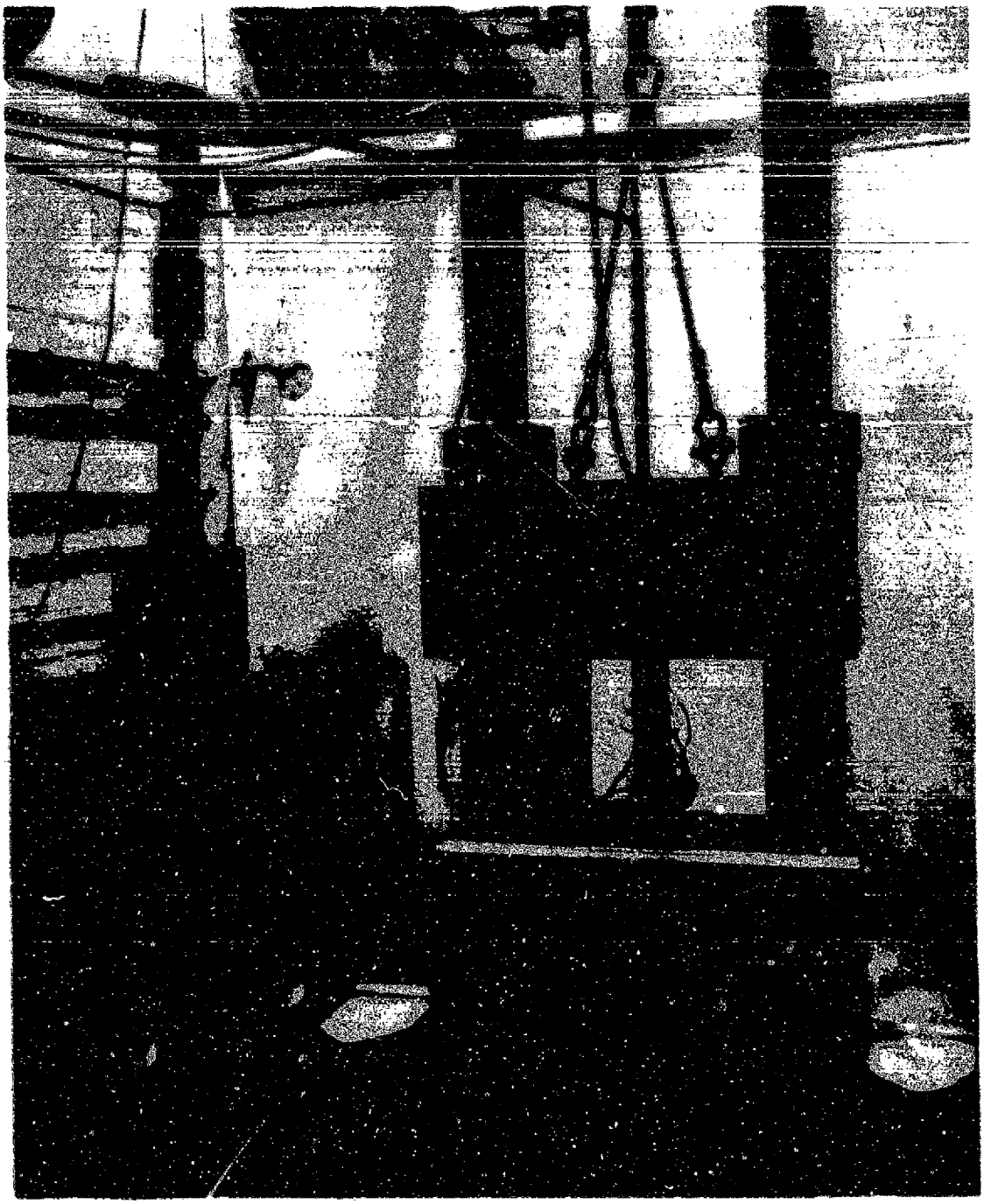

200,000 POUNDS PER SQUARE INCH TESTING SYSTEM
Figure 8.

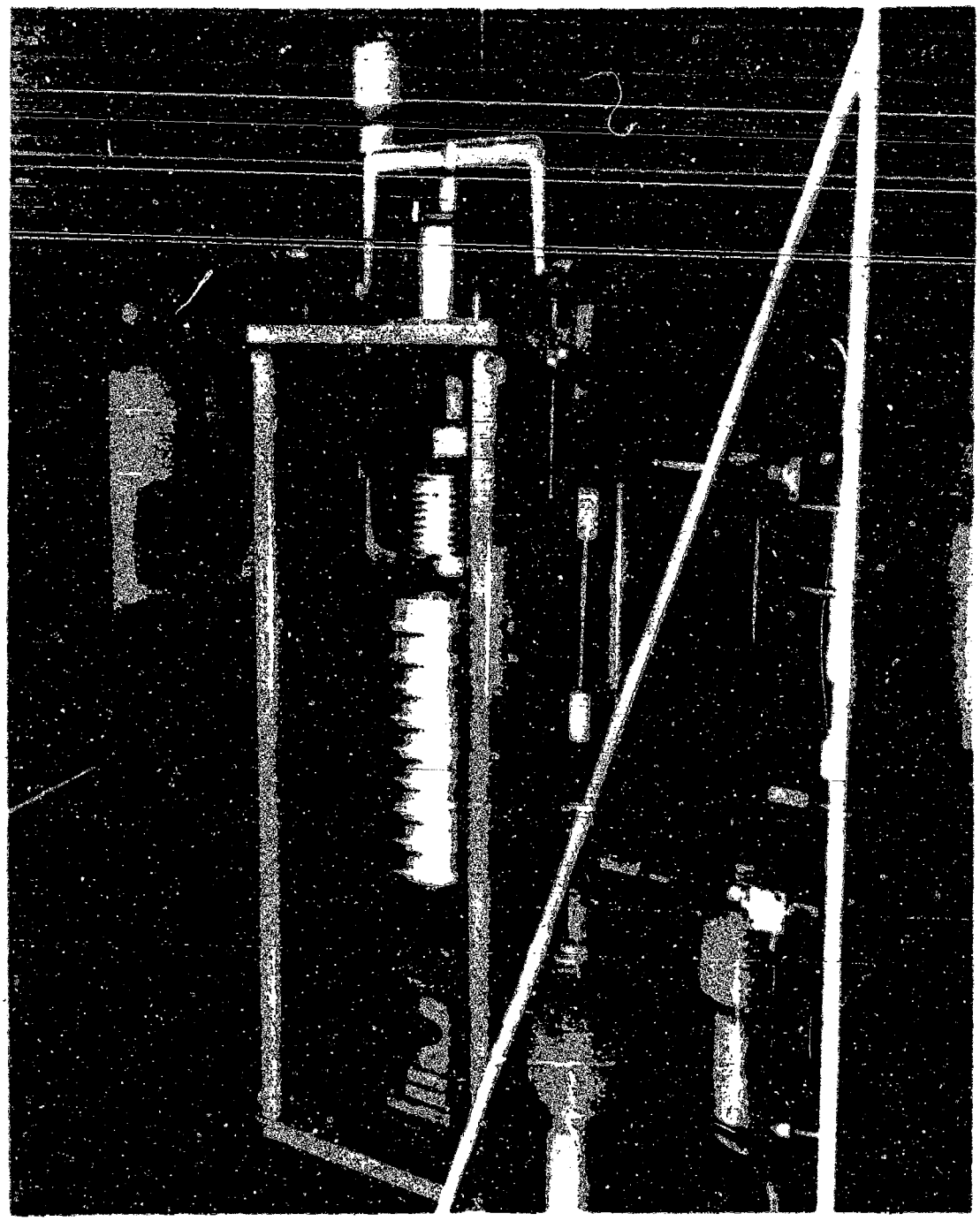

Figure 9. CONTROLLED CLEARANCE PISTON GAGE

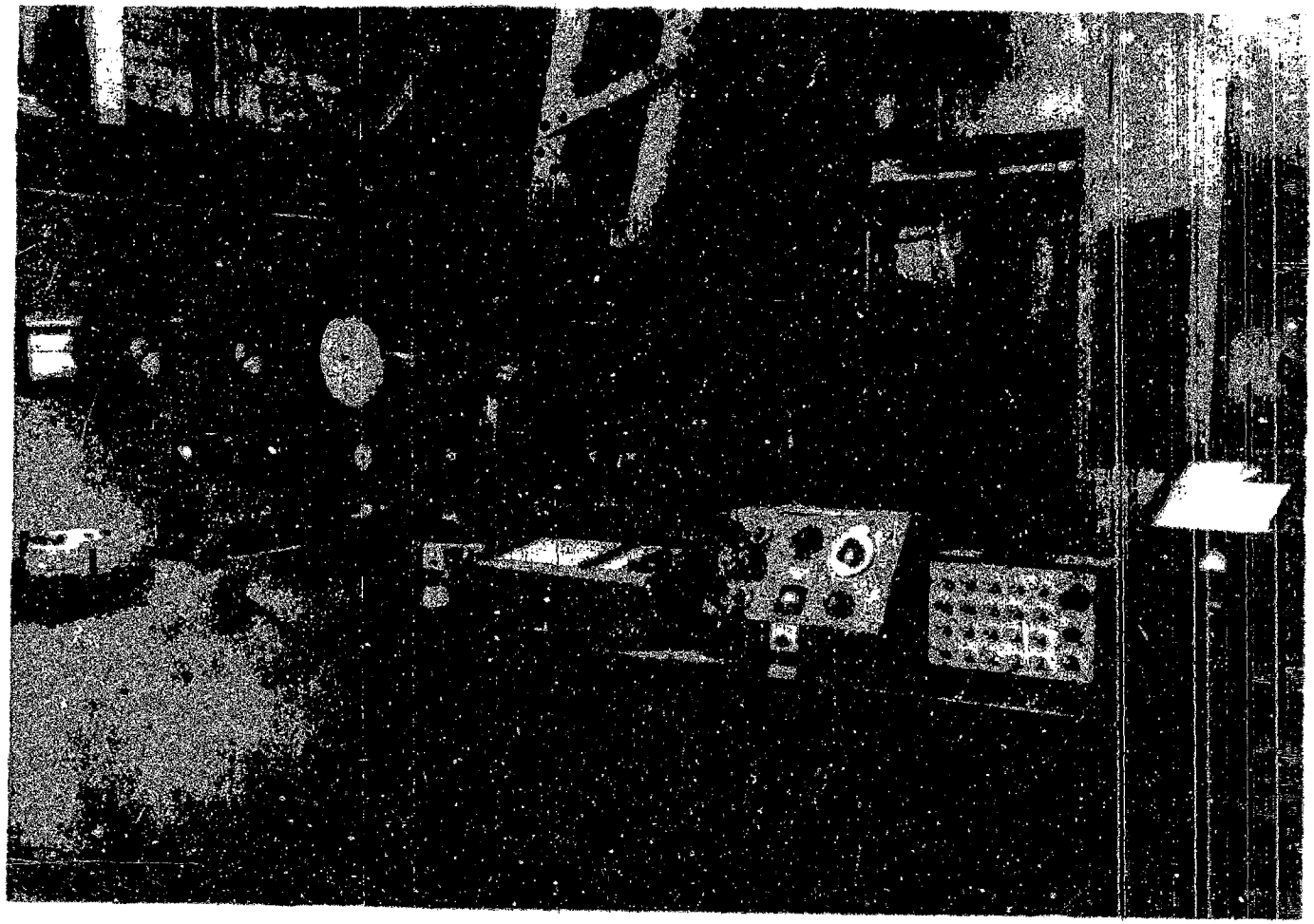

Figure 10. PRESSURE AND STRAIN MEASUREMENT EQUIPMENT

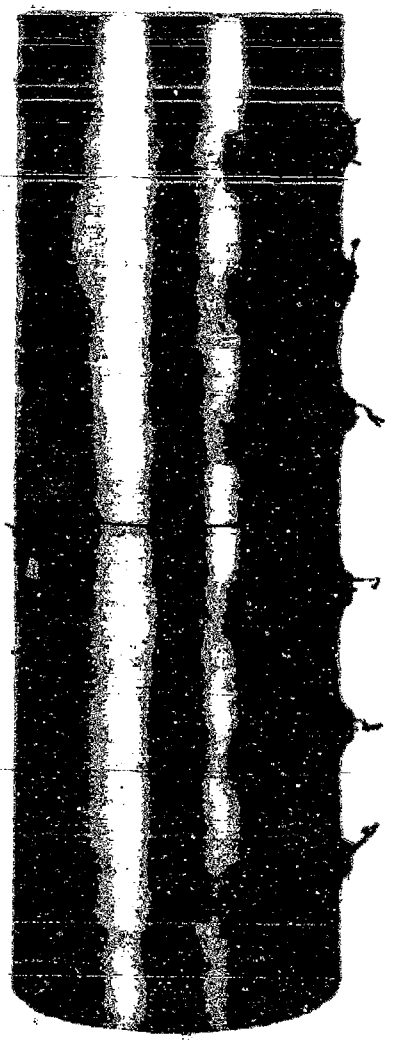

Figure 11. SPECIMEN AND CONTAINER ARRANGEMENT

Figure 11. SPECIMEN AND CONTAINER ARRANGEMENT

Figure 12. 200,000 POUNDS PER SQUARE INCH AUTOFRETTAGE SYSTEM

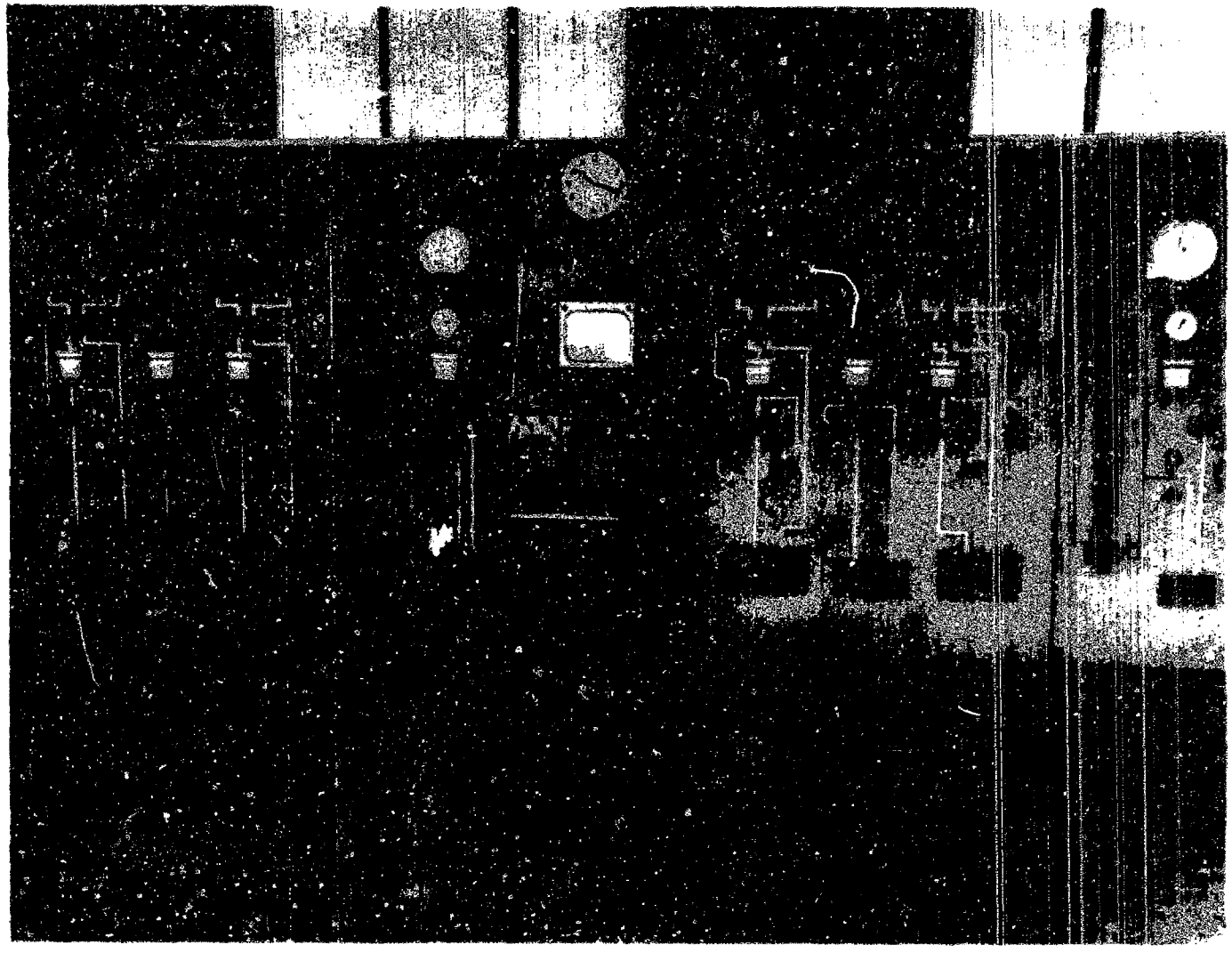

Figure 13. CONTROLS FOR 200,000 POUNDS PER SQUARE INCH AUTOFRETTAGE SYSTEM

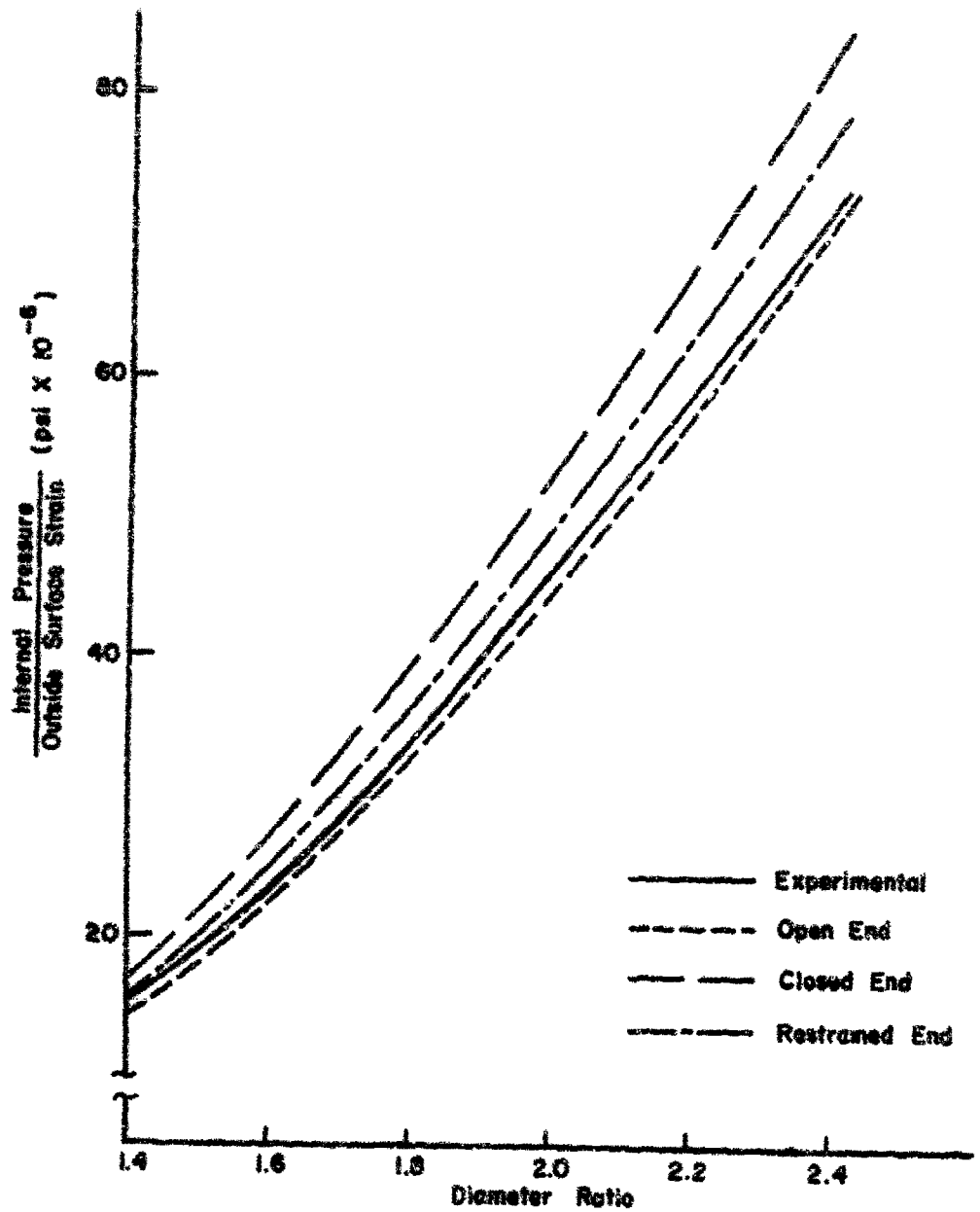

Figure 14. SLOPE IN THE ELASTIC RANGE OF INTERNAL PRESSURE OUTSIDE SURFACE STRAIN CURVE vs DIAMETER RATIO

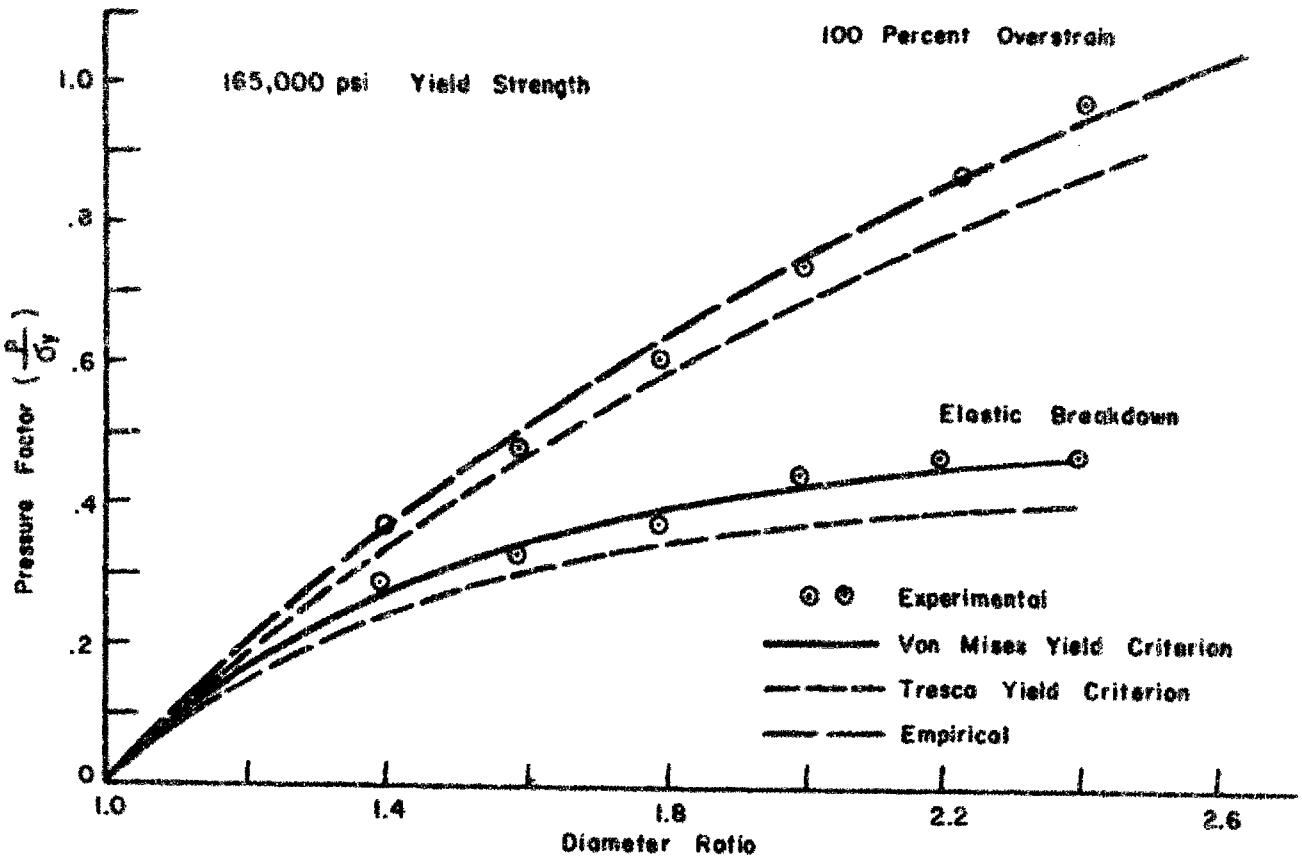

Figure 15. ELASTIC BREAKDOWN AND 100 PERCENT OVERSTRAIN PRESSURE FACTOR vs DIAMETER RATIO

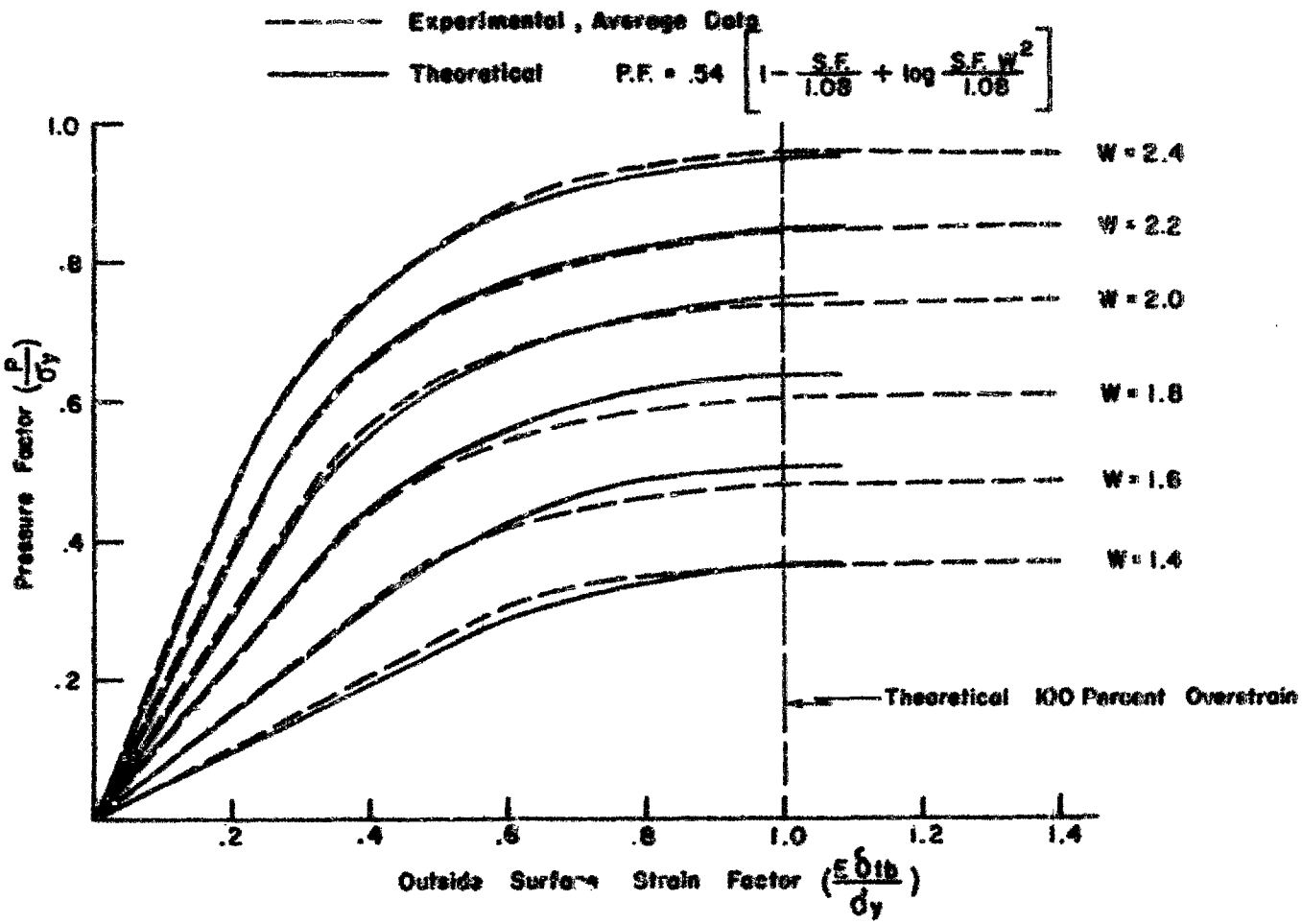

Figure 16. PRESSURE FACTOR vs OUTSIDE SURFACE STRAIN FACTOR FOR VARIOUS DIAMETER RATIOS

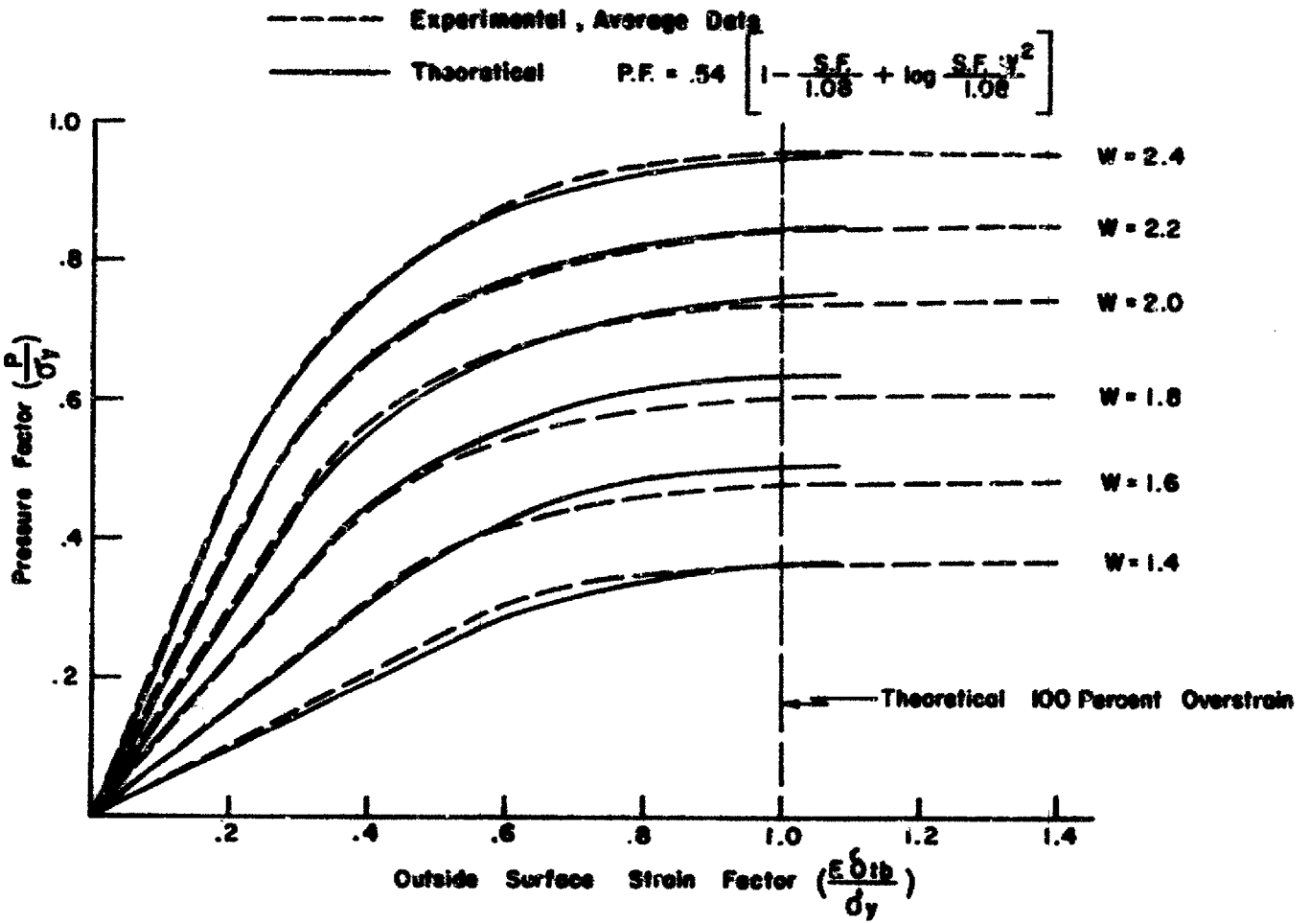

Figure 16. PRESSURE FACTOR vs OUTSIDE SURFACE STRAIN FACTOR FOR VARIOUS DIAMETER RATIOS

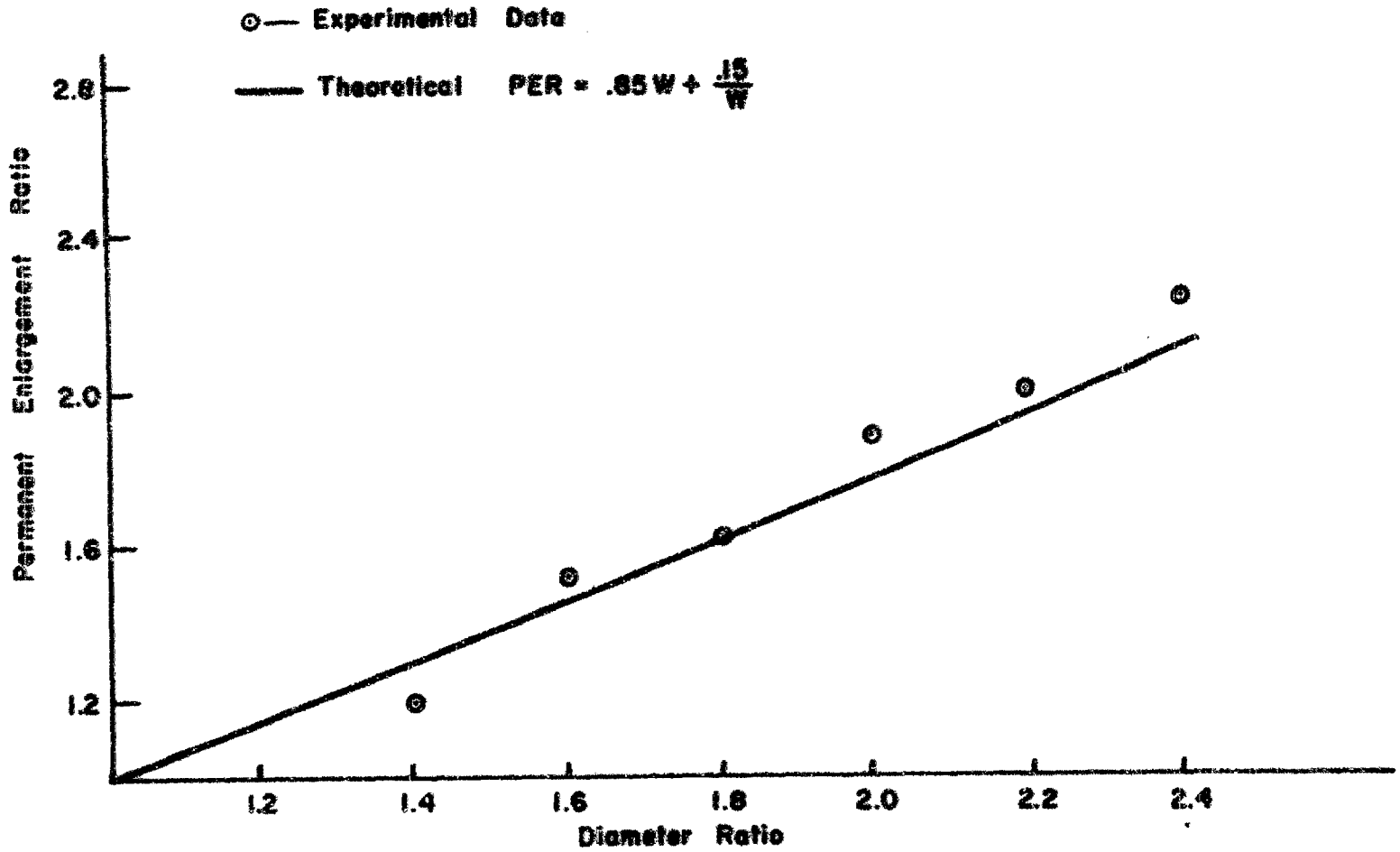

Figure 17. PERMANENT ENLARGEMENT RATIO vs DIAMETER RATIO

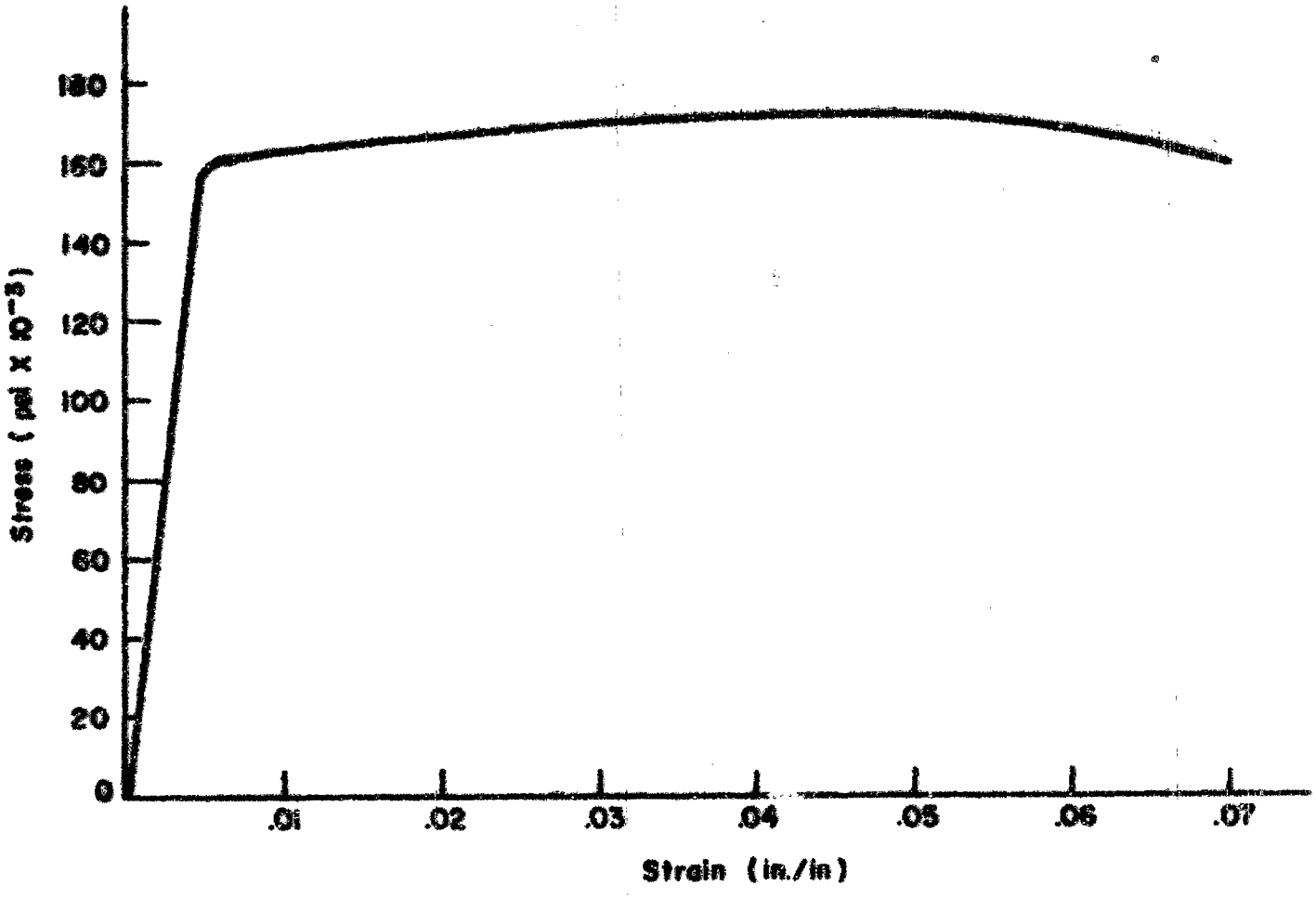

Figure 18. STRESS – STRAIN DIAGRAM

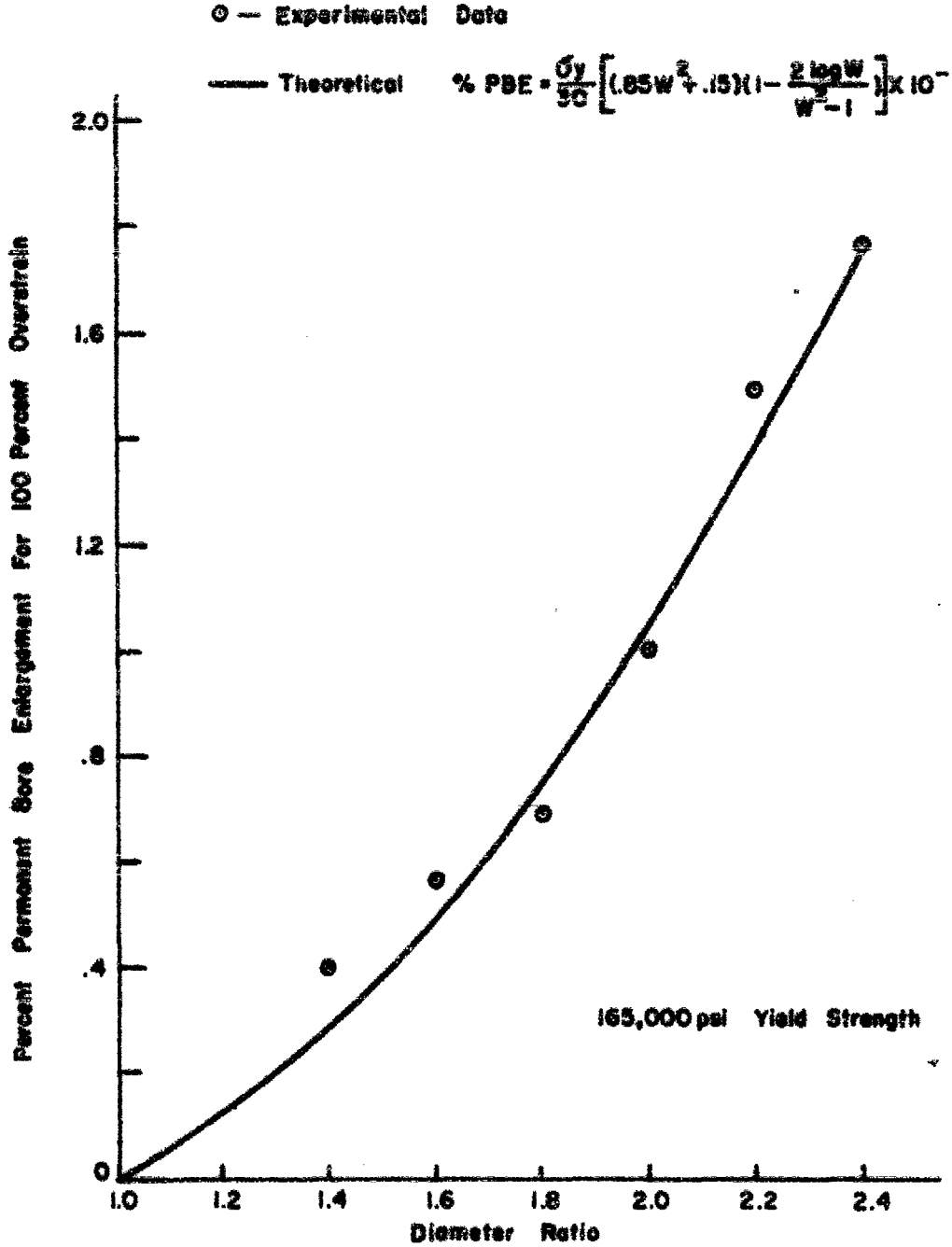

Figure 19. PERCENT PERMANENT BORE ENLARGEMENT FOR 100 PERCENT OVERSTRAIN vs DIAMETER RATIO

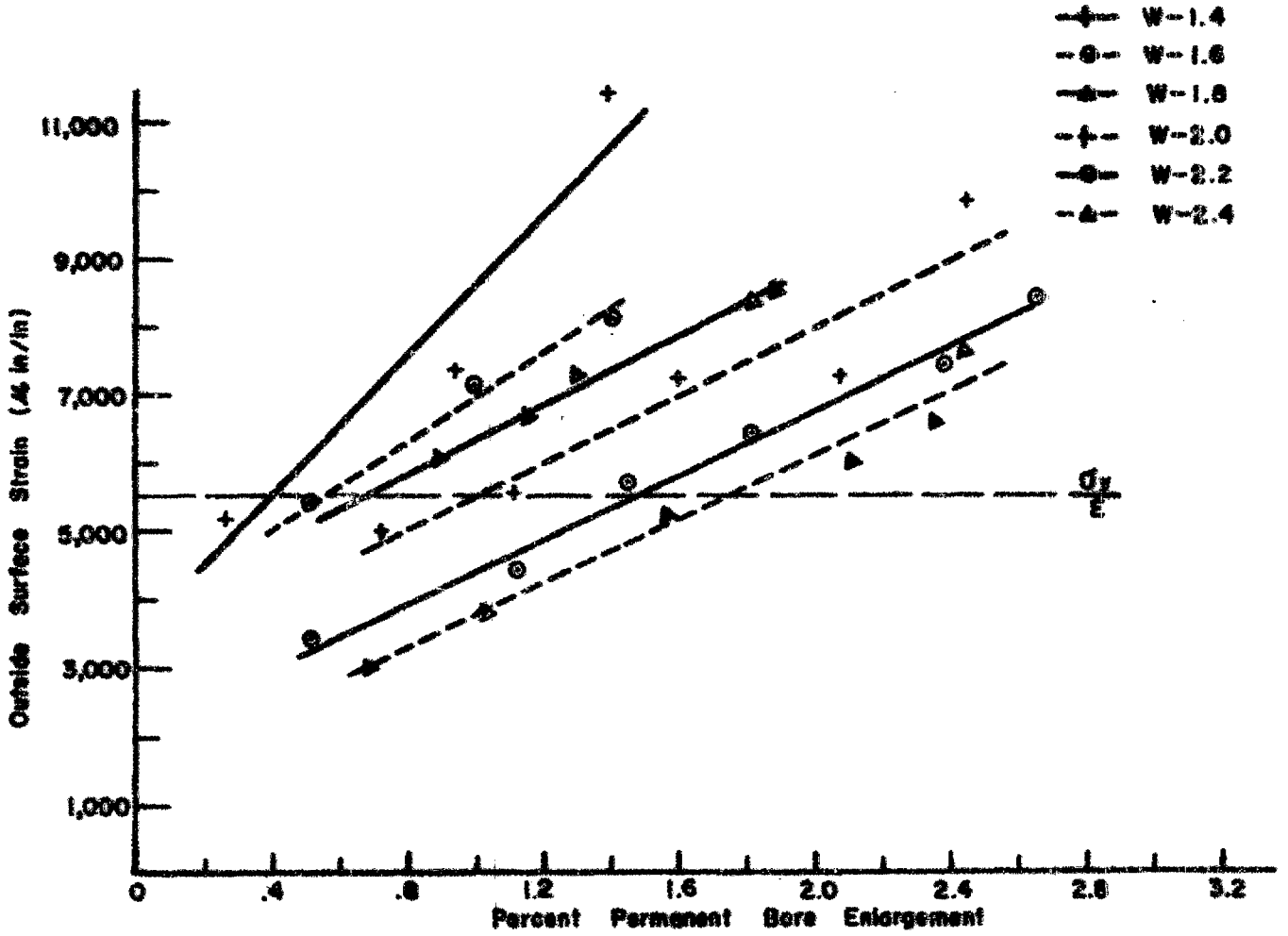

Figure 20 OUTSIDE SURFACE STRAIN vs PERCENT PERMANENT BORE ENLARGEMENT

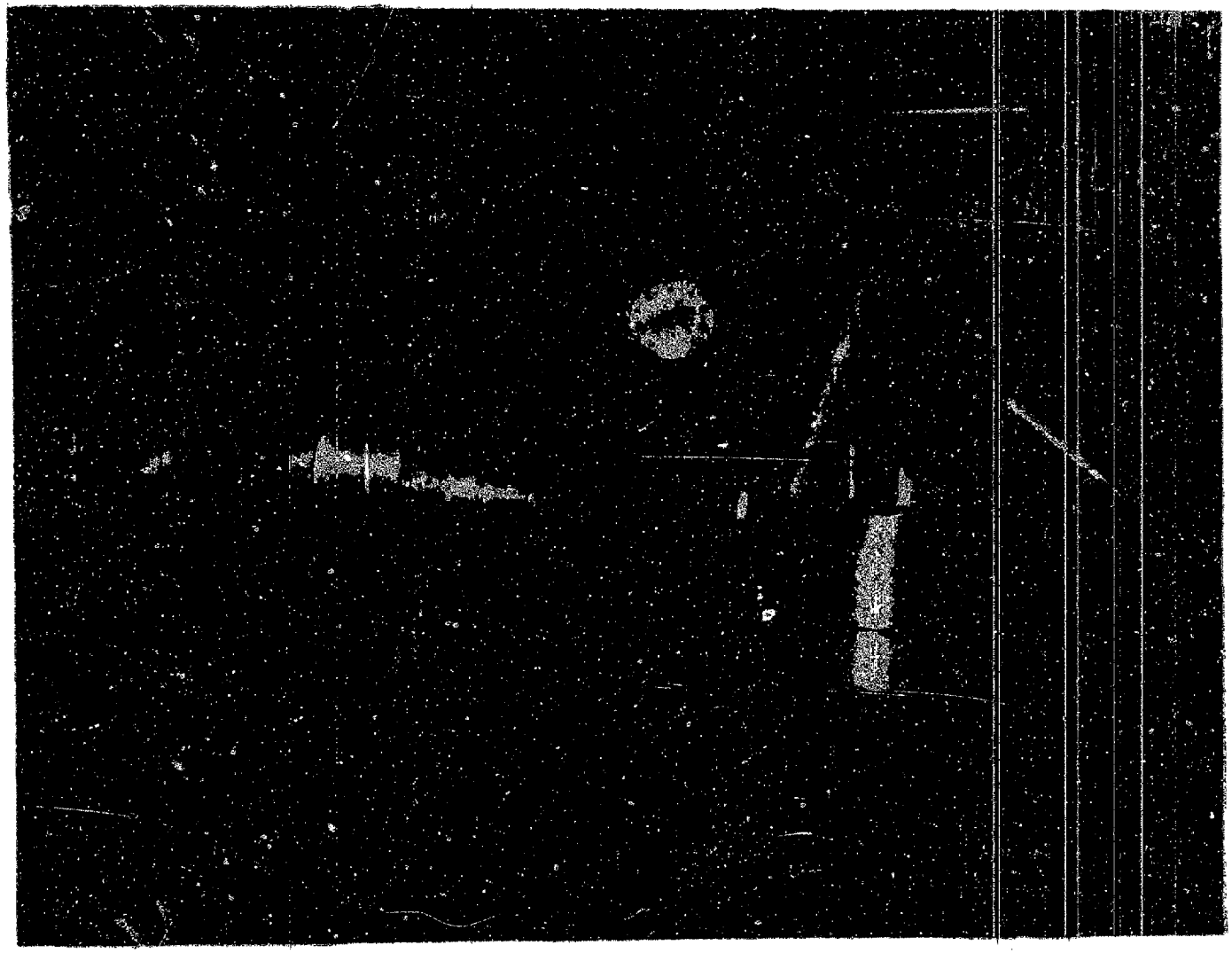

Figure 21. RESIDUAL STRESS ANALYSIS MACHINING FIXTURE AND TYPICAL SPECIMEN

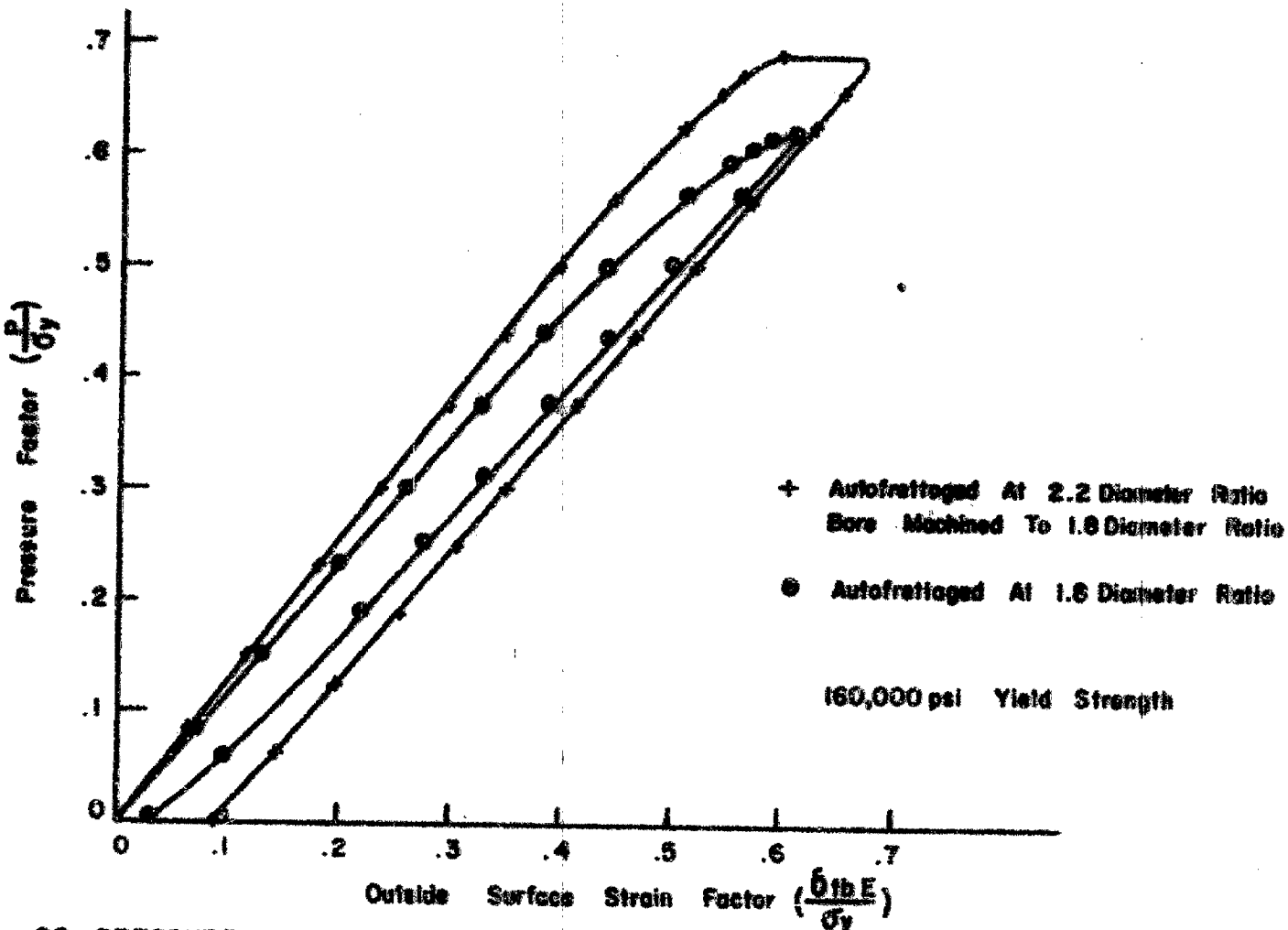

Figure 22. PRESSURE FACTOR vs OUTSIDE SURFACE STRAIN FACTOR FOR RE-APPLICATION OF OVERSTRAIN PRESSURE SHOWING EFFECT OF MACHINING

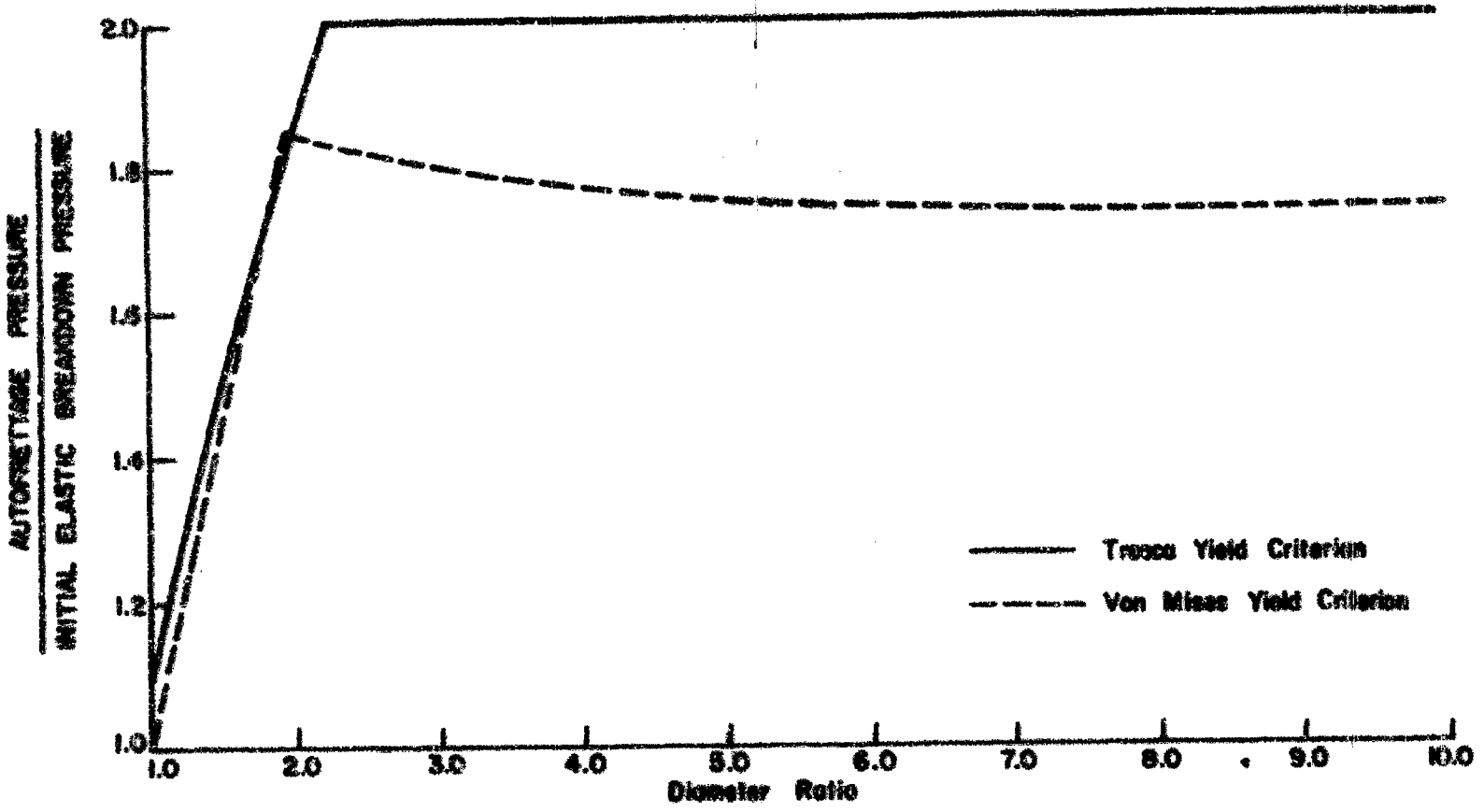

Figure 23. RATIO OF AUTOFRETTAGE TO INITIAL ELASTIC BREAKDOWN PRESSURE vs DIAMETER RATIO

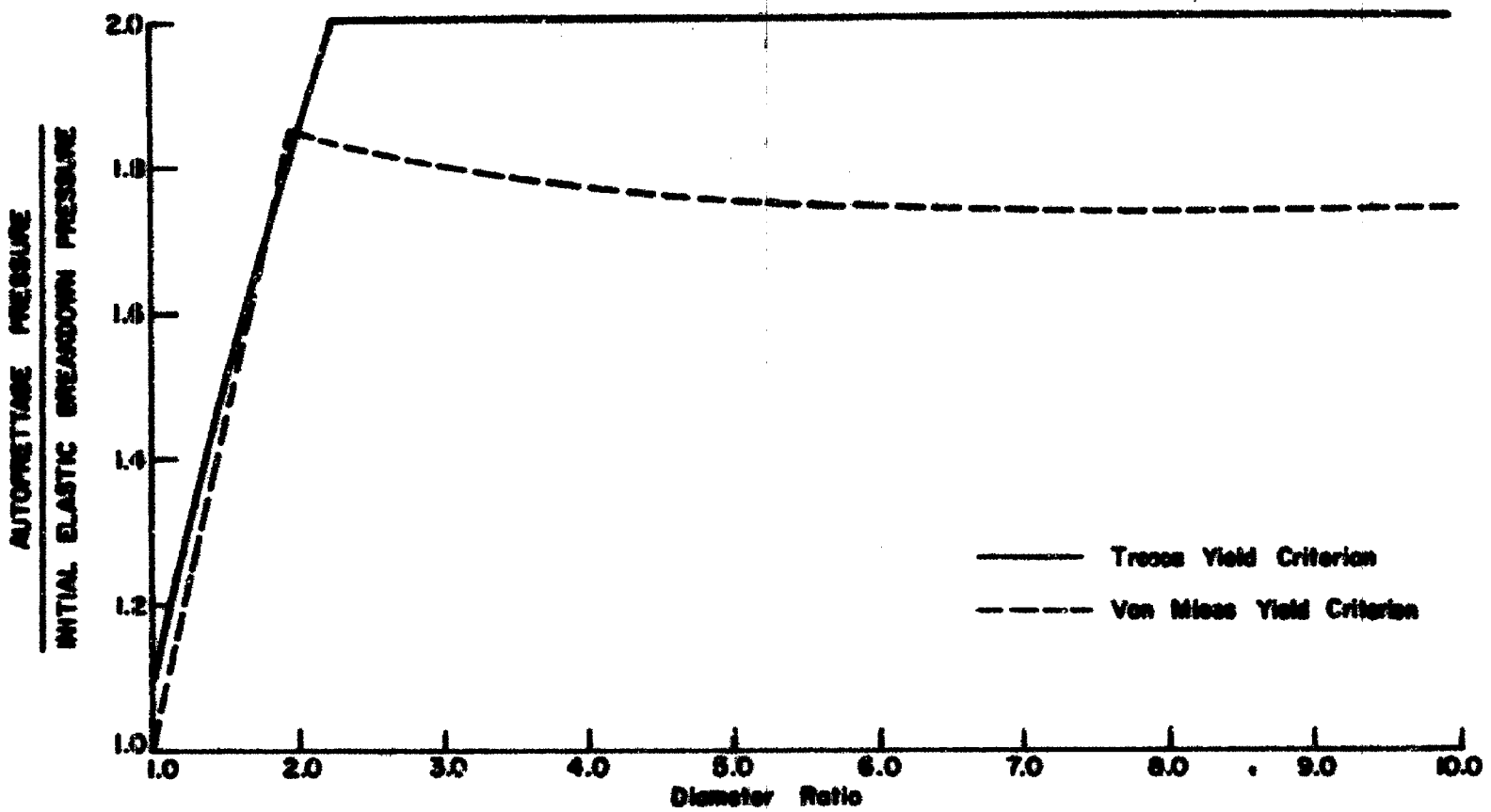

Figure 23. RATIO OF AUTOFRETTAGE TO INITIAL ELASTIC BREAKDOWN PRESSURE vs DIAMETER RATIO

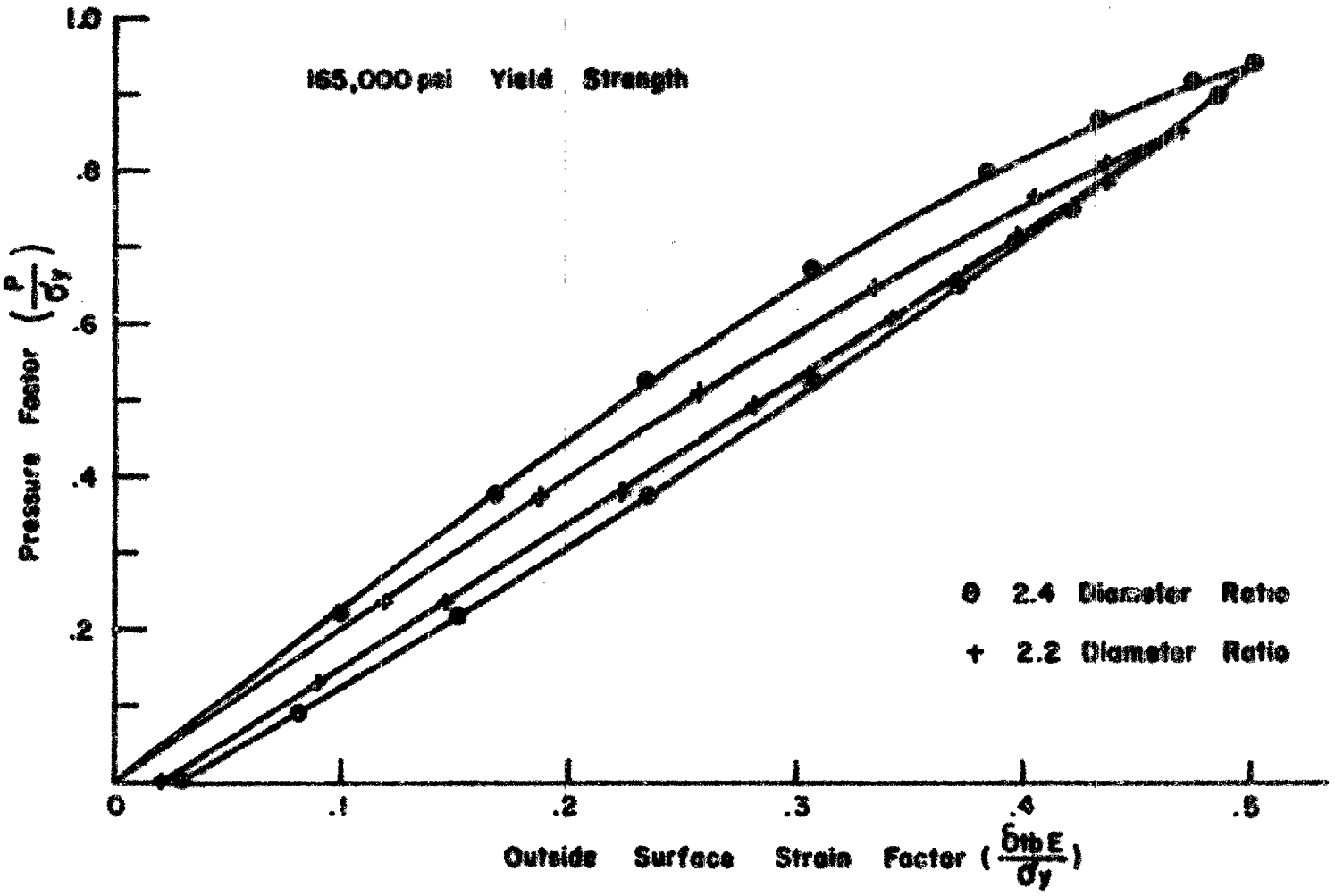

Figure 24. PRESSURE FACTOR vs OUTSIDE SURFACE STRAIN FACTOR FOR RE-APPLICATION OF OVERSTRAIN PRESSURE

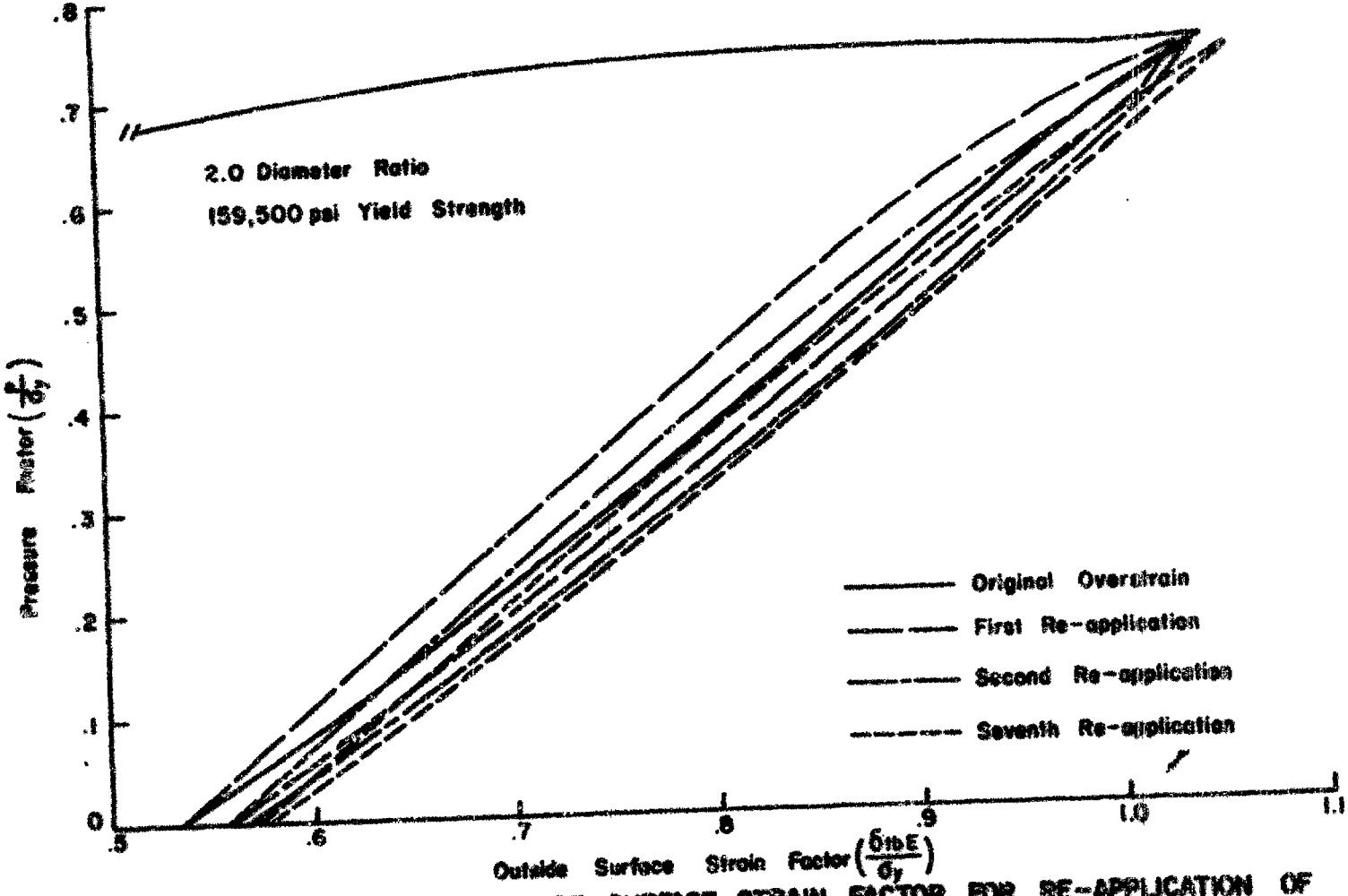

Figure 25. PRESSURE FACTOR vs OUTSIDE SURFACE STRAIN FACTOR FOR RE-APPLICATION OF OVERSTRAIN PRESSURE FOR NON-THERMAL TREATED SPECIMEN

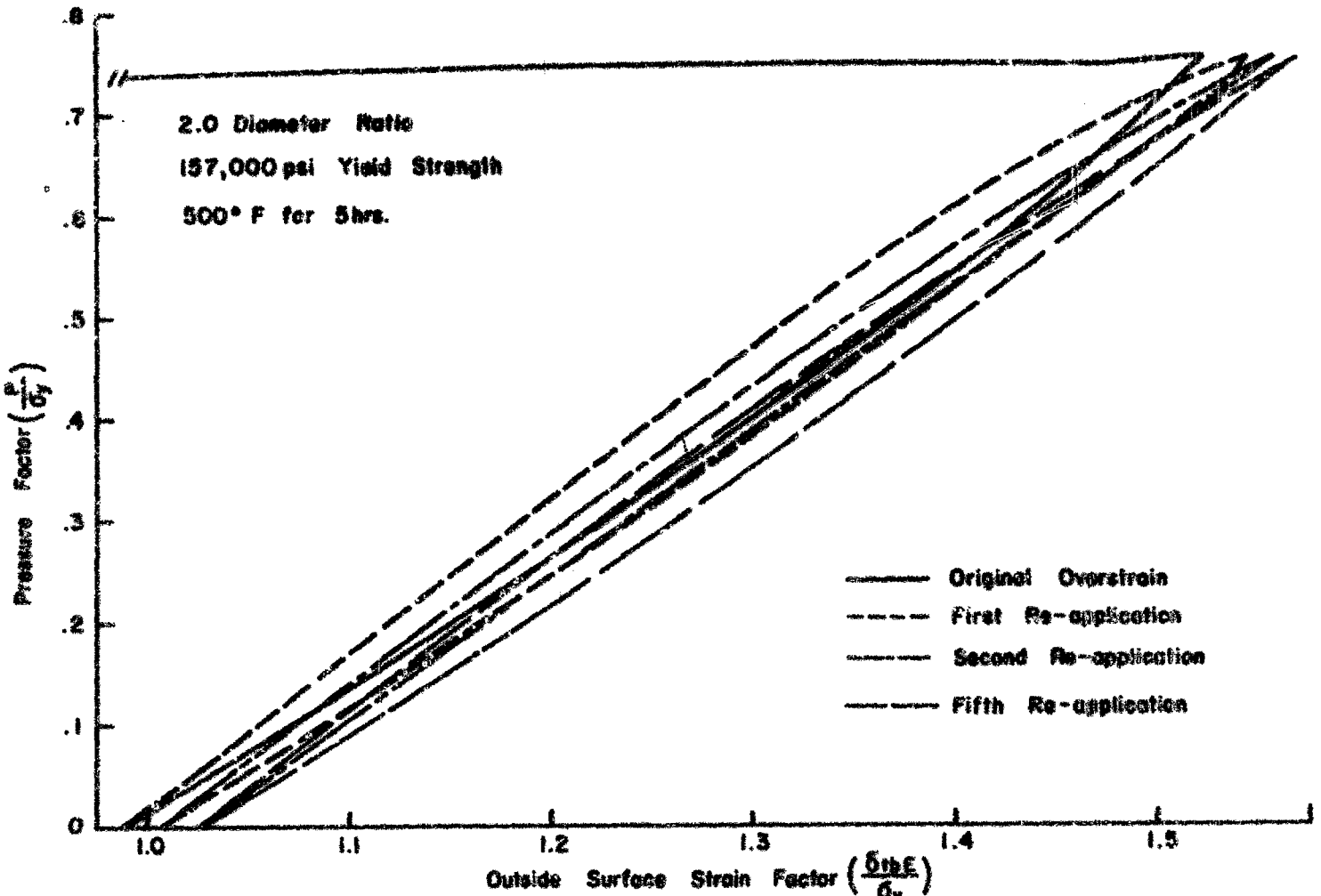

Figure 26. PRESSURE FACTOR vs OUTSIDE SURFACE STRAIN FACTOR FOR RE-APPLICATION OF OVERSTRAIN PRESSURE FOR THERMAL TREATED SPECIMEN

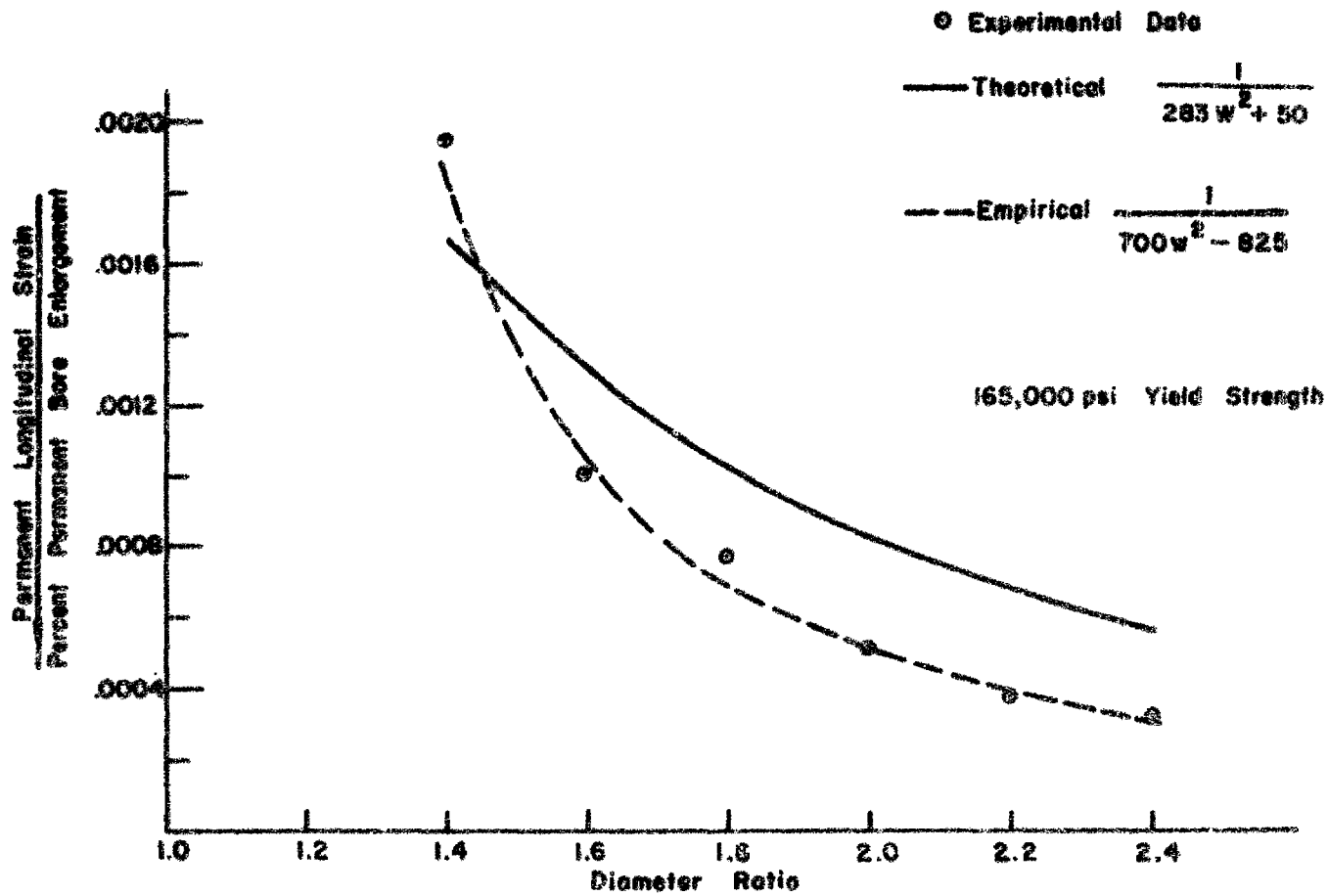

PERMANENT LONGITUDINAL STRAIN FACTOR vs DIAMETER RATIO

Figure 27.

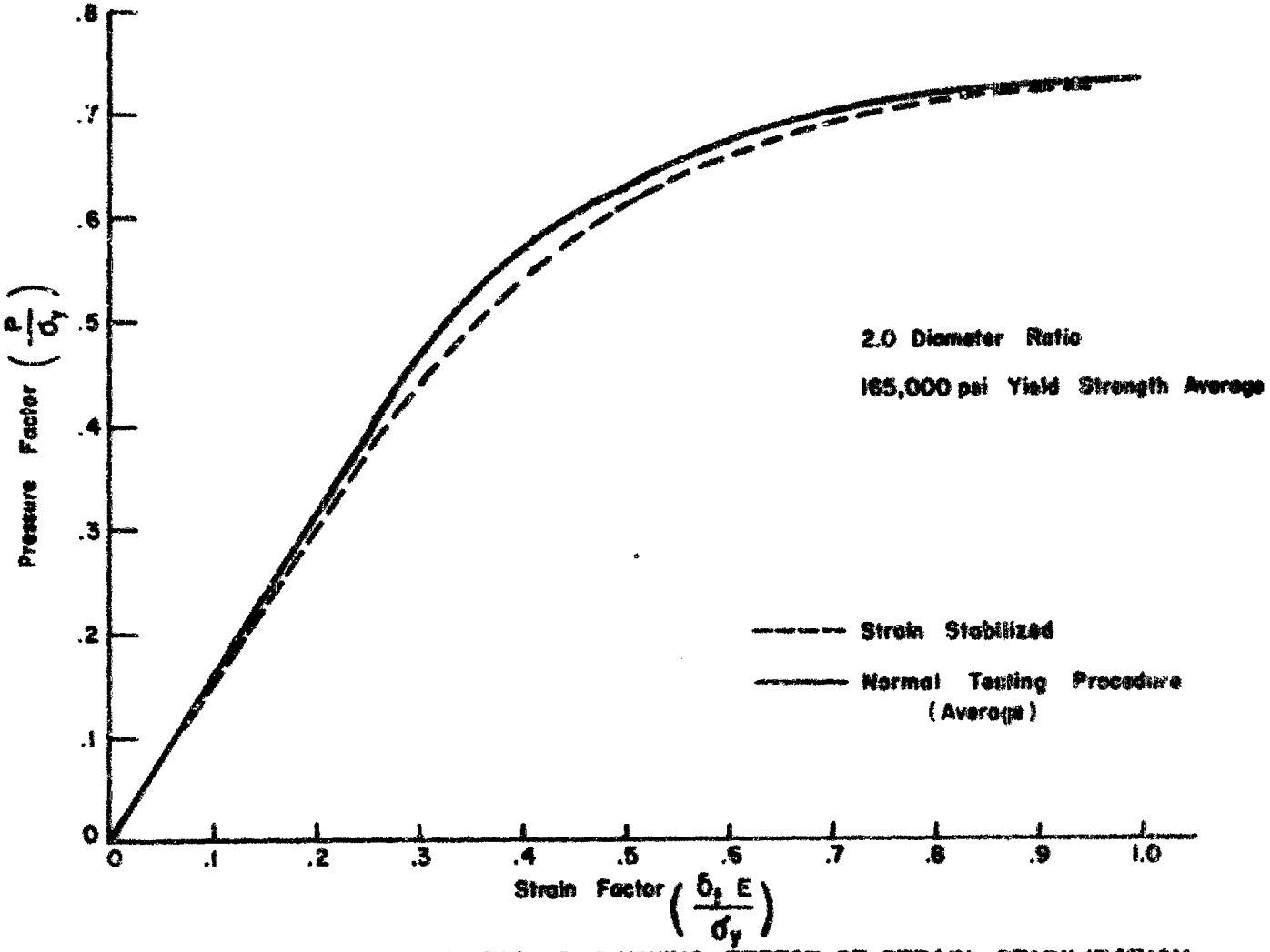

Figure 28. PRESSURE FACTOR vs STRAIN FACTOR SHOWING EFFECT OF STRAIN STABILIZATION

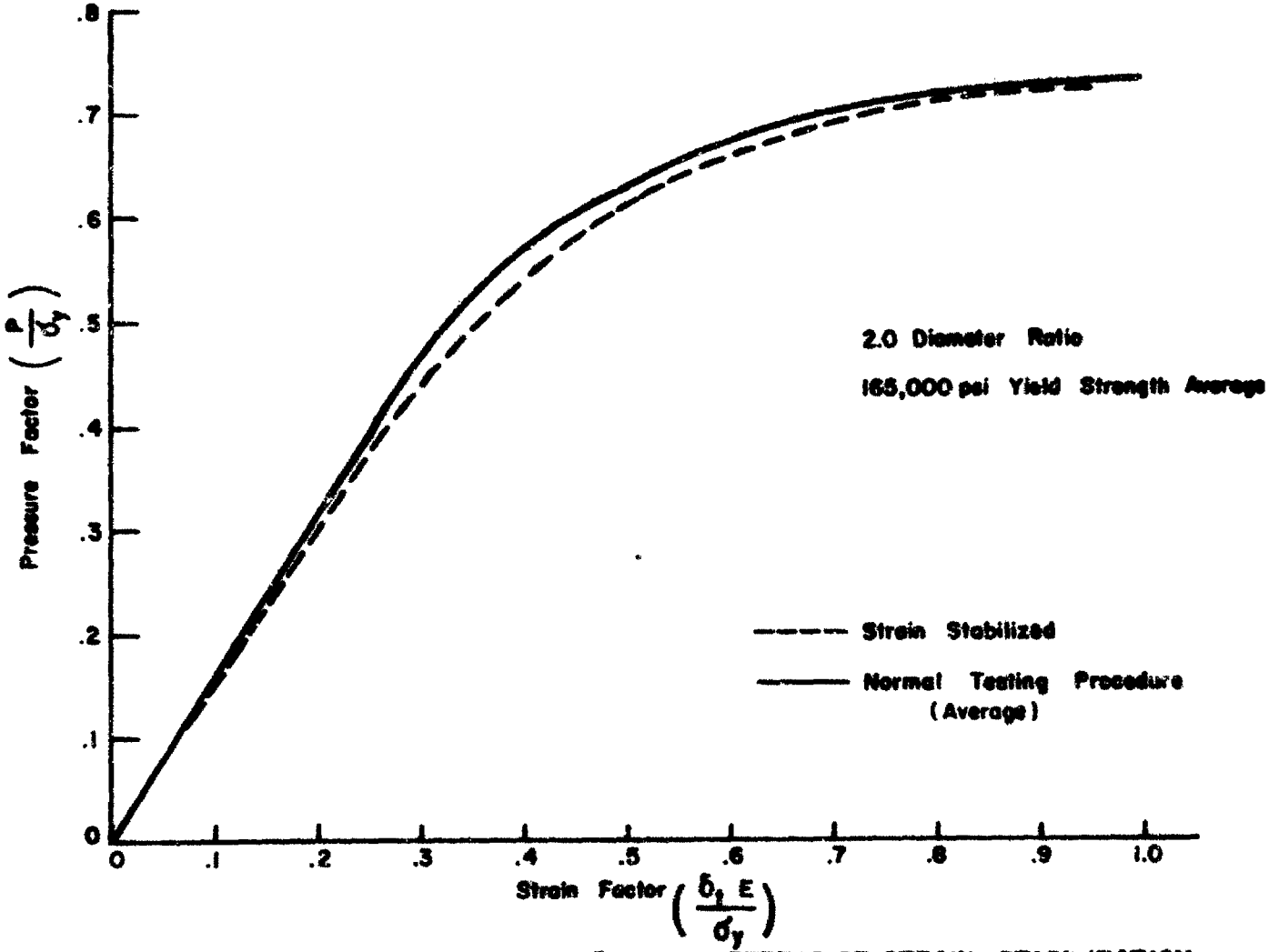

Figure 28. PRESSURE FACTOR vs STRAIN FACTOR SHOWING EFFECT OF STRAIN STABILIZATION

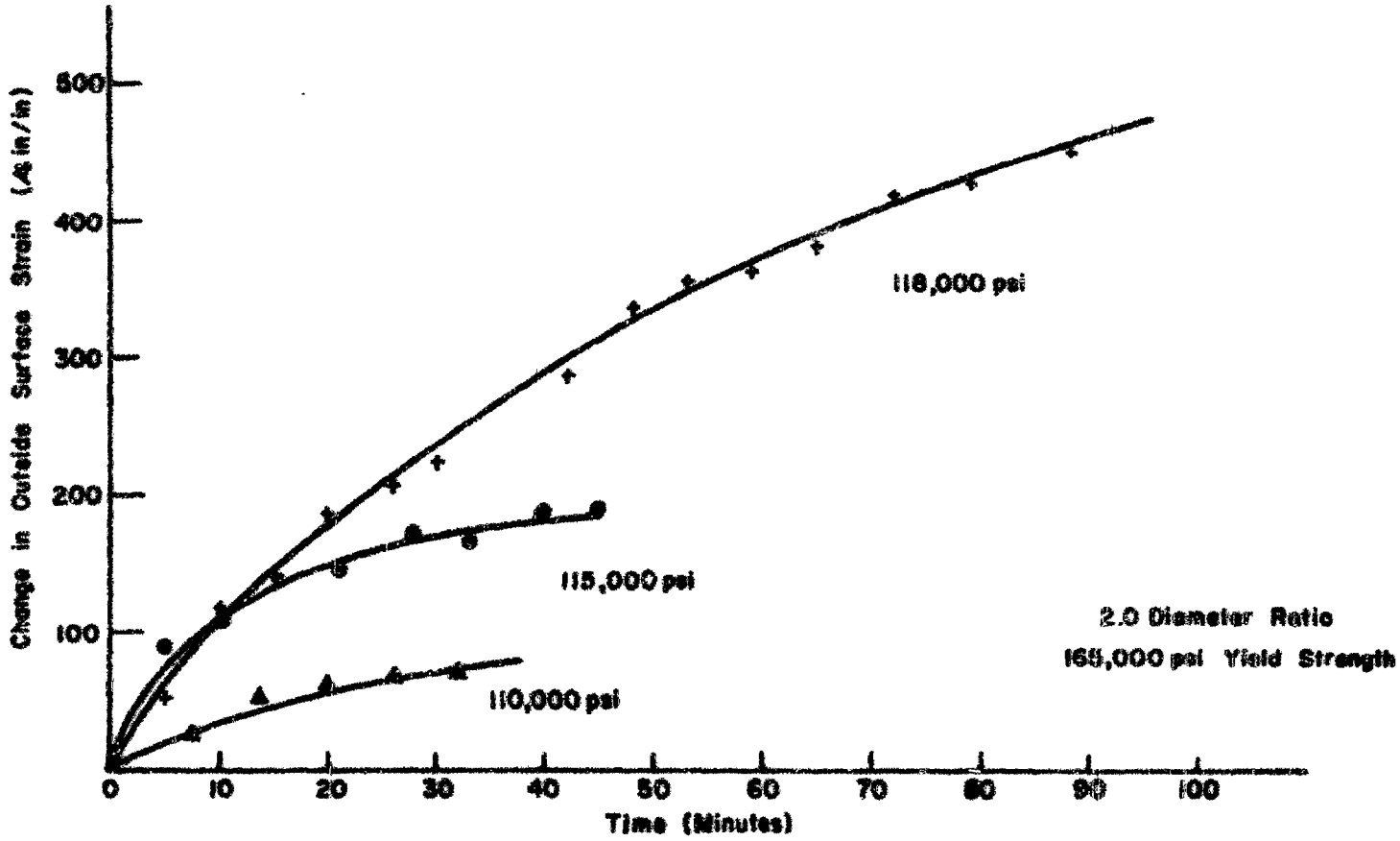

Figure 29. CHANGE IN OUTSIDE SURFACE STRAIN vs TIME

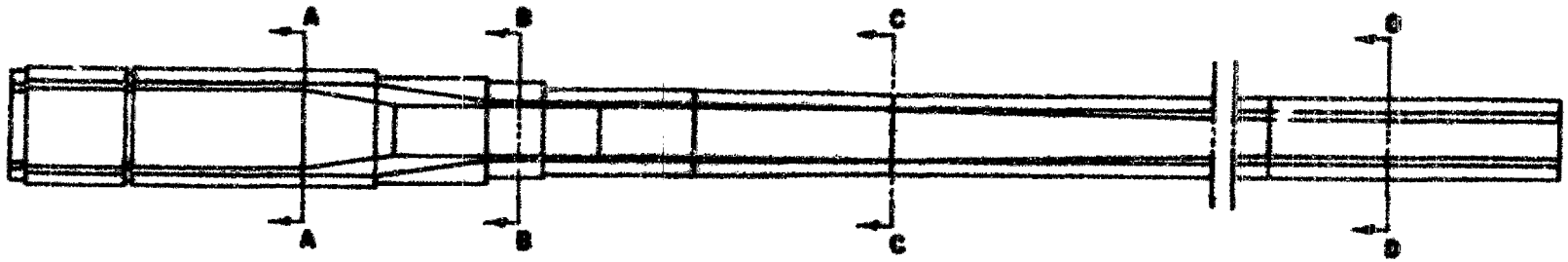

TUBE TYPE	A	B	C	D	WEIGHT
90m/m M 41	10.04	9.01	6.40	5.44	1180
90m/m AUTOFRETTAGED (SF = 1.46)	7.60	6.45	5.30	5.00	860
90m/m AUTOFRETTAGED (SF = 1.12)	6.79	5.81	5.10	4.50	840

Figure 30. COMPARISON OF 90m/m AUTOFRETTAGED AND NON-AUTOFRETTAGED TUBES

SPECIMEN NUMBER	TENSILE STRENGTH (psi)	YIELD STRENGTH (psi)	INITIAL YIELD PRESSURE (psi)	OVERSTRAIN PRESSURE (psi)	MAX. OUTSIDE SURFACE STRAIN (micro-in/in)	LONGITUDINAL SHRINKAGE (inch)	% PERMANENT HOOP ENLARGEMENT	PERMANENT ENLARGEMENT RATIO
1.4 DIAMETER RATIO								
3AA1	176,500	165,000	46,000	60,000	5,760	.0042	.268	1.15
3AA2	176,500	165,000	48,000	62,000	4,960	.0042	.269	-
3AA3	176,500	165,000	46,000	60,000	4,880	.0057	.244	-
3BB1	175,000	165,000	46,000	59,000	5,960	.0055	.544	1.14
3BB2	175,000	165,000	46,000	60,000	6,200	.0083	.525	1.18
3BB3	175,000	165,000	44,000	60,000	6,065	.0073	.470	1.24
4AA1	155,500	144,000	42,000	54,000	8,460	.0136	.973	1.22
4AA2	155,500	144,000	44,000	53,000	7,580	.0185	1.00	1.20
4AA3	155,500	144,000	44,000	54,500	5,880	.0174	.866	1.10
4BB1	177,000	167,500	44,000	60,000	10,620	.0289	1.31	1.19
4BB2	177,000	167,500	46,000	60,500	10,960	.0279	1.35	1.22
4BB3	177,000	167,500	46,000	61,000	12,470	.0286	1.51	1.19
1.6 DIAMETER RATIO								
3AA1	179,000	169,000	53,000	82,000	5,170	.0044	.52	1.53
3AA2	179,000	169,000	55,000	81,000	5,110	.0067	.48	1.46
3AA3	179,000	169,000	52,000	80,000	5,790	.0073	.53	1.51
3BB1	176,500	165,000	53,000	82,000	7,340	.0051	.92	1.45
3BB2	176,500	165,000	55,000	81,000	6,650	.0052	1.01	1.48
3BB3	176,500	165,000	53,000	80,000	7,400	-	1.02	1.50
3AA1	178,000	166,500	55,000	81,500	8,070	.0108	1.40	1.51
3AA2	178,000	166,500	55,000	80,000	7,300	.0119	1.40	1.54
3AA3	178,000	166,500	53,000	79,000	6,890	.0107	1.42	1.48

SPECIMEN DATA
SHEET 1 OF 5

TABLE 1

SPECIMEN NUMBER	TENSILE STRENGTH (psi)	YIELD STRENGTH (psi)	INITIAL YIELD PRESSURE (psi)	OVERSTRAIN PRESSURE (psi)	MAX. OUTSIDE SURFACE STRAIN (micro-in/in)	LONGITUDINAL SHRINKAGE (inch)	% PERMANENT BORE ENLARGEMENT	PERMANENT ENLARGEMENT RATIO
1.8 DIAMETER RATIO								
30B1	179,000	169,500	62,000	102,300	5,755	.0009	.68	1.51
30B2	179,000	169,500	64,000	102,500	6,110	.0051	.73	1.50
30B3	179,000	169,500	64,000	102,000	6,520	.0097	.81	1.84
30A1	179,000	167,500	64,000	104,000	7,380	.0040	1.10	1.51
30A2	179,000	167,500	60,000	102,000	7,250	.0044	1.15	1.59
30A3	179,000	167,500	66,000	101,000	7,115	.0066	1.14	1.42
36A1	170,000	160,000	57,000	98,000	5,370	RUPTURED		
36A2	170,000	160,000	56,000	97,000	6,470	.0100	1.18	1.76
36A3	170,000	160,000	56,000	95,000	6,830	.0088	1.14	1.73
36B1	172,000	161,000	57,000	100,000	8,500	.0126	1.74	1.65
36B2	172,000	161,000	58,000	97,000	9,000	.0175	1.97	1.68
36B3	172,000	161,000	58,000	95,500	7,520	.0148	1.74	1.61
40A1	170,000	160,000	62,000	101,000	8,470	.0110	1.90	1.69
40A2	170,000	160,000	61,000	102,000	9,300	.0142	1.80	1.63
40A3	170,000	160,000	60,000	100,000	9,030	.0157	1.95	1.63
28A1	170,000	161,000	55,000	99,000	8,000+	RUPTURED		
28A2	170,000	161,000	62,000	99,000	6,800	RUPTURED		
28B3	179,000	170,000	60,000	101,000	8,000+	RUPTURED		
2.0 DIAMETER RATIO								
24A1	174,000	163,500	69,000	120,000	4,885	.0016	.82	2.00
24A2	174,000	163,500	75,000	120,000	4,475	.0057	.77	1.98
24A3	174,000	163,500	73,000	115,000	5,440	.0011	.61	1.96

SPECIMEN DATA
SHEET 2 OF 5

TABLE 1

SPECIMEN NUMBER	TENSILE STRENGTH (psi)	YIELD STRENGTH (psi)	INITIAL YIELD PRESSURE (psi)	OVERSTRAIN PRESSURE (psi)	MAX. OUTSIDE SURFACE STRAIN (micro-in/in)	LONGITUDINAL SHRINKAGE (inch)	% PERMANENT BORE ENLARGEMENT	PERMANENT ENLARGEMENT RATIO
2.0 DIAMETER RATIO (CONT.)								
24B1	177,000	169,000	75,000	122,000	5,080	.0046	1.21	2.10
24B2	177,000	169,000	71,000	126,000	6,160	.0040	1.11	1.72
24B3	177,000	169,000	75,000	124,000	5,640	.0078	1.01	1.91
26A1	177,000	168,000	73,000	124,000	7,235	.0054	1.59	1.88
26A2	177,000	168,000	73,000	126,000	5,500+	RUPTURED		
26A3	177,000	168,000	67,000	127,000	4,700	RUPTURED		
40B1	170,000	160,500	73,000	121,000	7,135	.0072	1.76	1.69
23B1	172,000	163,000	67,000	121,000	9,600	-	2.25	-
23B2	172,000	163,000	70,000	122,000	7,970	-	2.00	1.61
23B3	172,000	163,000	73,000	122,000	6,400	-	2.14	1.61
23A2	171,000	161,000	69,000	122,000	9,970	-	2.55	1.80
23A3	171,000	161,000	69,000	121,000	9,910	-	2.54	1.78
2.2 DIAMETER RATIO								
37A1	175,000	164,000	83,000	135,000	3,350	.0009	.54	1.93
37A2	175,000	164,000	83,000	134,000	3,300	.0010	.49	2.07
37A3	175,000	164,000	83,000	135,000	3,600	.0012	.53	2.00
37B1	155,000	143,000	75,000	125,000	4,370	.0016	1.12	1.98
37B2	155,000	143,000	75,000	125,000	-	.0013	1.11	2.01
37B3	155,000	143,000	75,000	128,000	4,370	.0024	1.12	1.96
44B1	182,000	172,000	81,000	146,000	5,530	.0014	1.39	1.95
44B2	182,000	172,000	81,000	145,000	5,900	.0021	1.48	1.99
44B3	182,000	172,000	81,000	141,000	5,770	.0033	1.41	2.09

SPECIMEN DATA
SHEET 3 OF 5

TABLE 1

SPECIMEN NUMBER	TENSILE STRENGTH (psi.)	YIELD STRENGTH (psi.)	INITIAL YIELD PRESSURE (psi)	OVERSTRAIN PRESSURE (psi.)	MAX. OUTSIDE SURFACE STRAIN (micro-in/in)	LONGITUDINAL SHRINKAGE (inch)	% PERMANENT BORE ENLARGEMENT	PERMANENT ENLARGEMENT RATIO
2.2 DIAMETER RATIO (CONT.)								
44A1	181,500	171,000	79,000	145,000	6,760	.0069	1.93	2.15
44A2	181,500	171,000	77,000	143,000	6,475	.0055	1.80	2.04
44A3	181,500	171,000	79,000	141,500	5,875	.0069	1.74	1.96
34A1	176,000	164,000	77,000	139,000	7,265	.0136	2.41	1.97
34A2	176,000	164,000	77,000	135,000	7,505	.0065	2.36	1.96
34A3	176,000	164,000	75,000	135,000	--	.0080	2.36	2.00
34B1	180,000	169,500	79,000	138,000	8,265	.0125	2.66	1.95
34B2	180,000	169,500	79,000	136,000	8,795	-	2.70	2.01
24B3	180,000	169,500	77,000	135,000	7,955	.0140	2.38	1.99
2.4 DIAMETER RATIO								
48A1	172,000	163,000	82,000	140,000	3,090	.0051	.75	2.09
48A2	172,000	163,000	82,000	139,000	3,145	.0008	.46	2.08
48A3	172,000	163,000	80,000	135,000	2,460	.0020	.44	2.25
48B1	172,500	163,000	75,000	143,000	3,560	.0020	.49	2.41
48B2	172,500	163,000	73,000	145,000	3,700	.0016	1.01	2.30
48B3	172,500	163,000	67,000	145,000	4,170	.0034	1.09	2.32
58A1	177,000	167,500	77,000	155,000	5,470	.0023	1.09	2.40
58A2	177,000	167,500	82,000	158,000	4,870	.0012	1.45	2.39
58B1	158,000	146,000	72,000	144,000	5,950	.0048	2.17	2.25
58B2	158,000	146,000	73,000	144,000	6,180	.0079	2.13	2.25
58B3	158,000	146,000	71,000	145,000	5,770	.0063	2.05	2.27

SPECIMEN DATA
SHEET 4 OF 5

TABLE 1

SPECIMEN NUMBER	TENSILE STRENGTH (psi.)	YIELD STRENGTH (psi.)	INITIAL YIELD PRESSURE (psi.)	OVERSTRAIN PRESSURE (psi.)	MAX. OUTSIDE SURFACE STRAIN (micro-in/in)	LONGITUDINAL SHRINKAGE (inch)	% PERMANENT BORE ENLARGEMENT	PERMANENT ENLARGEMENT RATIO
2.4 DIAMETER RATIO (CONT.)								
4SA1	171,000	160,500	78,000	151,000	6,700	.0072	2.44	2.21
4SA2	171,000	160,500	77,000	151,000	6,400	.0052	2.28	2.17
4SA3	171,000	160,500	76,000	154,000	6,660	.0075	2.37	2.32
4SB1	168,000	157,500	79,000	150,000	7,250	.0055	2.43	2.15
4SB2	168,000	157,500	76,000	151,000	7,910	.0091	2.45	2.01
4SB3	168,000	157,500	78,000	152,000	7,610	.0085	2.42	2.09

SPECIMEN DATA
SHEET 5 OF 5

TABLE 1

SPECIMEN NUMBER	TENSILE STRENGTH (psi.)	YIELD STRENGTH (psi.)	INITIAL YIELD PRESSURE (psi.)	OVERSTRAIN PRESSURE (psi.)	MAX. OUTSIDE SURFACE STRAIN (micro-in/in)	LONGITUDINAL SHRINKAGE (inch)	% PERMANENT BORE ENLARGEMENT	PERMANENT ENLARGEMENT RATIO
2.4 DIAMETER RATIO (CONT.)								
45A1	171,000	160,500	78,000	151,000	6,700	.0072	2.44	2.22
45A2	171,000	160,500	77,000	151,000	6,400	.0061	2.28	2.17
45A3	171,000	160,500	76,000	154,000	6,600	.0075	2.37	2.32
45B1	168,000	157,500	79,000	150,000	7,250	.0065	2.43	2.15
45B2	168,000	157,500	76,000	151,000	7,910	.0091	2.45	2.01
45B3	168,000	157,500	78,000	152,000	7,610	.0085	2.42	2.09

SPECIMEN DATA
SHEET 5 OF 5

TABLE 2

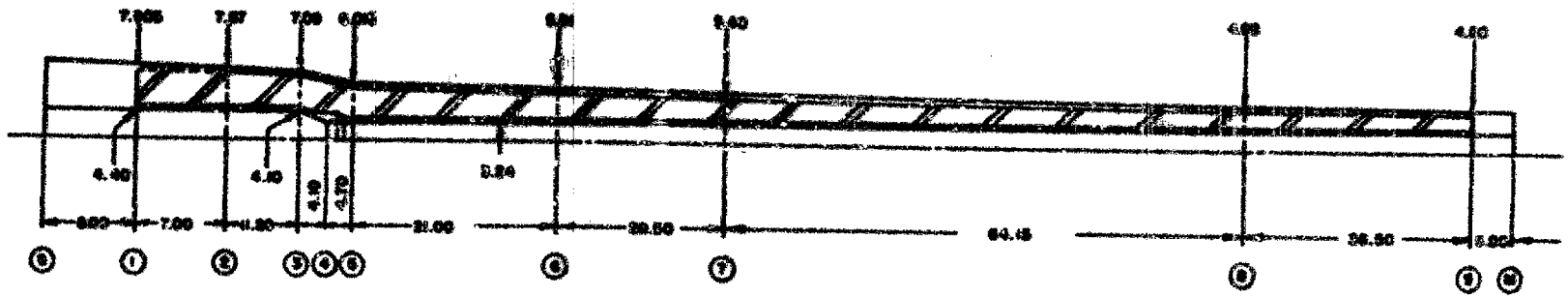

	TUBE																CONTAINER						LONGITUDINAL STRAIN				
	RECLAIMED		FIRST APPROXIMATION							SECOND APPROXIMATION																	
	AFTER AF							AFTER AF		BEFORE AF						AFTER AF											
SECT	a	b	W	PRE	Δa	PRE	db	a	b	a	b	W	PRE	Δa	PRE	db	a	b	P_0	P_{LZ}	ε_{aa}	W	ε_{bb}	ε_0	ΔT (deg)	ΔPRE	ε (Δdiff)	Δε	ε (Δdiff)
A										4.365	7.905														7.905				
1	4.60	7.903	1.80	.85	.037	1.60	.023	4.343	7.882	4.365	7.905	1.81	.87	.038	1.61	.024	4.403	7.909	109	26	.018	3.79	.010	7.919	1.60	.60	8.00	.001	8.00
2	4.084	7.87	1.84	.92	.040	1.64	.024	4.264	7.846	4.250	7.850	1.85	.94	.040	1.65	.024	4.280	7.874	119	28	.020	3.92	.009	7.883	1.85	.90	7.70	.004	7.69
3	4.30	7.09	1.73	.75	.031	1.55	.020	4.069	7.070	4.065	7.090	1.74	.76	.032	1.55	.020	4.096	7.090	102	23	.018	4.25	.013	7.087	1.79	.85	11.20	.007	11.21
4	3.84	6.95	2.02	2.3	.063	1.82	.032	3.338	6.887	3.800	6.868	2.01	2.34	.063	1.84	.033	3.963	6.902	130	5	.022	4.55	.018	6.912	1.99	2.35	4.70	.005	4.70
5		6.015	1.85	2.0	.052	1.66	.029	3.208	5.956		5.995	1.87	.97	.033	1.69	.029	3.852	6.014	115	20	.016	5.00	.005	6.036	1.86	.95	23.00	.013	23.01
6		5.98	1.82	.90	.029	1.62	.018	3.213	5.892		5.890	1.84	.92	.029	1.64	.018	3.209	5.908	112	23	.015	5.05	.0095	5.932	1.76	.79	25.50	.010	25.52
7		5.60	1.67	.65	.021	1.47	.014	3.219	5.386		5.585	1.68	.66	.021	1.50	.014	3.222	5.599	95	60	.0135	5.56	.010	5.567	1.68	.57	64.15	.028	64.29
8		4.88	1.54	.47	.013	1.38	.012	3.285	4.969		4.972	1.55	.48	.013	1.39	.013	3.335	4.983	80	25	.0120	6.02	.0125	6.003	1.55	.45	26.50	.020	26.52
9		4.80	1.48	.40	.013	1.33	.010	3.227	4.790	3.200	4.790	1.50	.43	.013	1.34	.010	3.273	4.800	74	66	.0135	6.25	.013	6.799	1.30	.20	5.00	.008	5.08
B	3.85									3.800	4.985														4.796				

Table 2. SAMPLE AUTOFRETTAGE DESIGN COMPUTATION